The University Of Sheffield.

Antenna Array Design for Directional Modulation

By

Bo Zhang

A doctoral thesis submitted in fulfilment of the requirements for the award of

Doctor of Philosophy

The University of Sheffield

Department of Electrical and Electronic Engineering

July 2018

Supervisor

Dr. Wei Liu

Antenna Array Design for Directional Modulation

Bo Zhang

PHD THESIS

Communications Group

Department of Electrical and Electronic Engineering

The University of Sheffield

July 2018

Abstract

Directional modulation (DM) as a physical layer security technique to keep known constellation points in the desired directions, while making the points scrambled in other directions has been achieved. DM is normally applied on uniform linear arrays (ULAs) where the maximum spacing between adjacent antennas is a half wavelength of the frequency of interest in order to avoid spatial aliasing. In this thesis, to have a larger aperture and a higher spatial resolution given a fixed number of antennas, compressive sensing (CS) based sparse antenna array design for DM is formulated. Two practical scenarios are considered in the proposed design: robust design with model errors, and design with practical non-zero-sized antennas. To extend the frequency spectrum, multi-carrier based phased antenna array design for DM by using Inverse Discrete Fourier Transform (IDFT) is introduced. The modified Wideband Beampattern Formation via Iterative Techniques (modified WBFIT) method is proposed to reduce the peak to average power ratio (PAPR) to a given threshold for a given antenna array geometry. Moreover, polarisation states of signals are exploited on crossed-dipole array for DM to further increase the channel capacity. Based on a multi-path model, positional modulation design is proposed to make sure that only in desired locations the received signal can be recovered successfully, while in the positions around, the received modulation patterns are scrambled.

Contents

List of Publications

Journal papers

1. B. Zhang and W. Liu. "Multi-carrier based phased antenna array design for directional modulation". IET Microwaves, Antennas & Propagation, 12(5), 765 – 772, April 2018.

2. B. Zhang, W. Liu, and X. Gou. "Compressive sensing based sparse antenna array design for directional modulation", IET Microwaves, Antennas & Propagation 11(5), 634 – 641, April 2017.

Conference papers

1. B. Zhang and W. Liu, "Antenna array based positional modulation with a two-ray multi-path model", In Proc. Sensor Array and Multichannel Signal Processing Workshop (SAM), 2018 IEEE, Sheffield, UK, July, 2018, to appear.

2. B. Zhang, W. Liu, and X. Lan. "Directional modulation design based on crossed-dipole arrays for two signals with orthogonal polarisations". In Proc. European Conference on Antennas and Propagation (EuCAP), London, UK, April, 2018, to appear.

3. B. Zhang, W. Liu, and X. Gou. "Sparse antenna array design for directional modulation", In Proc. Sensor Array and Multichannel Signal Processing Workshop (SAM), 2016 IEEE, Rio de Janerio, Brazil, September 2016.

Under review

1. B. Zhang, W. Liu, and X. Lan. "Orthogonally Polarised Dual-Channel Directional Modulation Based on Crossed-Dipole Arrays", IET Microwaves, Antennas & Propagation.

2. B. Zhang, W. Liu and Q. Li, "Multi-carrier Antenna Array Design for Directional Modulation under PAPR constraint", IEEE Transactions on Circuits and Systems I: Regular Papers.

List of Figures

List of Tables

Acknowledgements

I would like to express my sincere gratitude and appreciation to my supervisors Dr. Wei Liu and Dr. Xiaoli Chu. Thank you for guiding me into this area and imparting your wisdom to me.

To my parents, thank you for always listening to me, supporting me and encouraging me. You are the world to me. You bring me calm and safe.

To my cousin Xin Li, her husband Ian Booth and their lovely sons Stephen and Alex, thank you for bringing me happiness and knowledge. I am always the guy who says I am not alone in Christmas as I know I am going to spend time with you and I will be surrounded by love and presents.

To 61, thank you for coming here and thank you for making me laugh when I don't even want to smile. You are the person who I spend the most time with for the last three years. I can't imagine how the life would be if you weren't here.

To Ruilong, Terence, Martin and all friends, thank you for standing by my side when life is hard, and giving me your advice and showing your support in my PhD studies. Without you guys, life would be boring.

To all colleagues in the communication group, thank you for the unlimited support I have received for the last four years.

List of Abbreviations

AWGN	Additive White Gaussian Noise
BER	Bit Error Rate
CS	Compressive Sensing
DFT	Discrete Fourier Transform
DM	Directional Modulation
DOF	Degree of Freedom
GA	Genetic Algorithm
IDFT	Inverse Discrete Fourier Transform
IQ	In-phase Quadrature
LOS	Line of Sight
MIMO	Multiple Input Multiple Output
OFDM	Orthogonal Frequency-Division Multiplexing
PAPR	Peak to Average Power Ratio
PTS	Partial Transmit Sequences
QPSK	Quadrature Phase-Shift Keying
SA	Simulated Annealing

SLM	Selective Mapping
SNR	Signal to Noise Ratio
TDL	Tapped Delay Line
TEM	Transverse Electromagnetic
ULA	Uniform Linear Array
WBFIT	Wideband Beampattern Formation via Iterative Techniques

Chapter 1

Introduction

1.1 Introduction

Communication networks such as telephone networks, cable television, broadcast radio, etc. play an important role in social life. According to the connection method between transmitters and receivers, it can be classified into wired communication and wireless communication. Wired communication, as the name implies, transmits data over a wire, provides point to point connection and is stable to make sure that signals are not easy to be interfered, but the wire cost is a problem for long distance communication. While in wireless systems, radio wave is the carrier to transmit signal between transmitters and receivers, which is cost effective, flexible and convenient. However, it is easy to be attacked by intruders via transmitting jamming signals, pretending to be a legitimate user, etc [1]. Therefore, the security of information transfer is challenging, and it is critical to make sure that data are transmitted to the desired users only.

Beamforming is a traditional method to protect data transmission by keeping the maximum power to desired direction or directions, while making power to un-desired directions as low as possible. However, as the signal is modulated at base band and then up-converted to radio frequency, the same constellation mappings are used in all directions of the transmit antennas (the differences between different directions are power levels and phase rotation due to the different propagation path). To further increase the signal transmission security, the directional modulation (DM) technique has been devel-

oped by keeping the mainbeam pointing to the desired direction with known constellation mappings in a desired direction or directions, while lower the power and scrambling constellation mappings for the remaining directions [2–4].

Moreover, most existing research in DM is based on uniform linear arrays (ULAs) with a maximum half wavelength spacing to avoid grating lobes. However, cost and weight are problems when a large number of antennas are required for ULA applications. To have a similar antenna array performance with fewer antennas than ULA, sparse arrays are employed [5, 6], and the increased degrees of freedom (DOFs) in the spatial domain allows the system to incorporate more constraints into the design of various beamformers. Many methods have been proposed to design such a sparse array, including the genetic algorithm (GA) [7–11], simulated annealing (SA) [12], and compressive sensing (CS) [13–18]. In the thesis, CS-based design is considered, where l_1 norm and reweighted l_1 norm minimisation problems are both used and tested for sparse array designs, and it turns out that the reweighted l_1 norm minimisation, an iterative method can provide a closer minimisation to the l_0 norm than the usual l_1 norm minimisation. In this reweighted method, a larger weighting term is introduced to those coefficients with smaller non-zero values and a smaller weighting term to those coefficients with larger non-zero values.

1.2 Original Contributions

1. Directional modulation (DM) can be achieved based on ULAs where the maximum spacing between adjacent antennas is a half wavelength of the frequency of interest in order to avoid spatial aliasing. To exploit the additional degrees of freedom (DOFs) provided in the spatial domain, sparse antenna arrays can be employed for more effective DM. However, the set of optimised antenna locations would be different if the locations for each modulation symbol are optimised individually. To solve the problem, group sparsity is introduced to the CS optimisation process, which is to calculate the l_2 norm of weight coefficients for all symbols on this antenna position. If the result is higher than a given threshold, then the antenna location is kept; otherwise, the position is cancelled. Based on this, a common set of active

antennas can be found for all modulation symbols generating a response close to the desired one. Moreover, two practical scenarios for the proposed design are considered, including robust design with model errors, and design with practical non-zero-sized antennas.

2. For DM design, narrowband signal is normally considered. To use a wider spectrum, a multi-carrier based DM framework using antenna arrays are developed, where simultaneous data transmission over multiple frequencies can be achieved. In addition, such a framework allows possible frequency division based multi-user access to the system and also provides the flexibility of using different modulation schemes at different frequencies. Then, the antenna location optimisation problem for multi-carrier based DM is studied using a CS-based approach by employing the group sparsity concept. However, a potential problem of the multi-carrier design is the high peak to average power ratio (PAPR) of the resultant signals, leading to non-linear distortion when signal peaks pass through saturation regions of a power amplifier. To avoid this, a PAPR constraint to control the signal envelope needs to be considered in the design, and the relevant solution, the so-called modified Wideband Beampattern Formation via Iterative Techniques (modified WBFIT) method, is proposed.

3. In the context of one single carrier frequency, to increase channel capacity, a new DM scheme based on a crossed-dipole array is introduced which can simultaneously transmit two signals with orthogonal polarisations to the same direction at the same frequency. These two signals can also be considered as one composite signal using a four dimensional (4-D) modulation scheme across the two polarisation diversity channels. The set of weight coefficients to achieve directional modulation for the two signals based on crossed-dipole arrays is designed. Moreover, compressive sensing (CS) based formulations for sparse crossed-dipole array design in this context for a common set of optimised antenna locations are also introduced to further exploit the DOFs in the spatial domain.

4. Traditional DM designs are based on the assumption that there is no multi-path

effect between transmitters and receivers. One problem with these designs is that the resultant systems will be vulnerable to eavesdroppers which are aligned with or very close to the desired directions. To solve the problem, a two-ray multi-path model is studied for positional modulation and the coefficients design for a given antenna array geometry and a location-optimised antenna array are proposed, where the multi-path effect is exploited to generate a given modulation pattern at desired positions, with scrambled values at positions around them.

1.3 Outline

The outline of this thesis is as follows:

In Chapter 2, basics about narrowband beamforming, wideband beamforming and directional modulation are reviewed. Many methods to achieve DM are described, and the patterns of constellation points with and without DM technique are drawn to demonstrate their differences. Phased antenna array for DM is shown with its formulated design solutions.

In Chapter 3, a class of CS-based design methods for DM is presented for sparse antenna array design, including l_1 norm minimisation and reweighted l_1 norm minimisation. Then two practical scenarios are considered, consisting of a robust design in the presence of steering vector errors, and a design considering the non-zero size of antennas. Design examples including beam patterns, phase patterns and bit error rate (BER) for all cases are provided to verify the effectiveness of the designs.

In Chapter 4, to use a wider spectrum, the multi-carrier based structure and its design for DM are proposed, so that a much higher data rate can be obtained. In addition, such a framework allows possible frequency division based multi-user access to the system and also provides the flexibility of using different modulation schemes at different frequencies. However, a potential problem of the multi-carrier design is the high peak to average power ratio (PAPR) of the resultant signals, leading to non-linear distortion when signal peaks pass through saturation regions of a power amplifier. To avoid this, a PAPR constraint to control the signal envelope needs to be considered in the design.

In Chapter 5, a review of polarised beamforming based on crossed-dipole arrays is given firstly, where there is only a single signal transmitted at one carrier frequency to the desired direction and the weight coefficients are thus designed for one single signal. Then, for a higher channel capacity in the context of one carrier frequency, DM designs for two signals transmitted to the same direction, but with orthogonal polarisation states are proposed, based on a given fixed array geometry and an array with optimised crossed-dipole locations. Design examples are provided to show the effectiveness of the work.

In Chapter 6, a review of the two-ray model is given, where signals at receiver side are the sum of a line of sight (LOS) signal and a reflected signal. Then the multi-path effect is exploited and positional modulation design based on a given array geometry is provided with a closed-form solution based on the method of Lagrange multipliers. The CS-based design for a location-optimised array is also presented using the reweighted l_1 norm minimisation method, and a comparison between the ULA design and the sparse array designs is provided to show the effectiveness of the designs.

Finally in Chapter 7, conclusions are drawn and an outline for potential future work is provided.

Chapter 2

Review of Directional Modulation and Beamforming

2.1 Introduction to Directional Modulation

Beamforming is a traditional method to protect data transmission by keeping the maximum power to desired direction or directions, while making the power to un-desired directions as low as possible. However, for beamforming technique the same constellation mappings (complex value in the In-phase Quadrature (IQ) complex plane, e.g. for Quadrature Phase Shift Keying (QPSK), four complex-valued signals are $\sqrt{2}/2+(\sqrt{2}/2)i$, $-\sqrt{2}/2+(\sqrt{2}/2)i$, $-\sqrt{2}/2-(\sqrt{2}/2)i$, $\sqrt{2}/2-(\sqrt{2}/2)i$) are used in all directions of the transmit antennas (the differences between different directions are power levels and phase rotation due to the different propagation path). Then the problem is that the eavesdroppers located at the sidelobe of the radiation pattern still able to receive the same information as the desired receiver located at the mainlobe direction. The constellation points in different directions are shown in Fig. 2.1. To avoid this, the DM technique [2, 3] was developed to improve signal transmission security by keeping known constellation mappings in a desired direction or directions, but scrambling them for the other ones, as shown in Fig. 2.2.

In [2–4], a method called near-field direct antenna modulation (NFDAM) was introduced, applying to a parasitic array which includes a dipole antenna and several reflectors

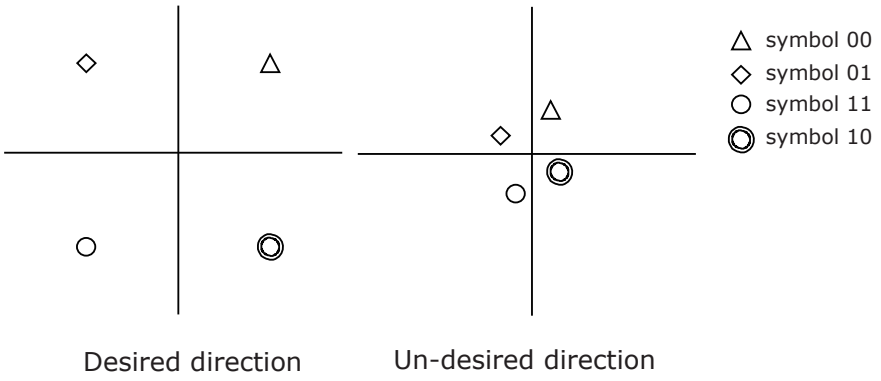

Figure 2.1: Baseband constellation points in IQ complex plane.

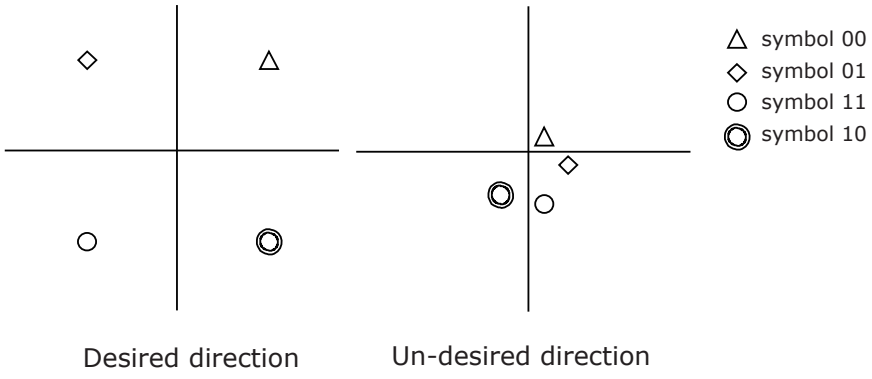

Figure 2.2: DM constellation points in IQ complex plane.

with switches. The dipole antenna radiates an un-modulated signal $A_0\cos(\omega t+\varphi_0)$. By controlling switches to change the reflectors' effective length and scattering properties, scattered signals radiated from reflectors to the desired direction $A_i\cos(\omega t+\varphi_i)$ are different. Therefore, the far-field signal can be given by $A_0\cos(\omega t+\varphi_0)+A_i\cos(\omega t+\varphi_i)$. Given the scattering properties of these reflectors, the phase and magnitude of scattered signals are different with angles. Therefore in un-desired directions, constellation points are scrambled.

Similarly, in [19], a four-element reconfigurable array was designed by switching elements for each symbol to change the element radiation pattern to make their constellation points not scrambled in desired directions, but distorted in other directions. In this paper, reconfigurable arrays implement beam steering without the use of phase shifters, which reduces cost and size to the system caused by phase shifters. The procedure for determining how to switch the corresponding elements to transmit only in a specified direction was outlined.

A method named dual beam DM was introduced in [20]. Unlike the methods where In-phase and Quadrature data are transmitted by the same antennas, in this technique they are transmitted by different antennas. $F_1(\varphi)$ and $F_2(\varphi)$ are defined as transmit beams or antenna patterns (φ denotes the azimuth angle of the receiver). For normalizable solutions the magnitude was 1 (0 dB) in mainlobe and 0 (negative infinity dB) at sidelobe directions) associated with the excitation signal $s_1(t)=b_m\cos\omega t$ and $s_2(t)=c_m\sin\omega t$, respectively, where $b_m\in\{+1,-1\}$ and $c_m\in\{+1,-1\}$ for QPSK modulation. The received signals are given as follows

$$\begin{aligned}E(t,\phi)=&b_mF_1(\varphi)\cos(\omega t+\phi)+c_mF_2(\varphi)\sin(\omega t+\phi)\\=&\sqrt{F_1^2(\varphi)+F_2^2(\varphi)}\cos[\omega t+\phi-\arctan(c_mF_2(\varphi)/b_mF_1(\varphi))],\end{aligned}\tag{2.1}$$

where ϕ represents a random phase delay, $\sqrt{F_1^2(\varphi)+F_2^2(\varphi)}$ and $\arctan(c_mF_2(\varphi)/b_mF_1(\varphi))$ are respectively magnitude and phase of the received signals. Therefore, to keep standard QPSK constellation points in the mainlobe, i.e. the complex values for four symbols are $\sqrt{2}/2+(\sqrt{2}/2)i$, $-\sqrt{2}/2+(\sqrt{2}/2)i$, $-\sqrt{2}/2-(\sqrt{2}/2)i$, $\sqrt{2}/2-(\sqrt{2}/2)i$, but scrambled

over sidelobe directions, the antenna patterns $F_1(\varphi)$ and $F_2(\varphi)$ are designed

$$\Lambda = |F_1(\varphi) - F_2(\varphi)|, \tag{2.2}$$

where $\Lambda \to 0$ in desired direction, but $\Lambda \to 1$ in other directions. However, the mainlobe direction cannot be steered with fixed beams $F_1(\varphi)$ and $F_2(\varphi)$.

In [21–30], phased arrays are employed to show that DM can be implemented by phase shifting the transmitted antenna signals properly, and DM also enables an array to send independent data in multiple directions. The radiation pattern of an arbitrarily-spaced array of N elements is

$$E(\theta, \phi) = \sum_{n=0}^{N-1} f_n(\theta, \phi) e^{jkr_n}, \tag{2.3}$$

where $f_n(\theta, \phi)$ is the active element pattern of element n (e.g. for an isotropic antenna, which is a hypothetical lossless antenna having equal radiation in all directions, $f_n(\theta, \phi)$ can be considered as one), and

$$kr_n = \frac{2\pi}{\lambda}(x_n \sin(\theta)\cos(\phi) + y_n \sin(\theta)\sin(\phi) + z_n \cos(\theta)). \tag{2.4}$$

(x_n, y_n, z_n) is the location of element n and λ is the wavelength at the carrier frequency. The radiation pattern can also be made time-varying by adding excitations $w_n^*(t)$ to each element

$$E(t, \theta, \phi) = \sum_{n=0}^{N-1} f_n(\theta, \phi) e^{j\mathbf{k}\mathbf{r}_n} w_n^*(t). \tag{2.5}$$

Assume there are Θ directions, and then the desired modulation symbol in the i-th direction for $i = 0, 1, \ldots, \Theta - 1$ is given by $E_{desired}(t, \theta_i, \phi_i)$ and the calculated modulation symbol from the current set of phase shifts is given by $E_{calculated}(t, \theta_i, \phi_i)$. The genetic algorithm (GA) in [21] was chosen for this application. The cost function is defined as

$$\sum_{i=0}^{\Theta-1} |E_{desired}(t, \theta_i, \phi_i) - E_{calculated}(t, \theta_i, \phi_i)|^2. \tag{2.6}$$

The objective of the design is to optimise the phase shift γ_i of the excitation $w_i^*(t)$ for the i-th element

$$w_i^*(t) = e^{j\gamma_i(t)}. \tag{2.7}$$

Members of the population are sets of four phase angles γ, one for each element. The population size was set to four, with children formed from random crossover of the two best members.

A design to enhance the transmission security by using direction dependent antenna modulation based on a directional antenna array with wide element spacing was presented in [26]. The directional error rate characteristics of the system can be significantly improved by replacing the isotropic elements with directional array elements in a given direction. Moreover, it is shown that the DM system shows a better error rate performance to the counterpart of the conventional system where signals are modulated at baseband in the grating lobe directions. The error rate characteristics of the proposed system were also analysed for two scenarios, i.e., when the angular separation between an eavesdropper and the intended recipient is small and when a potential eavesdropper is located much closer to the transmit antenna than the intended recipient.

In [31], the BER was employed for DM transmitter synthesis by linking the BER performance to the settings of phase shifters. The signals are modulated for QPSK with Gray coding; therefore, the symbols 11, 01, 00, and 10 are respectively located in the first, second, third and fourth quadrants. The received constellation patterns are always rotated to align the phase of symbol 11 to $\pi/4$ as a reference in the first quadrant. The BER can be calculated as follows

$$BER_{DM\_QPSK} = \frac{1}{4}\sum [Q(\sqrt{\frac{l_1^2 \times sin^2(\pi/4)}{N_0/2}}) + Error_{01} + Error_{00} + Error_{10}], \quad (2.8)$$

where $N_0/2$ is the noise power spectral density, l_i is the distance between coordinate origin to the constellation point, $Error_{11}$ is $Q(\sqrt{\frac{l_1^2 \times sin^2(\pi/4)}{N_0/2}})$. For the other three symbols, the $Error_{xy}$ is $Q(\sqrt{\frac{l_i^2 \times sin^2(\beta_i)}{N_0/2}})$ $(i = 2, 3, 4)$ where β_i is the minimum angel between the symbol and the decoding boundary when the $symbol_{xy}$ is located in the quadrants where it should be; otherwise the error would be 0.5 or 1 depending on how many bits the error occurs. By minimising the desired and designed BER as follows, the phases of symbols can be calculated and set randomly

$$V_{cf} = \int_0^{\pi} W \cdot (BER_{DM\_QPSK} - BER_{tem})^2 d(\theta), \quad (2.9)$$

where BER_{tem} is the desired BER (i.e. 1 over the sidelobe directions and a small value in the mainlobe direction depending on what the SNR is), and W is the pre-defined spatial weights.

A more systematic pattern synthesis approach was presented in [32]. An information pattern pointing to the desired direction θ_0 with its array excitations P is created first, and then far-field patterns are generated with main beams pointing to sidelobes of the information pattern. Then steer these far-field pattern nulls along the desired direction θ_0 by power pattern projection method in [33], the resultant patterns are the interference patterns, where excitation is B_i. Finally, the excitation S_m for the m-th symbol is given as follows

$$S_m = D_m \times P + \sum_{i=1}^{N-1} (R_{im} \times B_i), \tag{2.10}$$

where N is the number of antennas, R_{im} is a random complex number imposed by the practical hardware limitations in the DM transmitter [32], for example, amplitude and phase shifter increment for the analogue DM architecture [21, 25], and D_m represents the m-th data with phase and magnitude. The design is achieved by a digital DM transmitter architecture, as described in [34].

In [35, 36], a far-field patterns synthesis approach (magnitude and phase patterns) was proposed to calculate weight coefficients to ensure optimal constellation pattern production along pre-specified communication directions, whereas simultaneously conserving energy dispersal in other directions.

Recently, an eight-element time-modulated antenna array with constant instantaneous directivity in desired directions was proposed in [37, 38]. The main idea of the design is that the array transmits signals without time modulation in the desired direction, while transmitting time-modulated signals in other directions. Due to the time modulation, the radiation pattern of the array changes with time. In the design, during one T_p time modulation period, the second and seventh antenna elements with their corresponding phase shifters are turned-off from the time 0 to $0.2T_p$ and from $0.8T_p$ to $1.0T_p$, while in the rest of the time period, the switched-off elements are the first and eighth elements with their phase shifters.

2.2 Beamforming Based on Antenna Arrays

2.2.1 Narrowband Beamforming

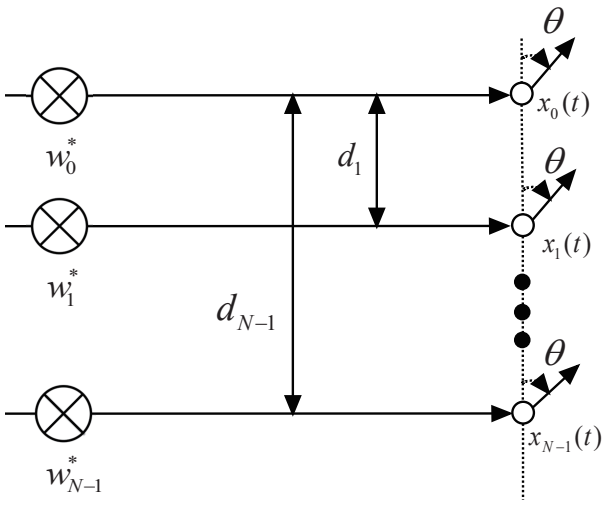

Figure 2.3: A general structure for narrowband beamforming.

A narrowband linear array for transmit beamforming is shown in Fig. 2.3, consisting of N equally spaced omnidirectional antennas, represented by $\circ$. The spacing from the zeroth antenna to its subsequent antennas is represented by d_n for $n = 1, \ldots, N-1$, and the transmission angle $\theta \in [0°, 180°]$. The output signal and weight coefficient for each antenna are respectively denoted by x_n and w_n for $n = 0, \ldots, N-1$. The beamformer weight vector w_n^* is often defined to take the complex conjugates of the coefficients, as it allows the resultant response to be expressed as vector inner products. The steering vector of the array is a function of angular frequency ω and transmission angle θ, given by

$$\mathbf{s}(\omega, \theta) = [1, e^{j\omega d_1 \cos\theta/c}, \ldots, e^{j\omega d_{N-1} \cos\theta/c}]^T, \tag{2.11}$$

where $\{\cdot\}^T$ is the transpose operation, and c is the propagation speed. Moreover, spatial aliasing needs to be considered, which implies signals transmitted to different directions having the same steering vector, e.g. $\mathbf{s}(\omega, \theta_0) = \mathbf{s}(\omega, \theta_1)$, where θ_0 and θ_1 represent

different transmission directions. Therefore,

$$\begin{aligned} e^{j\omega d\cos\theta_0/c} &= e^{j\omega d\cos\theta_1/c} \\ e^{j2\pi d\cos\theta_0/\lambda} &= e^{j2\pi d\cos\theta_1/\lambda}. \end{aligned} \tag{2.12}$$

In order to avoid spatial aliasing, the condition $|2\pi d\cos\theta/\lambda| \leq \pi$ needs to be satisfied. As $|\cos\theta| \leq 1$, $d \leq \lambda/2$ can be derived. Then for a ULA with a half-wavelength spacing ($d_n - d_{n-1} = \lambda/2$), the steering vector is simplified to

$$\mathbf{s}(\omega,\theta) = [1, e^{j\pi\cos\theta}, \ldots, e^{j\pi(N-1)\cos\theta}]^T. \tag{2.13}$$

Then, the beam response of the array is given by

$$p(\theta) = \mathbf{w}^H\mathbf{s}(\omega,\theta), \tag{2.14}$$

where $\{\cdot\}^H$ represents the Hermitian transpose, and $\mathbf{w}$ is the weight vector including all corresponding coefficients

$$\mathbf{w} = [w_0, w_1, \ldots, w_{N-1}]^T. \tag{2.15}$$

To describe the sensitivity of a beamformer with respect to signals transmitted to different directions, beampattern (amplitude response), represented by $|p(\theta)|$ is used. For example, the weight coefficients of an $N = 6$ elements antenna array is given by

$$\mathbf{w} = [1, 1, 1, 1, 1, 1]^T. \tag{2.16}$$

The beampattern (BP) in decibel (dB) of the antenna array is given as follows and is shown in Fig. 2.4.

$$BP = 20\log_{10}\frac{|p(\theta)|}{\max|p(\theta)|}. \tag{2.17}$$

2.2.2 Wideband Beamforming

Compared to the narrowband beamforming structure where one set of weight coefficients is designed for a single frequency, for wideband signals which consist of an infinite number of different frequency components, tapped delay-lines (TDL) are used to compensate the phase difference for different frequency components. Fig. 2.5 shows a wideband

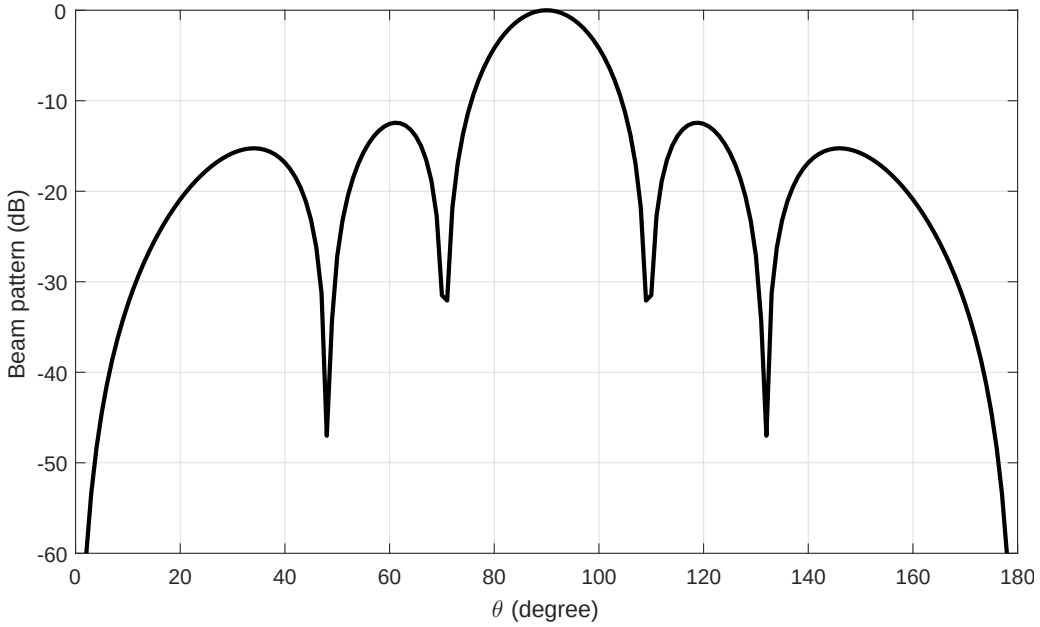

Figure 2.4: Resultant narrowband beam pattern based on the 6 elements ULA.

beamforming linear array, consisting of N equally spaced omni-directional antennas where each element links with a TDL [39, 40]. The spacing from the zeroth antenna to its subsequent antennas is represented by d_n for $n = 1, 2, \ldots, N-1$ and $\theta \in [0°, 180°]$. The weight coefficient at the j-th tap position of the n-th antenna is represented by $w_{n,j}$ for $n = 0, 1, \ldots, N-1$ and $j = 0, 1, \ldots, J-1$. Here the input wave is assumed to be $e^{j\omega t}$, then the output $x_n(t)$ is a linear combination of different delayed transmit signals $w_{n,j}^* e^{j\omega(t-jT_s)}$ through the n-th antenna, and the steering vector of the array as a function of frequency ω and transmission angle θ is given by

$$\begin{aligned}\mathbf{s}(\omega,\theta) =&[1, e^{-j\omega T_s}, \ldots, e^{-j\omega(J-1)T_s}, e^{j\omega\tau_1}, \ldots, \\ &e^{j\omega(\tau_1-(J-1)T_s)}, \ldots, e^{j\omega(\tau_{N-1}-(J-1)T_s)}]^T,\end{aligned} \tag{2.18}$$

where $\{\cdot\}^T$ indicates the transpose operation, T_s is the temporal sampling period of the system and is no more than half the period T_{min} of the signal component with the highest frequency according to the Nyquist sampling theorem, i.e. $T_s \leq \frac{T_{min}}{2}$. $\tau_n = \frac{d_n \cos\theta}{c}$ represents the time advance for the n-th antenna. The array response is given by

$$p(\omega,\theta) = \mathbf{w}^H \mathbf{s}(\omega,\theta), \tag{2.19}$$

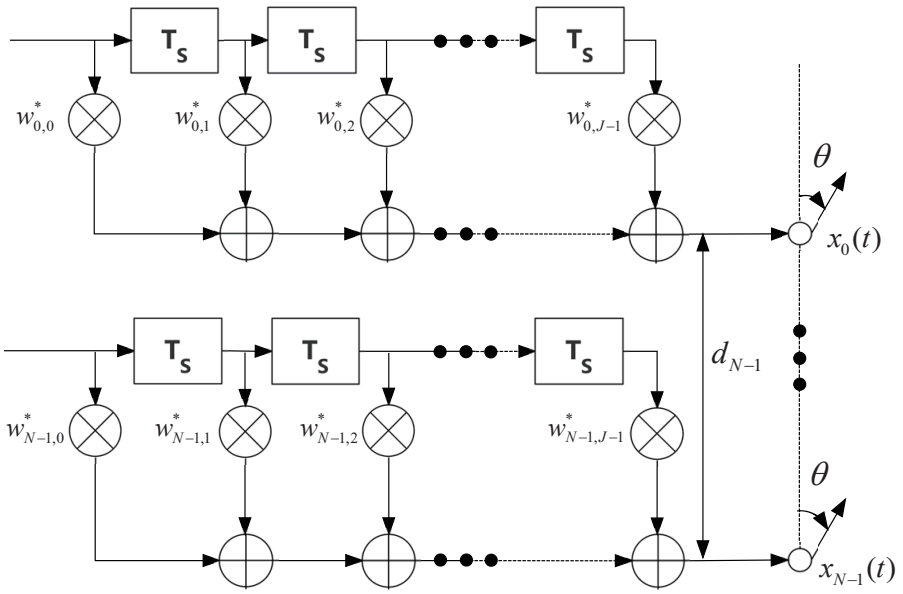

Figure 2.5: A general structure for wideband beamforming.

where $\mathbf{w}$ is a vector of the array, given by

$$\mathbf{w} = [\mathbf{w}_1, \mathbf{w}_1, \ldots, \mathbf{w}_{N-1}]^T, \tag{2.20}$$

$$\mathbf{w}_n = [w_{n,0}, w_{n,1}, \ldots, w_{n,J-1}]^T. \tag{2.21}$$

For example, an $N = 5$ elements antenna array with $J = 3$ tapped delay lines for each antenna is designed. The transmission angle $\theta \in [0°, 180°]$ and the frequency band is from $[0.8\pi, \pi]$ with $I = 10$ discrete temporal frequencies. The weight coefficients is given by

$$w = [0, 0.3, 0, 0, 0.3, 0, 0, 0.3, 0, 0, 0.3, 0, 0, 0.3, 0]^T; \tag{2.22}$$

Then the beam pattern of this array is shown in Fig. 2.6.

2.3 Phased Array Antenna Design for DM

The objective of DM design for a given array geometry is to find the set of weight coefficients giving the desired constellation values in the directions of interest while scrambling the values and simultaneously maintaining a magnitude response as low as possible

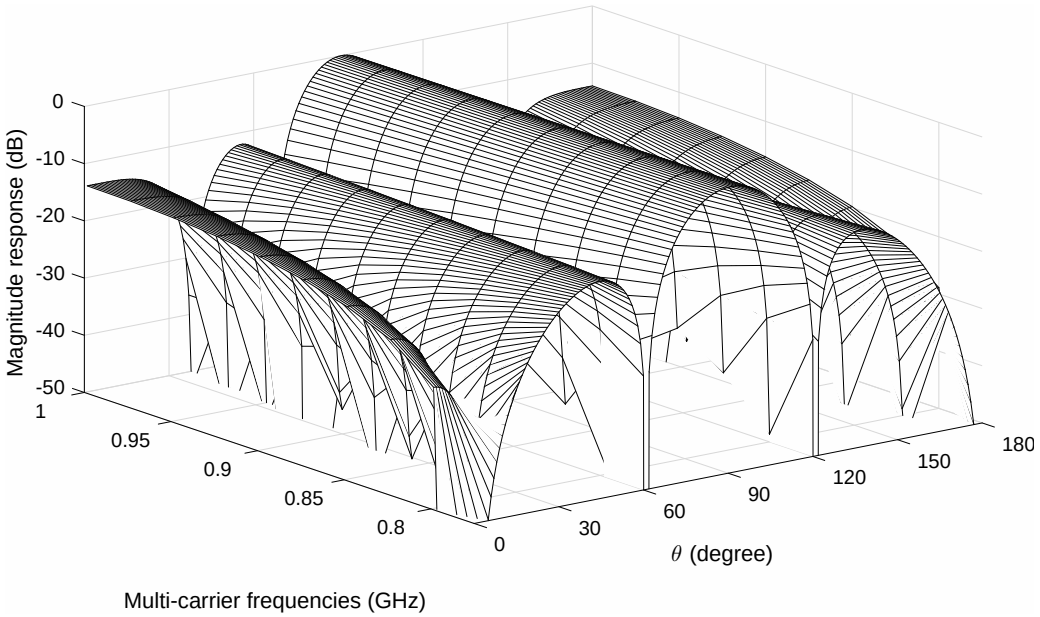

Figure 2.6: Resultant wideband beam pattern based on the 5 elements ULA.

in other directions. For M-ary signaling, such as multiple phase shift keying (MPSK), there are M sets of desired array responses $p_m(\theta)$, with a corresponding weight vector $\mathbf{w}_m = [w_{m,0}, \ldots, w_{m,N-1}]^T$, $m = 0, \ldots, M-1$. Each desired response $p_m(\theta)$ as a function of θ is split into two regions: the mainlobe and the sidelobe, represented by $\mathbf{p}_{m,ML}$ and $\mathbf{p}_{m,SL}$, respectively. Assume Θ sampling points are considered, where r sampling points in the mainlobe and $\Theta - r$ points $\theta_0, \theta_1, \ldots, \theta_{\Theta-r-1}$ in the sidelobe region. Therefore,

$$\begin{aligned} \mathbf{p}_{m,SL} &= [p_m(\theta_0), p_m(\theta_1), \ldots, p_m(\theta_{\Theta-r-1})], \\ \mathbf{p}_{m,ML} &= [p_m(\theta_{\Theta-r}), p_m(\theta_{\Theta-r+1}), \ldots, p_m(\theta_{\Theta-1})]. \end{aligned} \tag{2.23}$$

All constellation points for a fixed θ share the same steering vector and all the $\Theta - r$ steering vectors at the sidelobe region are put into an $N \times (\Theta - r)$ matrix $\mathbf{S}_{SL}$, and the steering vectors at the mainlobe directions are denoted by $\mathbf{S}_{ML}$. For the m-th constellation point, its corresponding weight coefficients can be found by

$$\begin{aligned} \min_{\mathbf{w}_m} \quad & ||\mathbf{p}_{m,SL} - \mathbf{w}_m^H \mathbf{S}_{SL}||_2 \\ \text{subject to} \quad & \mathbf{w}_m^H \mathbf{S}_{ML} = \mathbf{p}_{m,ML}, \end{aligned} \tag{2.24}$$

where $||\cdot||_2$ denotes the l_2 norm. The objective function and constraint in (2.24) ensure a minimum difference between desired and designed responses in the sidelobe, and a

desired constellation value to the mainlobe or the direction of interest. To guarantee scrambled constellations in the sidelobe, the phase of the desired response $\mathbf{w}_m^H \mathbf{S}_{SL}$ at different sidelobe directions can be randomly generated. The problem in (2.24) can be solved by the method of Lagrange multipliers.

The Lagrangian function $\mathscr{L}$ is formed by the cost function $||\mathbf{p}_{m,SL} - \mathbf{w}_m^H \mathbf{S}_{SL}||_2$ and the real part (complex number cannot be compared) of the constraint $\mathbf{w}_m^H \mathbf{S}_{ML} = \mathbf{p}_{m,ML}$,

$$\begin{aligned}\mathscr{L} =&(\mathbf{p}_{m,SL} - \mathbf{w}_m^H \mathbf{S}_{SL})(\mathbf{p}_{m,SL}^H - \mathbf{S}_{SL}^H \mathbf{w}_m) + \lambda^H(\mathbf{w}_m^H \mathbf{S}_{ML} - \mathbf{p}_{m,ML}) \\ &+ \lambda^T(\mathbf{w}_m^T \mathbf{S}_{ML}^* - \mathbf{p}_{m,ML}^*).\end{aligned} \tag{2.25}$$

Differentiating the function $\mathscr{L}$ with respect to w^*, where $\mathbf{R} = \mathbf{S}_{SL}\mathbf{S}_{SL}^H$

$$\frac{\partial \mathscr{L}}{\partial w^*} = -\mathbf{S}_{SL}\mathbf{p}_{m,SL} + \mathbf{R}\mathbf{w}_m + \lambda^H \mathbf{S}_{ML}. \tag{2.26}$$

Setting the result to zero,

$$\mathbf{w}_m = \mathbf{R}^{-1}(\mathbf{S}_{SL}\mathbf{p}_{m,SL}^H - \lambda^H \mathbf{S}_{ML}). \tag{2.27}$$

Then substitute the $\mathbf{w}_m$ to the constraint $\mathbf{w}_m^H \mathbf{S}_{ML} = \mathbf{p}_{m,ML}$,

$$\lambda = (\mathbf{p}_{m,SL}^H \mathbf{S}_{ML}^H \mathbf{R}^{-1} \mathbf{S}_{SL} - \mathbf{p}_{m,ML})(\mathbf{S}_{ML}^H \mathbf{R}^{-1} \mathbf{S}_{ML})^{-1}. \tag{2.28}$$

Therefore, the optimum value for the weight vector $\mathbf{w}_m$ is given in (2.29),

$$\begin{aligned}\mathbf{w}_m =&\mathbf{R}^{-1}(\mathbf{S}_{SL}\mathbf{p}_{m,SL}^H - \mathbf{S}_{ML} \\ &\times ((\mathbf{S}_{ML}^H \mathbf{R}^{-1} \mathbf{S}_{ML})^{-1}(\mathbf{S}_{ML}^H \mathbf{R}^{-1} \mathbf{S}_{SL}\mathbf{p}_{m,SL}^H - \mathbf{p}_{m,ML}^H))).\end{aligned} \tag{2.29}$$

2.4 Design Examples

In this section, a design example is provided to show the performance of the DM designs based on a 24-element ULA. Without loss of generality, the mainlobe direction is $\theta_{ML} = 90^\circ$ and the sidelobe region is $\theta_{SL} \in [0^\circ, 85^\circ] \cup [95^\circ, 180^\circ]$, sampled every 1°. The desired response is a value of one (magnitude) with 90° phase shift at the mainlobe (QPSK) and a value of 0.1 (magnitude) with random phase shifts over the sidelobe regions.

The resultant beam pattern for each constellation point is shown in Fig. 2.7, where all main beams are exactly pointed to 90° with a reasonable sidelobe level. Moreover, the phase at the main beam direction follows the given QPSK modulation pattern and random in the sidelobe directions, as shown in Fig. 2.8, satisfying the DM requirements.

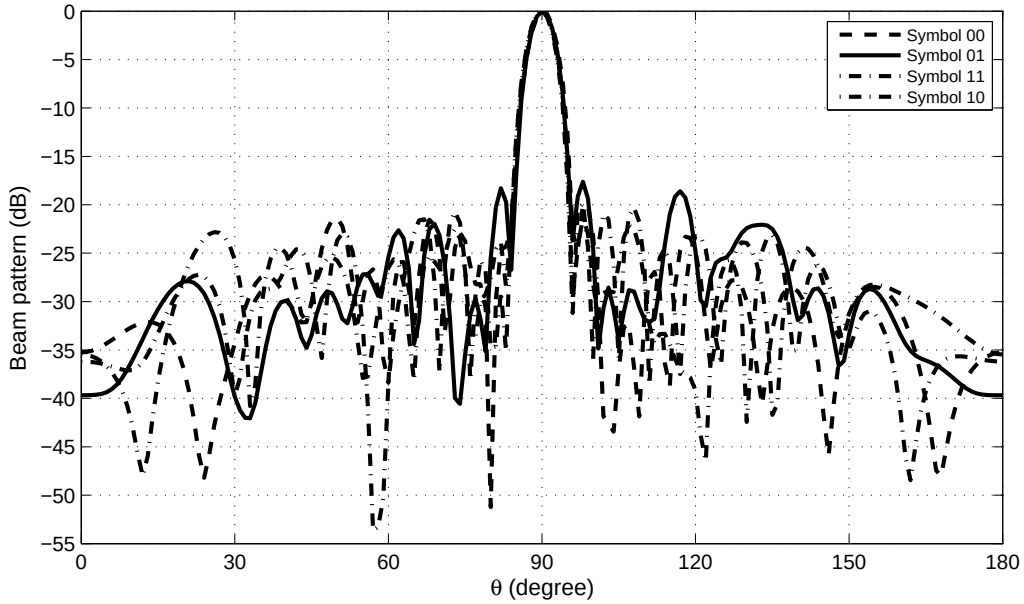

Figure 2.7: Resultant beam pattern based on the ULA for DM using (2.24).

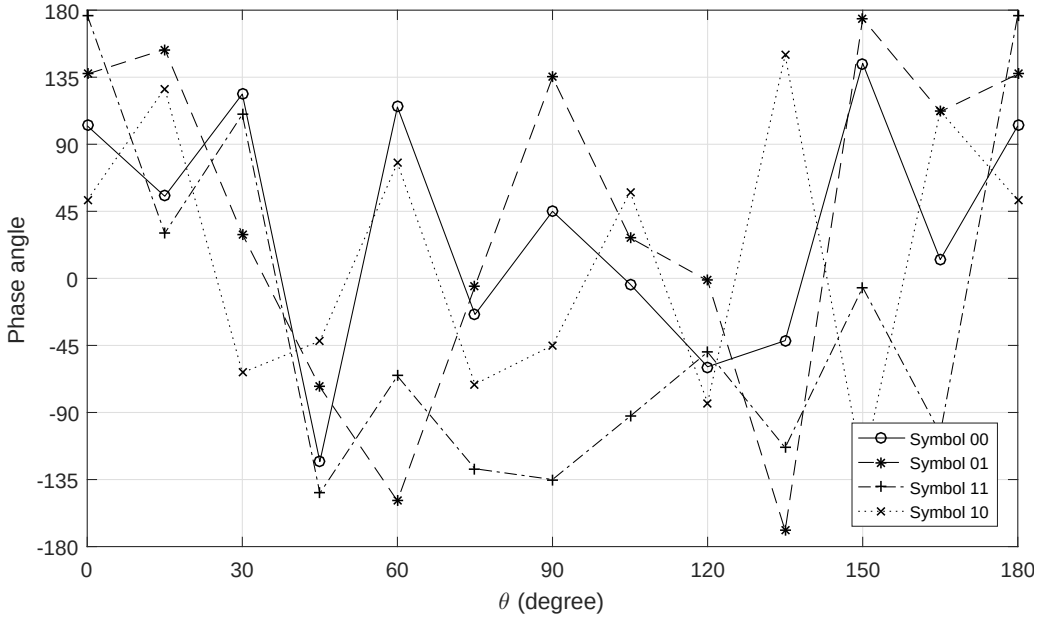

Figure 2.8: Resultant phase pattern based on the ULA for DM using (2.24).

2.5 Summary

In this chapter a review of narrowband beamforming, wideband beamforming and DM has been presented. Many methods and structures to achieve DM are described, and the patterns of constellation points with and without DM technique are drawn to demonstrate their differences. Phased antenna array design for DM based on a given array geometry is formulated, and as shown in the aforementioned figures, all main beams are exactly pointed to desired directions with a reasonable sidelobe level. The phase at the main beam directions follows the given phase pattern and random over the sidelobe ranges. The designs of compressive sensing on DM in narrowband situation, multi-carrier frequencies situation and multi-path model situation are described in the following chapters.

Chapter 3

Compressive Sensing Based Sparse Antenna Array Design for Directional Modulation

3.1 Introduction

This chapter describes the compressive sensing based sparse antenna array design for DM. For most existing research in DM, designs are based on ULAs with a maximum half wavelength spacing to avoid grating lobes. To have a larger aperture and a higher spatial resolution given a fixed number of antennas, sparse arrays are normally employed in traditional array signal processing [5, 6]. The increased DOFs in the spatial domain allow the system to incorporate more constraints into the design of various beamformers.

In this chapter, the CS-based sparse array design is extended to the area of DM and the antenna locations are optimised for a given set of modulation symbols and desired transmission directions by matching designed beam responses to desired ones. The key to the solution is to realise that this optimisation cannot be performed individually for each symbol; otherwise different transmission symbols would end up with different antenna locations. Therefore, a common set of optimised antenna locations needs to be found for all required transmission symbols with the desired directions. As a result, a group sparsity based approach is proposed to tackle the problem. The new CS-based formulation

for sparse array design in the context of DM can then be solved using standard convex optimisation toolboxes in the CS area.

One common issue in practical design of antenna arrays is the robustness of the resultant system against various model perturbations, such as errors in antenna locations, mutual coupling and discrepancies in individual antenna responses. Many methods have been proposed to design robust adaptive arrays, such as diagonal loading, worst case optimisation and robust Capon beamformers [41–44]. In this chapter this idea is used to place an extra constraint on the CS-based design process. As a result, the difference between the designed and achieved modulation responses can be kept below an acceptable level.

Another problem is the size of the antenna. In the design of antenna arrays, the antennas are often considered to be an ideal point without a physical size. As a result, it is possible that the resulting antenna locations will be too close for the antennas to physically fit in, especially for multiband or wideband arrays, where the antenna size may be much larger than $\lambda/2$ [45]. Following the approach in [18], the design of sparse arrays with physical size constraint is also considered in the context of DM.

The remaining part of this chapter is structured as follows. A class of CS-based design methods is presented in Sec. 3.2, including l_1 norm minimisation and reweighted l_1 norm minimisation. Two practical scenarios are considered in Sec. 3.3, including a robust design in the presence of steering vector errors, and a design considering the nonzero size of antennas. In Sec. 3.4, design examples are provided, with conclusions drawn in Sec. 3.5.

3.2 Proposed Design Method

3.2.1 Group Sparsity Based Design

DM design for a given antenna array geometry is reviewed in Sec. 2.3, and the solution to the design is formulated in

$$\begin{aligned} \min_{\mathbf{w}_m} \quad & ||\mathbf{p}_{m,SL} - \mathbf{w}_m^H \mathbf{S}_{SL}||_2 \\ \text{subject to} \quad & \mathbf{w}_m^H \mathbf{S}_{ML} = \mathbf{p}_{m,ML}. \end{aligned} \tag{3.1}$$

Here, for a standard sparse array design method, a given aperture is densely sampled with

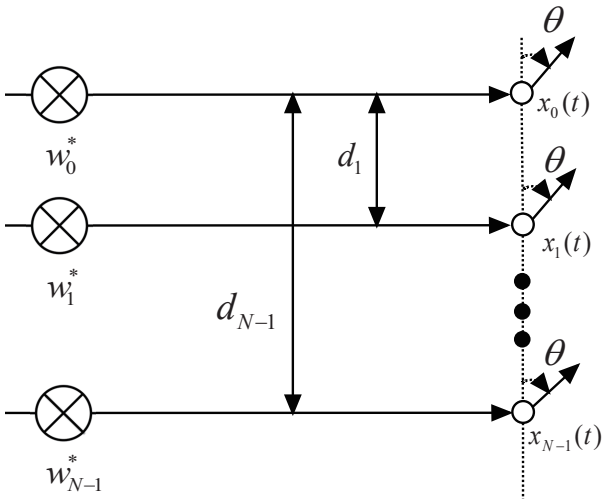

Figure 3.1: A general structure for narrowband beamforming.

a large number of potential antennas. First, consider Fig. 3.1 as a grid of potential active antenna locations, represented by $\circ$. Then d_{N-1} is the aperture of the array and the values of d_n, for $n = 1, 2, \ldots, N-1$, are selected to give a uniform grid, with N being a very large number. Through selecting the minimum number of non-zero valued weight coefficients to generate a response close to the desired one, sparseness is introduced. In other words, if a weight coefficient is zero-valued, the corresponding antenna will be inactive and therefore can be removed, leading to a sparse result. Assume $\mathbf{p}$ is the vector holding the desired responses at the Θ sampled angles, and $\mathbf{S}$ is the $N \times \Theta$ matrix composed of the Θ steering vectors. Then the design can be formulated as follows

$$\min_{\mathbf{w}} \quad ||\mathbf{w}||_1 \quad \text{subject to} \quad ||\mathbf{p} - \mathbf{w}^H \mathbf{S}||_2 \leq \alpha, \tag{3.2}$$

where the l_1 norm $||\cdot||_1$ is used as an approximation to the l_0 norm $||\cdot||_0$, and α is the allowed difference between the desired and designed responses.

Now, without loss of generality, assume $\Theta - 1$ sampling points in the sidelobe regions and one sampling point in the mainlobe direction. In the context of sparse array design for DM, it is necessary to modify (3.2) and find the sparse set of weight coefficients $\mathbf{w}_m$

through the following formulation

$$\min_{\mathbf{w}_m} \quad ||\mathbf{w}_m||_1 \ \text{ subject to } \quad ||\mathbf{p}_{m,SL} - \mathbf{w}_m^H \mathbf{S}_{SL}||_2 \leq \alpha \\ \mathbf{w}_m^H \mathbf{s}_{ML} = p_{m,ML}. \tag{3.3}$$

However, the solution to (3.3) cannot guarantee the same set of active antenna positions for all constellation points. If a weight coefficient is zero in an antenna position for one constellation point, but non-zero for others, the corresponding antenna still cannot be removed. To solve the problem, similar to [40], group sparsity is introduced here, which is to calculate the l_2 norm of weight coefficients for all symbols on this antenna position. If the result is higher than a given threshold, then the antenna location is kept; otherwise, the position is cancelled. Based on this, a common set of active antennas can be found for all modulation symbols generating a response close to the desired one. In other words, fewer antennas are used than the design without group sparsity consideration. To achieve this, the following matrices are constructed

$$\mathbf{W} = [\mathbf{w}_0, \mathbf{w}_1, \ldots, \mathbf{w}_{M-1}], \tag{3.4}$$

$$\mathbf{P}_{SL} = [\mathbf{p}_{0,SL}, \mathbf{p}_{1,SL}, \ldots, \mathbf{p}_{M-1,SL}]^T, \tag{3.5}$$

and the vector

$$\mathbf{p}_{ML} = [p_{0,ML}, p_{1,ML}, \ldots, p_{M-1,ML}]^T. \tag{3.6}$$

Each row of the $N \times M$ weight matrix $\mathbf{W}$ holds the weight coefficients at the same antenna location for different constellation points and it is denoted by $\tilde{\mathbf{w}}_n = [w_{n,0}, \ldots, w_{n,M-1}]$ for $n = 0, \ldots, N-1$. Now define $\hat{\mathbf{w}}$ as a vector of l_2 norm of $\tilde{\mathbf{w}}_n$, given by

$$\hat{\mathbf{w}} = [||\tilde{\mathbf{w}}_0||_2, ||\tilde{\mathbf{w}}_1||_2, \ldots, ||\tilde{\mathbf{w}}_{N-1}||_2]^T. \tag{3.7}$$

Then the group sparsity based sparse array design for DM can be formulated as

$$\min_{\mathbf{W}} \ ||\hat{\mathbf{w}}||_1 \quad \text{subject to } \quad ||\mathbf{P}_{SL} - \mathbf{W}^H \mathbf{S}_{SL}||_2 \leq \alpha \\ \mathbf{W}^H \mathbf{s}_{ML} = \mathbf{p}_{ML}. \tag{3.8}$$

The problem in (3.8) can be solved using cvx, a package for specifying and solving convex programs [46, 47].

3.2.2 Reweighted l_1 Norm Minimisation

Different from l_0 norm which uniformly penalises all non-zero valued coefficients, the l_1 norm penalises larger weight coefficients more heavily than smaller ones. To make the l_1 norm a closer approximation to the l_0 norm, a reweighted l_1 norm minimisation method can be adopted here [48–50], where a larger weighting term is introduced to those coefficients with smaller non-zero values and a smaller weighting term to those coefficients with larger non-zero values. This weighting term will change according to the resultant coefficients at each iteration. Applying this idea to the group sparsity problem in (3.8), for the i-th iteration, it is formulated as follows

$$\begin{aligned} \min_{\mathbf{W}} \quad & \sum_{n=0}^{N-1} \delta_n^i ||\tilde{\mathbf{w}}_n^i||_2 \\ \text{subject to} \quad & ||\mathbf{P}_{SL} - (\mathbf{W}^i)^H \mathbf{S}_{SL}||_2 \leq \alpha \\ & (\mathbf{W}^i)^H \mathbf{s}_{ML} = \mathbf{p}_{ML}, \end{aligned} \tag{3.9}$$

where the superscript i indicates the value of the corresponding parameters at the i-th iteration, and δ_n is the reweighting term for the n-th row of coefficients, given by $\delta_n^i = (||\tilde{\mathbf{w}}_n^{i-1}||_2 + \kappa)^{-1}$. The iteration processes are described as follows:

1. For the $i = 0$ iteration, calculate the initial value $||\tilde{\mathbf{w}}_n||_2$ by solving (3.8).

2. Set $i = i + 1$. Use the value of the last $||\tilde{\mathbf{w}}_n^{i-1}||_2$ to calculate δ_n^i, and then find $\mathbf{W}^i$ and $||\tilde{\mathbf{w}}_n^i||_2$ by solving the problem in (3.9).

3. Repeat step 2 until the positions of non-zero values of the weight coefficients do not change any more for some number of iterations (three in our design examples).

Here $\kappa > 0$ is required to provide numerical stability to prevent δ_n^i becoming infinity at the current iteration if the value of a weight coefficient is zero at the previous iteration, and it is chosen to be slightly less than the minimum weight coefficient that will be implemented in the final design (i.e. the value below which the associated antenna will be considered inactive and therefore removed from the obtained design result), where $\delta_n^i ||\tilde{\mathbf{w}}_n^i||_2 = \frac{||\tilde{\mathbf{w}}_n^i||_2}{||\tilde{\mathbf{w}}_n^i||_2 + \kappa}$.

3.2.3 Discussion with Multiple-Point Constraints in the Mainlobe

The proposed design can work irrespective of the number of points chosen at the mainlobe area. However, one potential problem is, if multiple points are chosen at the mainlobe and are still required to make sure the transmission is in the desired modulation pattern over those chosen direction points, the performance of the whole system on other aspects has to be sacrificed, such as sidelobe level and main beamwidth. The reason is, each additional modulation constraint on the mainlobe area will take up one DOF away from the system and therefore leave less number of DOFs to meet other requirements of the design.

For r sampling points in the mainlobe and $\Theta - r$ points in the sidelobe, the reweighted l_1 norm minimisation formulation for sparse array design in the context of DM becomes

$$\begin{aligned} \min_{\mathbf{W}} \quad & \sum_{n=0}^{N-1} \delta_n^i ||\tilde{\mathbf{w}}_n^i||_2 \\ \text{subject to} \quad & ||\mathbf{P}_{SL} - (\mathbf{W}^i)^H \mathbf{S}_{SL}||_2 \leq \alpha \\ & (\mathbf{W}^i)^H \mathbf{S}_{ML} = \mathbf{P}_{ML}, \end{aligned} \tag{3.10}$$

where $\mathbf{W}$ is unchanged (i.e. $\mathbf{W} = [\mathbf{w}_0, \mathbf{w}_1, \ldots, \mathbf{w}_{M-1}]$), $\mathbf{S}_{SL}$ is the $N \times (\Theta - r)$ matrix including $\Theta - r$ steering vectors in the sidelobe directions and $\mathbf{S}_{ML}$ is the $N \times r$ matrix composed of the r steering vectors at the mainlobe directions. The $M \times (\Theta - r)$ matrix $\mathbf{P}_{SL}$ holds the M desired modulation responses in the sidelobe directions, while the $M \times r$ matrix $\mathbf{P}_{ML}$ holds the M desired modulation responses at the r mainlobe directions, given by

$$\mathbf{P}_{SL} = [\mathbf{p}_{0,SL}, \mathbf{p}_{1,SL}, \ldots, \mathbf{p}_{M-1,SL}]^T, \tag{3.11}$$

$$\mathbf{p}_{m,SL} = [p_{m,0}, p_{m,1}, \ldots, p_{m,\Theta-r-1}], \tag{3.12}$$

$$\mathbf{P}_{ML} = [\mathbf{p}_{0,ML}, \mathbf{p}_{1,ML}, \ldots, \mathbf{p}_{M-1,ML}]^T, \tag{3.13}$$

$$\mathbf{p}_{m,ML} = [p_{m,\Theta-r}, p_{m,\Theta-r+1}, \ldots, p_{m,\Theta-1}]. \tag{3.14}$$

Note that for a fixed m (one of the M constellation points), $p_{m,\Theta-r}$, $p_{m,\Theta-r+1}$, …, $p_{m,\Theta-1}$ should have the same value to make sure the same information is transmitted for all the r chosen direction points in the mainlobe.

3.3 Two Practical Scenarios

3.3.1 Steering Vector Error

The above design methods are based on an ideal situation where the designed steering vectors are the same as the actual ones. To have the resultant sparse array robust against various steering vector errors, an error vector $\mathbf{e}$ is first introduced, and the actual steering vector is described by $\hat{\mathbf{s}} = \mathbf{s} + \mathbf{e}$, where $\mathbf{s}$ indicates the assumed steering vector. The difference between actual and designed array responses satisfies

$$|\mathbf{w}^H\hat{\mathbf{s}} - \mathbf{w}^H\mathbf{s}| = |\mathbf{w}^H\mathbf{e}| \leq \varepsilon||\mathbf{w}||_2, \tag{3.15}$$

where ε is the upper norm-bound of $\mathbf{e}$. Then a constraint to the previous formulations is added to make sure the difference between the actual and designed array responses does not exceed a predetermined threshold value β, and the new optimisation problem is formulated as

$$\begin{aligned} \min_{\mathbf{W}} \quad & \sum_{n=0}^{N-1} \delta_n^i ||\tilde{\mathbf{w}}_n^i||_2 \\ \text{subject to} \quad & ||\mathbf{P}_{SL} - (\mathbf{W}^i)^H\mathbf{S}_{SL}||_2 \leq \alpha \\ & (\mathbf{W}^i)^H\mathbf{S}_{ML} = \mathbf{P}_{ML} \\ & \varepsilon||\mathbf{w}_m^i||_2 \leq \beta \qquad \forall m = 0, 1, \ldots, M-1. \end{aligned} \tag{3.16}$$

3.3.2 Size Constraint

In practice, the antennas may not fit into the optimised locations obtained by the above design methods since so far the antennas with no physical size are assumed, which is obviously not true. The most straightforward method is to merge closely located optimised antenna positions into a new one to meet the minimum spacing requirement, although clearly this may lead to a solution far away from the optimum one. To deal with this problem, two methods for enforcing a minimum spacing d_{min} between adjacent antennas in the design result are proposed.

Iterative Sampling Method

This method iteratively samples a remaining range to obtain its following optimised antenna location until the remaining range is less than d_{min}, where in each iteration the starting point of the sampling aperture is at least d_{min} away from the previous optimised locations. The details are as follows.

Step 1 At the zeroth iteration ($u = 0$), the zeroth antenna is fixed at the starting point of the original aperture, i.e. $\hat{d}_{op(0)}$. A range from $\hat{d}_{op(0)} + d_{min}$ to the end of the original aperture is set as the sampling aperture, and by solving (3.9) all initial optimised locations $d_{op(0)}, d_{op(1)}, \ldots$ (i.e. $\hat{d}_{op(0)} = d_{op(0)}$) are calculated. To make sure the zeroth active location $\hat{d}_{op(0)}$ is included in the final result, the reweighting term for this location is set to be a very small value. Now the first active location $\hat{d}_{op(1)}$ is the average of the first cluster of optimised locations whose range is from $d_{op(1)}$ to $d_{op(1)} + d_{min}$.

Step 2 With the previously fixed active locations meeting the minimum spacing requirements, at the u-th iteration, $u = 1, 2, ...$, a range from $\hat{d}_{op(u)} + d_{min}$ to the end of the original aperture is set as the sampling aperture, and by solving (3.9) and taking an average of the new cluster which is within the range from $d_{op(u+1)}$ to $d_{op(u+1)} + d_{min}$, $\hat{d}_{op(u+1)}$ is found. The process is repeated until the remaining range is less than d_{min}.

Modified Reweighted l_1 Norm Minimisation Method

It is based on (3.9) and the idea is to modify the reweighting term δ_n^i to make sure when the resultant active antenna locations are too close to each other, the value of the reweighting term will be increased significantly so that it will be penalised more heavily in the optimisation process. To achieve this, δ_n^i in (3.9) is modified as

$$\delta_n^i = \begin{cases} (||\tilde{\mathbf{w}}_n^{i-1}||_2 + \kappa)^{-1}, & n = 0 \\ (||\tilde{\mathbf{w}}_n^{i-1}||_2 + \kappa)^{-1}, & n > 0 \ \& \text{ constraint met} \\ \kappa^{-1}, & \text{otherwise} \end{cases} \tag{3.17}$$

The process is repeated until all spacings between adjacent active antennas are larger than d_{min}.

3.4 Design Examples

In this section, several design examples are provided to show the performance of the proposed sparse designs in comparison with a standard ULA. The mainlobe direction is $\theta_{ML} = 90^\circ$ and the sidelobe region is $\theta_{SL} \in [0^\circ, 85^\circ] \cup [95^\circ, 180^\circ]$, sampled every 1°. The desired response is a value of one (magnitude) with 90° phase shift at the mainlobe (QPSK) and a value of 0.1 (magnitude) with random phase shifts over the sidelobe regions.

To have a fair comparison, the DM result using the method in (3.1) is first obtained based on a 24-element ULA with half-wavelength spacing between adjacent antennas. Based on the design result, the error norm between the designed and the desired responses of this ULA is then calculated and this value is used as α in the sparse array design formulations in (3.8) and (3.9).

To assess the performance of each design, the bit error rate (BER) is also calculated by setting the signal to noise ratio (SNR) at 12 dB in the main lobe direction. As the additive white Gaussian noise (AWGN) level is assumed to be the same for all directions, the SNR value will be much smaller at the sidelobe directions.

3.4.1 ULA Design Example

For the 24-element ULA with half-wavelength spacing between adjacent antennas, the resultant beam pattern for each constellation point is shown in Fig. 3.2, where all main beams are exactly pointed to 90° with a reasonable sidelobe level. Moreover, the phase at the main beam direction is 90° spaced and random in the sidelobe directions, as shown in Fig. 3.3.

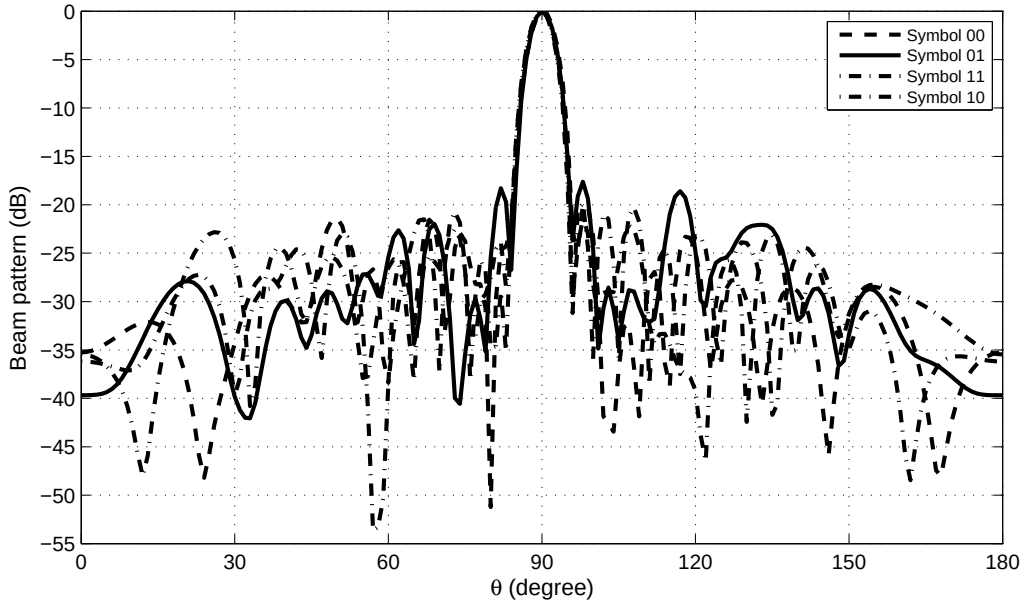

Figure 3.2: Simulated beam pattern based on the ULA for DM using (3.1).

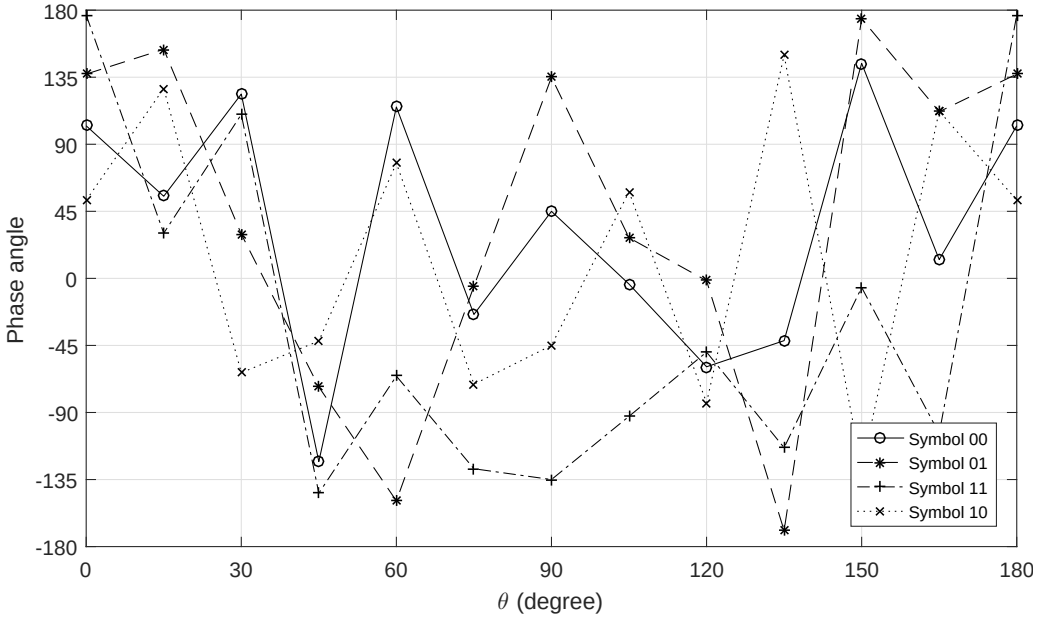

Figure 3.3: Simulated phase pattern based on the ULA for DM using (3.1).

3.4.2 Usual l_1 Norm Based Design Example

With the above ULA design, the difference $\alpha = 2.5521$ is obtained. Since the resultant sparse array may have a larger aperture than the ULA, the maximum aperture is set to be 16.5λ, consisting of 500 equally spaced potential antennas.

By the standard group-sparsity based formulation in (3.8), 26 active antennas are obtained, with an average spacing of 0.655λ. The resultant beam pattern for each constellation point is shown in Fig. 3.4, where all main beams are exactly pointed to 90° with a reasonable sidelobe level. The phase at the main beam direction is 90° spaced and random in the sidelobe directions, as shown in Fig. 3.5. As shown in Table 3.1, although its resultant value for $||\mathbf{P}_{SL} - \mathbf{W}^H\mathbf{S}_{SL}||_2$ is a little better than the ULA, the number of antennas is larger than the ULA, which is not desirable.

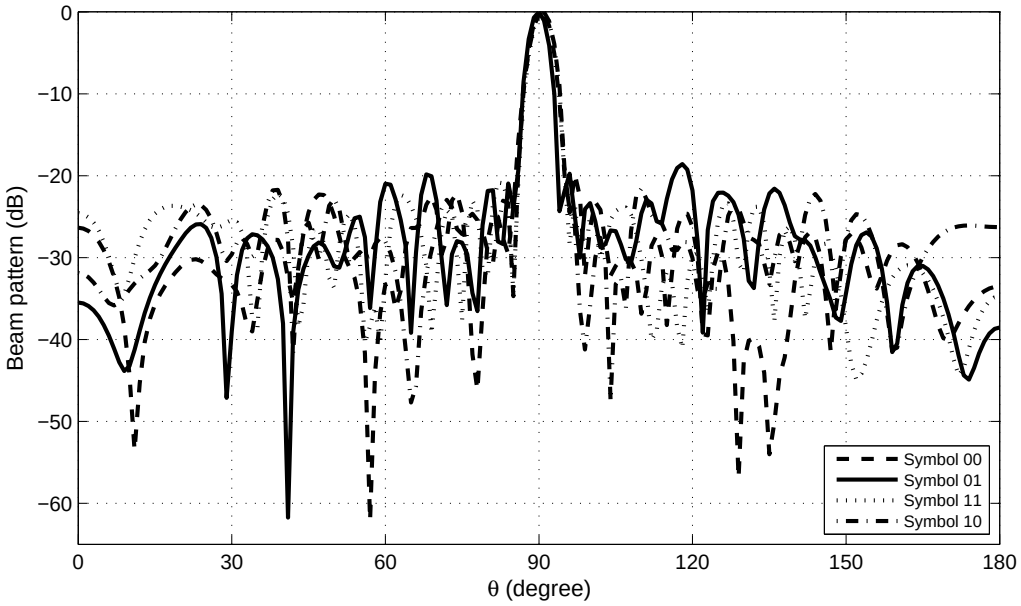

Figure 3.4: Simulated beam pattern based on the sparse antenna array for DM using l_1 norm minimisation method (3.8).

3.4.3 Reweighted l_1 Norm Based Sparse Design Example

In this design, there is an additional parameter κ, which should be small enough, and in the simulations $\kappa = 0.001$ is chosen, which means that antennas associated with a weight

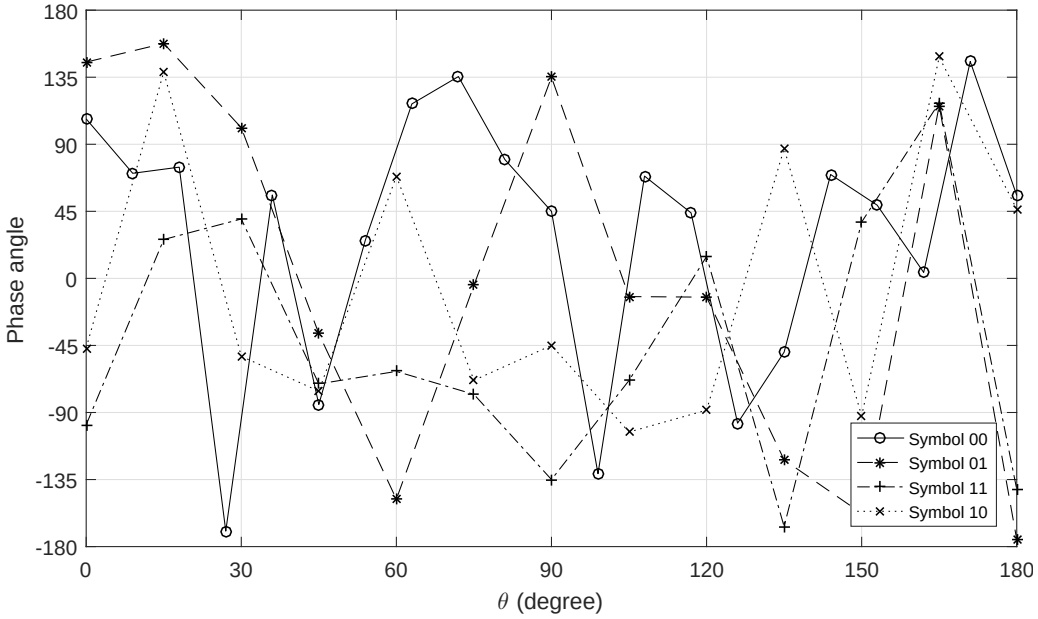

Figure 3.5: Simulated phase pattern based on the sparse antenna array for DM using l_1 norm minimisation method (3.8).

Table 3.1: Summary of performances of sparse arrays and ULAs for DM.

	ULA	Usual l_1	Reweighted	Robust
Antenna number	24	26	19	20
Aperture/λ	11.5	16.37	11.87	11.87
Average spacing/λ	0.5	0.655	0.660	0.625
$\|\|\mathbf{P}_{SL} - \mathbf{W}^H\mathbf{S}_{SL}\|\|_2$	2.5521	2.3742	2.5478	2.6754

coefficient value smaller than 0.001 will be considered inactive. With the other parameters same as in previous examples, it results in 19 active antennas with an average spacing of 0.660λ. So as expected, a sparser solution has been obtained compared to the design in (3.8). The array response for each constellation point is shown in Fig. 3.6 and the phase pattern in Fig. 3.7, all indicating a satisfactory design result. The array response is closer to the desired ones than the ULA according to the value of $||\mathbf{P}_{SL} - \mathbf{W}^H\mathbf{S}_{SL}||_2$, as shown in Table 3.1.

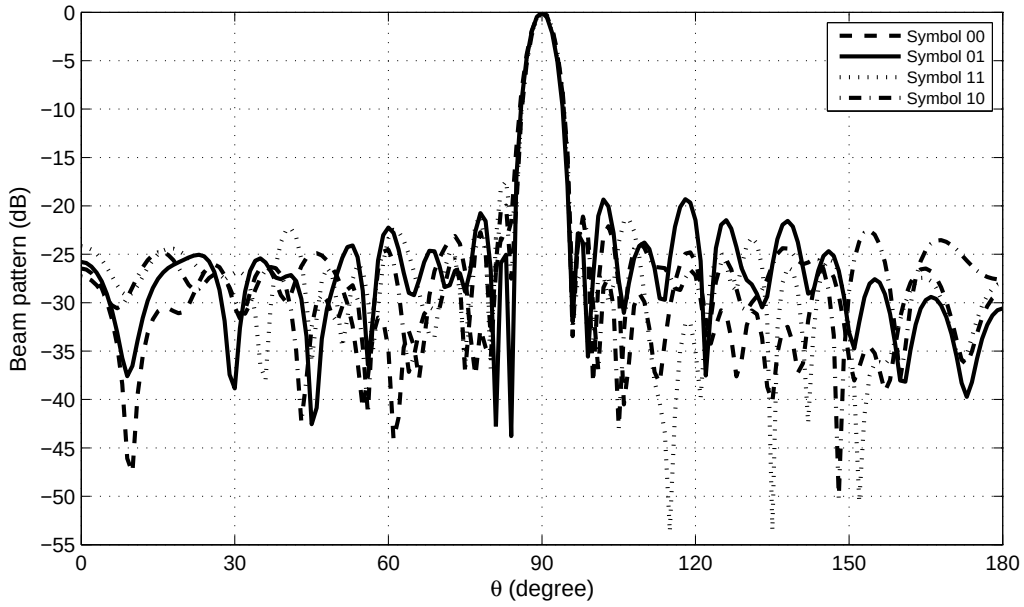

Figure 3.6: Simulated beam pattern based on the sparse antenna array for DM using reweighted l_1 norm minimisation method (3.9).

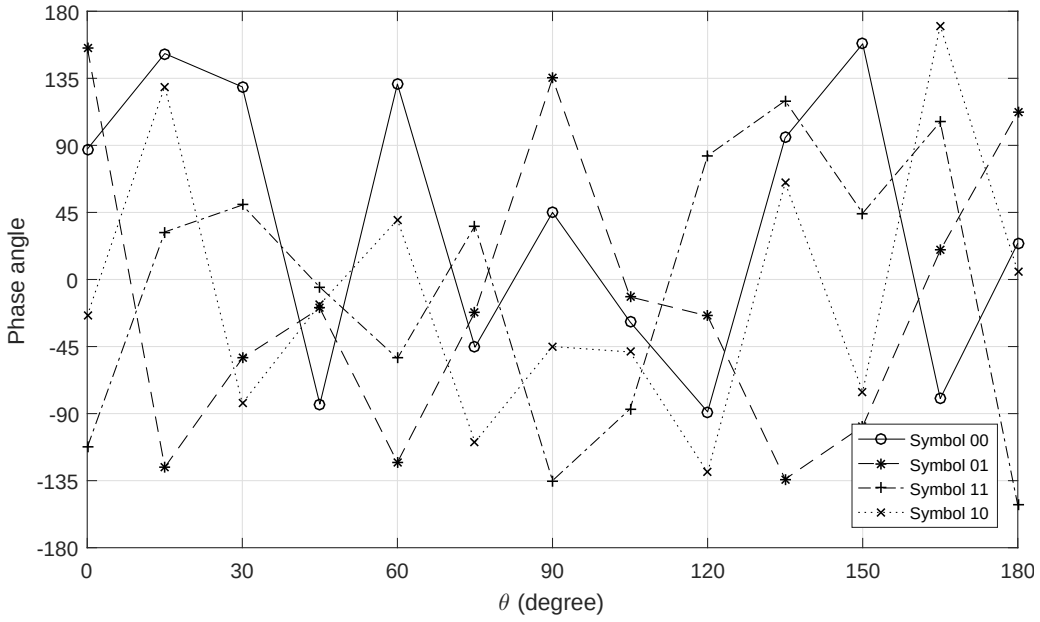

Figure 3.7: Simulated phase pattern based on the sparse antenna array for DM using reweighted l_1 norm minimisation method (3.9).

3.4.4 Robust Design Example

For the robust design, $\varepsilon = 1$ is set as the upper bound on the norm of the steering vector error and given the design result (20 antennas for the robust design) as shown in Table 3.1, this accounts for 22% of the real steering vector norm (the steering vector norm is 1 for each antenna, then for 20 antennas the steering vector norm is $\sqrt{1 \times 20}$). $\beta = 0.23$ is chosen to allow maximum 23% change in the magnitude response (1 in magnitude) at the main direction given the maximum allowable steering vector error. The result is a 20-antenna array with an average spacing of 0.625λ. The mean beam pattern obtained by averaging $L = 1000$ different responses resultant from randomly generated steering error vector $\mathbf{e}$ satisfying the norm-constraint are shown in Fig. 3.8, and the phase pattern is similar to the results in the earlier two designs. To show the robustness of the design, the normalised variance of the beam pattern is also calculated as follows,

$$var(\theta_r) = \frac{1}{L} \sum_{l=0}^{L-1} \frac{|p_l(\theta_r) - \bar{p}(\theta_r)|^2}{|\bar{p}(\theta_r)|^2}, \tag{3.18}$$

where $\bar{p}(\theta_r) = \frac{1}{L} \sum_{l=0}^{L-1} p_l(\theta_r)$ is the average achieved array response at θ_r for $r = 0, 1, \ldots, \Theta - 1$, and the results are shown in Fig. 3.9, with a value of almost zero in the designed main direction, less than 1 in other directions, indicating a robust geometrical layout of the antennas. The $||\mathbf{P}_{SL} - \mathbf{W}^H \mathbf{S}_{SL}||_2$ value is also shown in Table 3.1 as a comparison and a comparable result has been obtained.

3.4.5 BER Comparisions Between ULA and Sparse Arrays

As shown in Fig. 3.10, the BERs of the ULA and sparse arrays obtained by the usual l_1 norm algorithm and the reweighted l_1 norm minimisation are all down to 10^{-5} in the mainlobe direction, while in other directions BERs are around 0.5, further demonstrating the effectiveness of the designs. A very similar BER result is obtained for the robust design and the normalised variance of BER for the robust design is shown in Fig. 3.11, with a value of around 0.005 over sidelobe regions and 0.03 in mainlobe direction, indicating that BERs in the set are very close to the mean value and also very close to each other.

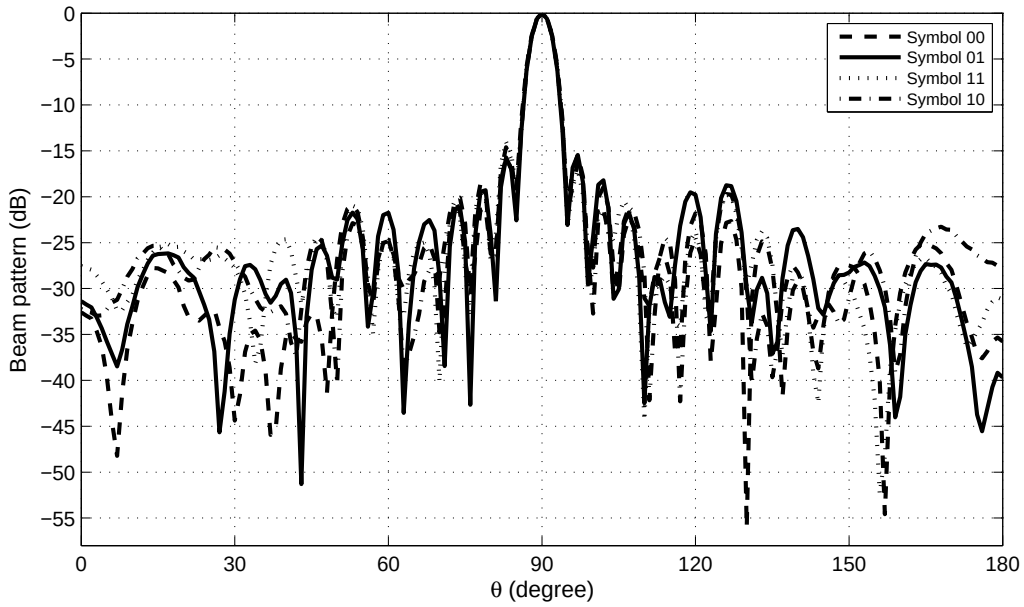

Figure 3.8: Simulated beam responses for robust design based on the sparse antenna array for DM using (3.16).

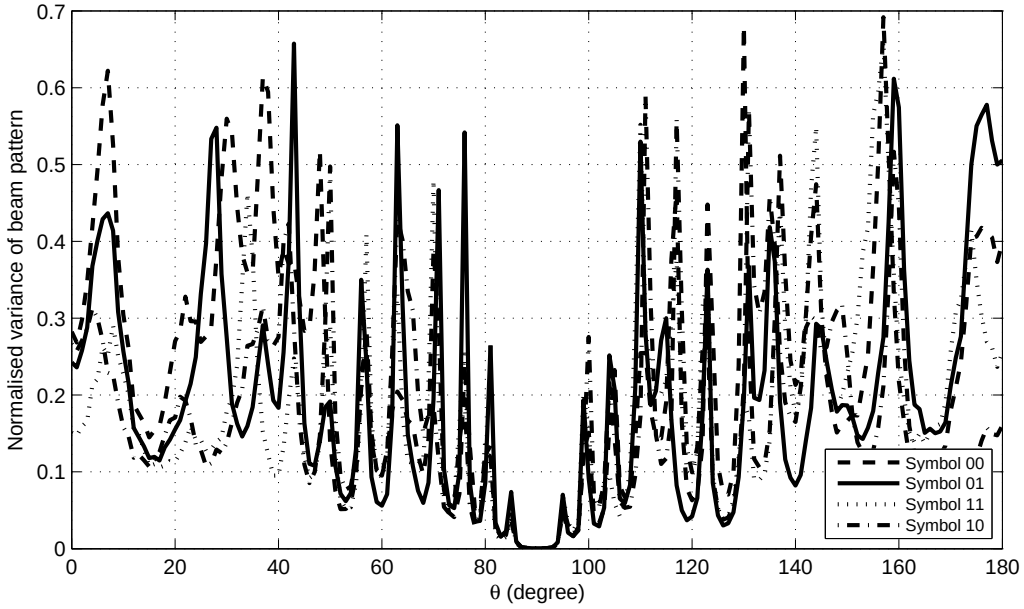

Figure 3.9: Normalised variance of beam pattern for robust design based on the sparse antenna array for DM using (3.16).

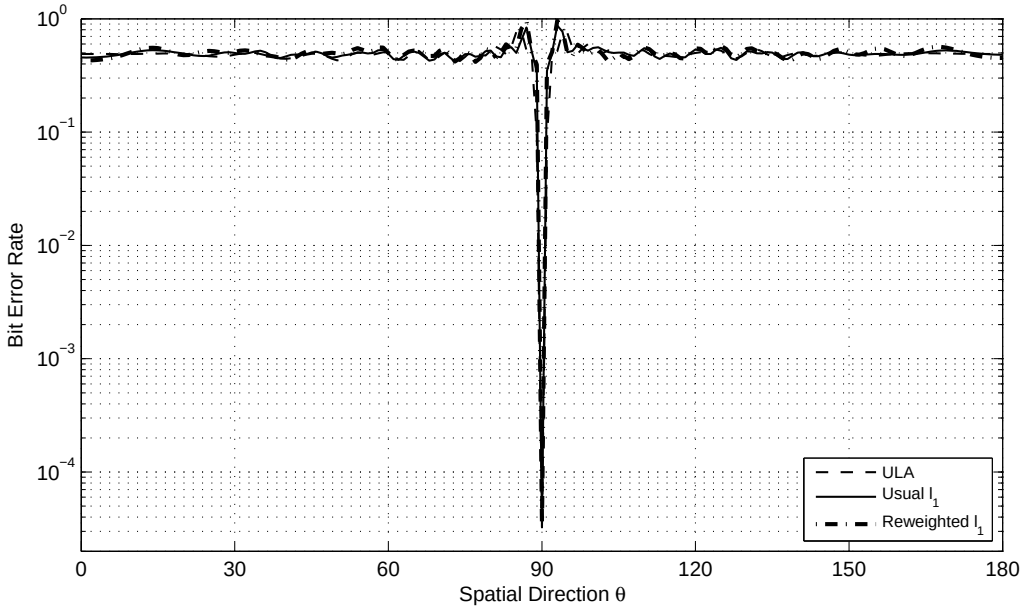

Figure 3.10: BER spatial distributions for DM based on different design results

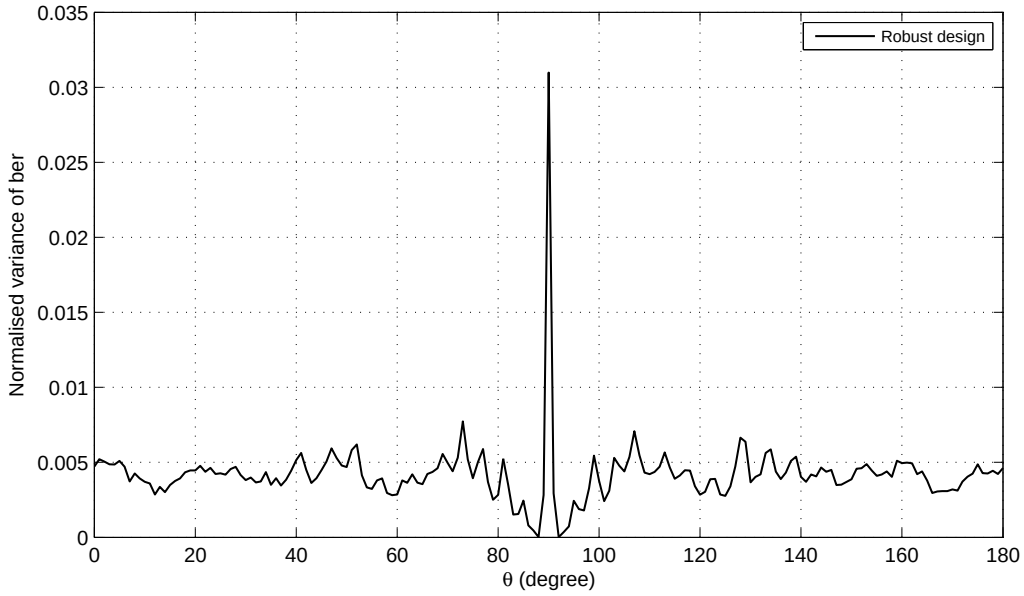

Figure 3.11: Normalised variance of BER for DM based on different design results.

Table 3.2: Optimised antenna locations based on the reweighted l_1 norm minimisation method (3.9).

n	d_n/λ	n	d_n/λ	n	d_n/λ
0	2.71	7	6.75	14	11.84
1	3.60	8	7.27	15	12.66
2	4.30	9	7.84	16	13.06
3	4.66	10	8.43	17	13.69
4	5.26	11	9.23	18	14.58
5	5.89	12	10.09		
6	6.38	13	10.94		

3.4.6 Reweighted l_1 Norm Based Sparse Array Design with Size Constraints

The minimum spacing d_{min} between adjacent antennas is set to be 0.55λ. For the design in (3.9), as shown in Table 3.2, the spacing between the 2nd and 3rd antennas, the spacing between the 5th and 6th, the spacing between the 6th and 7th, the spacing between the 7th and 8th, and the spacing between 15th and 16th are less than d_{min}, indicating an impractical design for an antenna with a physical size of 0.55λ.

Iterative Sampling Method

By this method, all main beams in Fig. 3.12 are pointed to the mainlobe direction, and their phases are 90° spaced, as shown in Fig. 3.13. The locations listed in Table 3.3 show that the size constraint d_{min} has been met.

Table 3.3: Optimised antenna locations given the minimum spacing using the iterative sampling method.

n	d_n/λ	n	d_n/λ	n	d_n/λ
0	0	6	6.61	12	11.95
1	2.70	7	7.60	13	12.88
2	3.49	8	8.41	14	13.71
3	4.29	9	9.30	15	14.75
4	5.04	10	10.19	16	15.41
5	5.83	11	11.07		

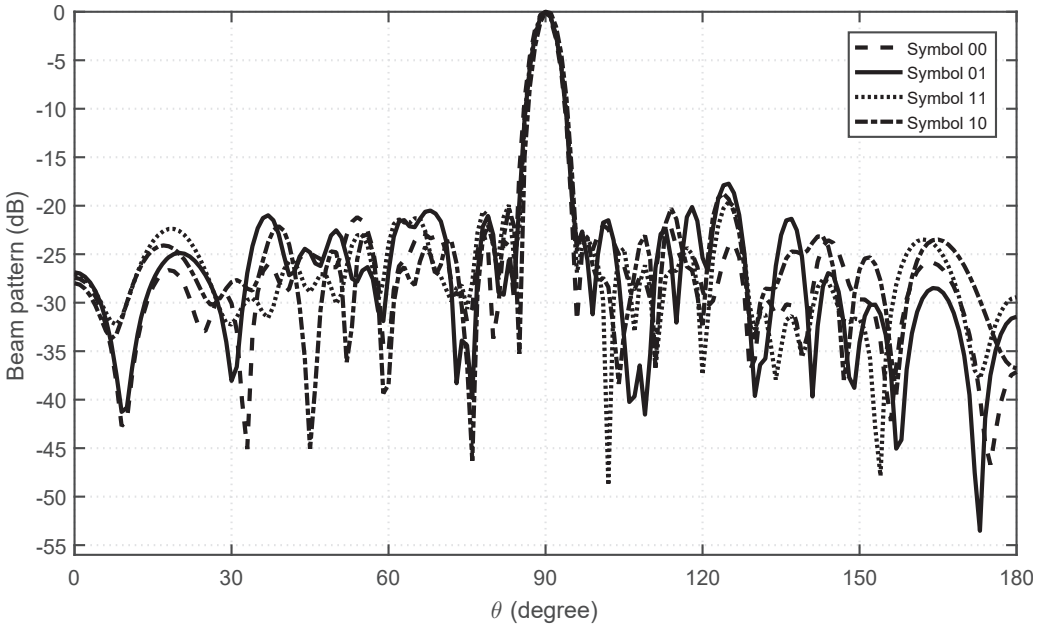

Figure 3.12: Simulated beam responses given the minimum spacing using the iterative sampling method.

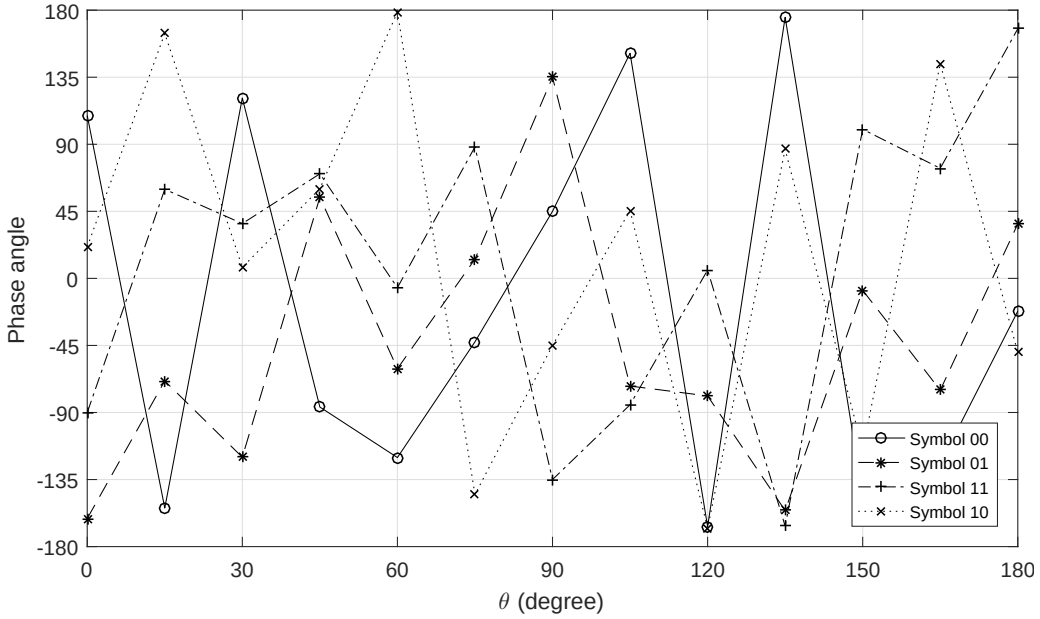

Figure 3.13: Simulated phase patterns given the minimum spacing using the iterative sampling method.

Modified Reweighted l_1 Norm Minimisation Method

The array responses in Fig. 3.14, the phase patterns in Fig. 3.15, and the positions in Table 3.4 all indicate a satisfactory design result by this method. Moreover, according to the value of $||\mathbf{P}_{SL} - \mathbf{W}^H\mathbf{S}_{SL}||_2$, the array response is closer to the desired one than the response resulted from the iterative sampling method, as shown in Table 3.5. Note that, with the optimised non-symmetrical antenna locations and weights, the implementation of such a sparse antenna array system would be more complicated. However, it is still feasible as for the proposed design an individual tailor-made feed circuit is needed (including phase shift and amplitude change) for each antenna.

3.5 Summary

The sparse antenna array design problem in the context of DM has been studied for the first time. The main contribution is to formulate the problem from the viewpoint of CS so that it can be solved using standard convex optimisation toolboxes in the CS area. In detail, a common set of active antennas for all modulation symbols needs to be found,

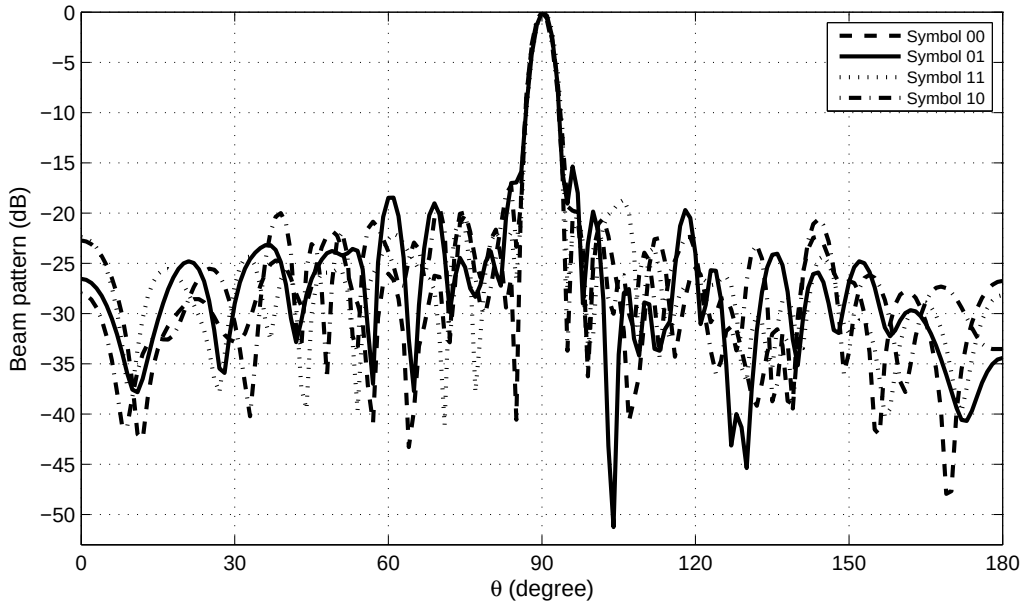

Figure 3.14: Simulated beam responses given the minimum spacing using the modified reweighted l_1 norm minimisation method.

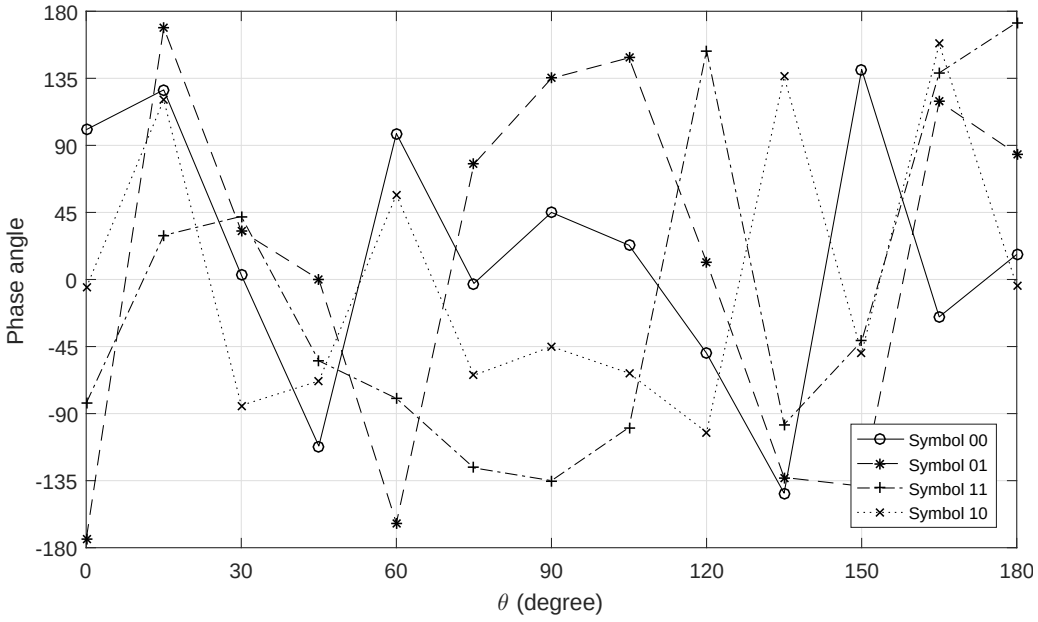

Figure 3.15: Simulated phase patterns given the minimum spacing using the modified reweighted l_1 norm minimisation method.

Table 3.4: Optimised antenna locations given the minimum spacing using the modified reweighted l_1 norm minimisation method.

n	d_n/λ	n	d_n/λ	n	d_n/λ
0	0	7	5.13	14	10.94
1	0.73	8	5.89	15	11.84
2	1.49	9	6.55	16	12.66
3	2.08	10	7.37	17	13.69
4	2.68	11	8.20	18	14.58
5	3.47	12	9.06	19	15.38
6	4.30	13	10.09	20	15.97

Table 3.5: Summary of performances of different designs with and without size constraint.

	No size constraint	With size constraint	
	Reweighted	Iterative	Modified Reweighted
The number of antennas	19	17	21
Aperture/λ	11.87	15.41	15.97
Average spacing/λ	0.660	0.963	0.799
$\|\|\mathbf{P}_{SL} - \mathbf{W}^H\mathbf{S}_{SL}\|\|_2$	2.5478	2.6157	2.5336
Size constraint satisfied	No	Yes	Yes

generating a response close to the desired one. The key to the solution is to realise the the group sparsity concept has to be employed, as a common antenna set cannot be guaranteed if antenna locations for each modulation symbol are optimised individually. Then, a class of CS based methods has been proposed, including the usual l_1 norm minimisation and the reweighted l_1 norm minimisation. Two practical scenarios are analysed where steering vector error happens and optimised locations are too close to each other. As shown in the provided design examples, in the context of DM, all sparse designs satisfy the mainlobe pointing to the desired direction with scrambled phases in other directions. In particular, the reweighted l_1 norm minimisation method can provide a sparer solution as expected, achieving a similar performance as the ULA but with less number of antennas.

Chapter 4

Multi-Carrier Based Phased Antenna Array Design for Directional Modulation

4.1 Introduction

Most of previous DM work is based on the assumption that the information is transmitted at one single frequency, which is not an efficient way to use the available spectrum. In this chapter, borrowing the idea of multi-carrier based transmission for traditional wireless communication systems [51–54], a novel multi-carrier based DM structure for antenna arrays is developed, which can be implemented efficiently by the Inverse Discrete Fourier Transform (IDFT). There are mainly three advantages for the proposed multi-carrier based DM: the first is that multiple low rate data streams can be transmitted in parallel to achieve a much higher overall data rate, extending the use of DM effectively and efficiently to a wider bandwidth; the second advantage is that different carriers can be assigned to different users allowing possible frequency division multi-user access, where the users can be located at the same directions or different directions and in the latter case, the beam pointing to different directions can be designed at different frequencies; the third advantage is that it provides the flexibility of using different modulation schemes at different carrier frequencies.

First, the traditional single-carrier design for DM is extended to the multi-carrier case for a given array geometry. Then the antenna location optimisation problem for multi-carrier based DM is studied using a CS based approach by extending the formulation developed for narrowband sparse arrays in [28]. For the single-carrier case, only a common set of antenna locations for all constellation points needs to be found. For the multi-carrier structure, since more than one carrier frequency are used, a common solution only for all constellation points at one frequency is not enough, and a common set of optimised antenna locations for all modulation symbols at all carrier frequencies are needed instead.

However, like traditional IDFT based multi-carrier wireless communication systems, a potential problem of the multi-carrier design in [30] is the high peak to average power ratio (PAPR) when multiple signals are added together, resulting in serious degradation in performance when signal peaks pass through the non-linear (clipping) region of a power amplifier [51–53, 55–58]. To avoid this, a PAPR constraint to control the signal envelope needs to be considered in the design.

Many methods have been proposed in traditional multi-carrier based communication to limit the PAPR of the transmitted signals. A clipping and filtering method was introduced in [59, 60], which iteratively limits the maximum amplitude until its corresponding output is under or equal to a pre-defined PAPR. Selective mapping (SLM) in [61, 62] was used to generate a set of phase sequences, and then each phase sequence is multiplied by the same data sequence to produce their corresponding transmitted sequences, and the one with the lowest PAPR is then chosen for transmission. In [63, 64], the partial transmit sequences (PTS) technique was studied, followed by the tone reservation method in [65]. The wideband beampattern formation via iterative techniques (WBFIT) method was introduced in [66] for wideband MIMO radar to directly link the beampattern to the signals through their Fourier transform. In the work, the idea of WBFIT is borrowed to solve the PAPR problem in the design of multi-carrier based DM antenna array system, and a modified WBFIT method is proposed to deal with both the PAPR constraint and the DM requirement.

The remaining part of this chapter is structured as follows. The proposed multi-carrier based structure and its design with a given array geometry is given in Sec. 4.2.

The CS-based antenna location optimisation method for multi-carrier based DM arrays is presented in Sec. 4.3, with design examples in Sec. 4.4. The modified WBFIT method to solve the PAPR $\leq \rho$ ($\rho \geq 1$) minimisation problem for DM is described in Sec. 4.5, along with the design examples provided in Sec. 4.6. Conclusions are drawn in Sec. 4.7.

4.2 The Proposed Structure for Multi-Carrier Based Directional Modulation

The proposed multi-carrier based transmit beamforming array structure for DM is shown in Fig. 4.1, where each antenna, represented by $\circ$, is associated with multiple frequency-dependent weight coefficients $w_{n,q}$, for $n = 0, \ldots, N-1$ and $q = 0, \ldots, Q-1$. The beamformer output $x_n(t)$ can be represented as follows

$$\begin{aligned} x_n(t) &= \sum_{q=0}^{Q-1} w_{n,q}^* e^{j2\pi(f_0+(-\frac{Q}{2}+q)\triangle f)t} \\ &= \sum_{q=0}^{Q-1} w_{n,q}^* e^{j2\pi(-\frac{Q}{2}+q)\triangle f t} \times e^{j2\pi f_0 t}, \end{aligned} \tag{4.1}$$

where f_0 represents the carrier frequency and $\triangle f$ denotes the subcarrier spacing.

To derive a discrete baseband representation of the structure, the carrier frequency f_0 is omitted, and $t = kt_s$ is substituted into (4.1) for $k = 0, 1, \ldots, Q-1$ and $t_s = \frac{1}{\triangle f \times Q}$ ($\triangle f \times Q$ represents the bandwidth of the baseband signal from $[-\frac{Q}{2} \times \triangle f, \frac{Q}{2} \times \triangle f]$). Therefore, the discrete baseband signal is given by

$$\begin{aligned} x_n(k) &= \sum_{q=0}^{Q-1} w_{n,q}^* e^{j2\pi(-\frac{Q}{2}+q)\triangle f k t_s} \\ &= \sum_{q=0}^{Q-1} w_{n,q}^* e^{j2\pi(-\frac{Q}{2}+q)\triangle f k \frac{1}{\triangle f Q}} \\ &= Q \times \frac{1}{Q} \sum_{q=0}^{Q-1} w_{n,q}^* e^{j2\pi(-\frac{Q}{2}+q)\frac{k}{Q}} \quad k = 0, 1, \ldots, Q-1, \end{aligned} \tag{4.2}$$

where $\frac{1}{Q}\sum_{q=0}^{Q-1} w_{n,q}^* e^{j2\pi(-\frac{Q}{2}+q)\frac{k}{Q}}$ is the IDFT expression of $w_{n,q}^*$. Therefore, mathematically modulating on each subcarrier and then adding them together is equivalent to taking an

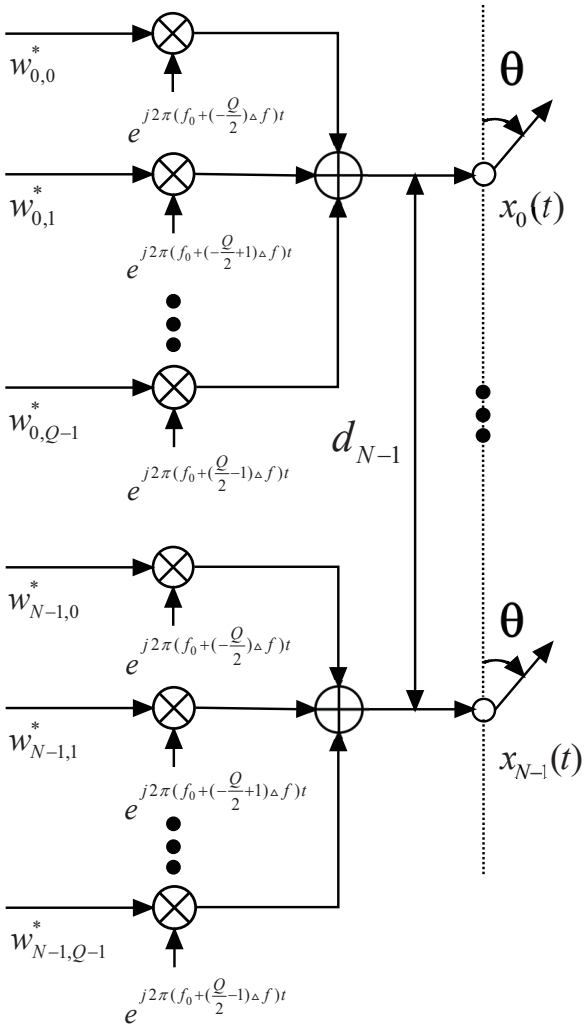

Figure 4.1: The proposed multi-carrier transmit beamforming structure for DM.

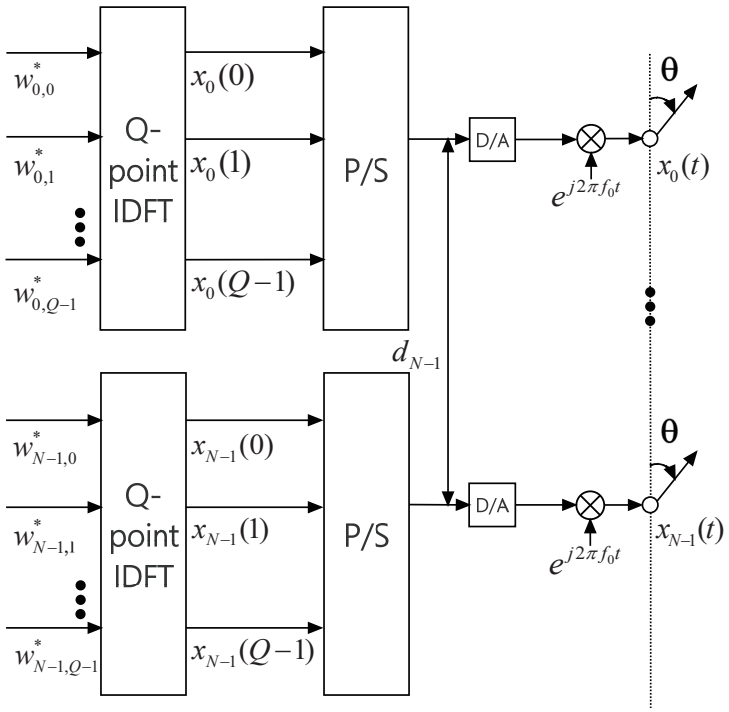

Figure 4.2: The proposed multi-carrier transmit beamforming structure for DM represented by IDFT.

IDFT. The outputs of IDFT are then followed by a parallel to serial converter (P/S) with the time interval t_s between adjacent samples and a digital to analogue converter (D/A). Finally, the multiple baseband signals are modulated to their corresponding carrier frequency and transmitted through the antennas. The new multi-carrier structure is represented in Fig. 4.2, which is the same as Fig. 4.1. To have a beam pointing to a certain direction, the steering vector at the q-th frequency is given by

$$\begin{aligned}\mathbf{s}(\omega_q,\theta) =& [1, e^{j\omega_q\tau_1}, \ldots, e^{j\omega_q\tau_{N-1}}]^T \\ =& [1, e^{j2\pi(f_0+(-\frac{Q}{2}+q)\triangle f)\tau_1}, \ldots, e^{j2\pi(f_0+(-\frac{Q}{2}+q)\triangle f)\tau_{N-1}}]^T,\end{aligned} \tag{4.3}$$

where τ_n for $n = 1, \ldots, N-1$ is the propagation advance for the signal from antenna n to antenna 0 and is a function of transmission angle θ, represented by $\frac{d_n \cos(\theta)}{c}$. Then, the beam response of the array at the q-th frequency is formulated as follows

$$\mathrm{p}(\omega_q,\theta) = \mathbf{w}(\omega_q)^H \mathbf{s}(\omega_q,\theta), \tag{4.4}$$

and $\mathbf{w}(\omega_q)$ is the weight vector at the q-th frequency, given by

$$\mathbf{w}(\omega_q) = [w_{0,q}, w_{1,q}, \ldots, w_{N-1,q}]^T. \tag{4.5}$$

Similarly, for M-ary signaling, $p_m(\omega_q, \theta)$ is defined as the desired array response to the m-th constellation point at the q-th frequency for $m = 0, \ldots, M-1$ and $q = 0, \ldots, Q-1$, and then is divided into $\mathbf{p}_m(\omega_q, \theta_{ML})$ (beam responses at the main lobe directions) and $\mathbf{p}_m(\omega_q, \theta_{SL})$ (beam responses over the sidelobe regions). Assume Θ sampling points, according to the direction of θ,

$$\begin{aligned} \mathbf{p}_m(\omega_q, \theta_{SL}) =& [p_m(\omega_q, \theta_0), p_m(\omega_q, \theta_1), \ldots, p_m(\omega_q, \theta_{\Theta-r-1})], \\ \mathbf{p}_m(\omega_q, \theta_{ML}) =& [p_m(\omega_q, \theta_{\Theta-r}), p_m(\omega_q, \theta_{\Theta-r+1}), \ldots, p_m(\omega_q, \theta_{\Theta-1})] \ . \end{aligned} \tag{4.6}$$

The corresponding weight vector is represented by

$$\mathbf{w}_m(\omega_q) = [w_{m,0,q}, \ldots, w_{m,N-1,q}]^T. \tag{4.7}$$

Moreover, $\mathbf{S}(\omega_q, \theta_{SL})$ is an $N \times (\Theta - r)$ matrix including all steering vectors at sidelobe regions at the q-th frequency, and the steering vector in the mainlobe θ_{ML} is an $N \times r$ matrix, denoted by $\mathbf{S}(\omega_q, \theta_{ML})$.

For the m-th constellation point at the q-th carrier frequency based on a given geometry, its corresponding weight coefficients can be obtained by solving the following constrained minimisation problem

$$\begin{aligned} \min_{\mathbf{w}_m(\omega_q)} \quad & ||\mathbf{p}_m(\omega_q, \theta_{SL}) - \mathbf{w}_m(\omega_q)^H \mathbf{S}(\omega_q, \theta_{SL})||_2 \\ \text{subject to} \quad & \mathbf{w}_m(\omega_q)^H \mathbf{S}(\omega_q, \theta_{ML}) = \mathbf{p}_m(\omega_q, \theta_{ML}). \end{aligned} \tag{4.8}$$

The objective function and constraint in (4.8) ensure a minimum difference between the desired and designed responses in the sidelobe, and a desired constellation value to the mainlobe or the direction of interest. To ensure that the constellation is scrambled in the sidelobe regions, the phase of the desired response $\mathbf{w}_m(\omega_q)^H \mathbf{S}(\omega_q, \theta_{SL})$ at different sidelobe directions can be randomly generated.

The problem in (4.8) can be solved by the method of Lagrange multipliers and the optimum value for the weight vector $\mathbf{w}_m(\omega_q)$ is given in (4.9), where $\mathbf{R} = \mathbf{S}(\omega_q, \theta_{SL})\mathbf{S}^H(\omega_q, \theta_{SL})$.

$$\begin{aligned}\mathbf{w}_m(\omega_q) =&\mathbf{R}^{-1}(\mathbf{S}(\omega_q,\theta_{SL})\mathbf{p}_m^H(\omega_q,\theta_{SL}) - \mathbf{S}(\omega_q,\theta_{ML}) \\ &\times ((\mathbf{S}^H(\omega_q,\theta_{ML})\mathbf{R}^{-1}\mathbf{S}(\omega_q,\theta_{ML}))^{-1}(\mathbf{S}^H(\omega_q,\theta_{ML})\mathbf{R}^{-1}\mathbf{S}(\omega_q,\theta_{SL})\mathbf{p}_m^H(\omega_q,\theta_{SL}) \\ &- \mathbf{p}^H(\omega_q,\theta_{ML}))))\end{aligned} \tag{4.9}$$

4.3 Multi-Carrier Design for DM with Location Optimisation

Equation (4.8) is only for designing the DM coefficients for a given set of antenna locations. In practice, the antenna locations may need to be optimised to achieve an even lower cost function in (4.8) or reduce the number of required antennas for a similar level of cost function minimisation result. This is a traditional sparse antenna array design problem [5, 6]. In the context of single-carrier DM, it has been studied using CS-based methods in the recent publication [28].

For CS-based sparse DM array design with a single carrier frequency [28], a given aperture represented by d_{N-1} is densely sampled with a large number (N) of potential antennas, where the values of d_n, for $n = 1, 2, \ldots, N-1$, are selected to give a uniform grid. Through selecting the minimum number of non-zero valued weight coefficients to generate a response close to the desired one, sparseness is achieved in the resultant design. In other words, if a weight coefficient is zero-valued, the corresponding antenna will be deemed inactive and therefore can be removed, leading to a sparse result.

Following this idea, for the multi-carrier structure in Fig. 4.2, where each antenna is connected to multiple frequency-dependent weight coefficients, the problem for the m-th constellation point at the q-th carrier frequency can be formulated as follows

$$\begin{aligned}\min_{\mathbf{w}_m(\omega_q)} \quad & ||\mathbf{w}_m(\omega_q)||_1 \\ \text{subject to} \quad & ||\mathbf{p}_m(\omega_q,\theta_{SL}) - \mathbf{w}_m(\omega_q)^H\mathbf{S}(\omega_q,\theta_{SL})||_2 \leq \alpha \\ & \mathbf{w}_m(\omega_q)^H\mathbf{S}(\omega_q,\theta_{ML}) = \mathbf{p}_m(\omega_q,\theta_{ML}),\end{aligned} \tag{4.14}$$

where $||\cdot||_1$ is the l_1 norm, used as an approximation to the l_0 norm, and α is the allowed

difference between the desired and designed responses.

However, the solution to (4.14) cannot guarantee the same set of active antenna positions for all constellation points at all frequencies. This means an antenna cannot be removed if the corresponding weight coefficients for all constellation points at all frequencies are not all zero-valued; in other words, to remove an antenna, all elements in the vector $\tilde{\mathbf{w}}_n$ need to be zero-valued or $||\tilde{\mathbf{w}}_n||_2 = 0$, where

$$\begin{aligned}\tilde{\mathbf{w}}_n =&[w_{0,n,0}, w_{1,n,0}, \ldots, w_{M-1,n,0},\\ &w_{0,n,1}, \ldots, w_{M-1,n,1}, \ldots, w_{M-1,n,Q-1}].\end{aligned} \tag{4.15}$$

Here $w_{m,n,q}$ represents the weight coefficient corresponding to the n-th antenna location for the m-th constellation point at the q-th frequency. Then, to reduce the number of elements for an N-element antenna array, all $||\tilde{\mathbf{w}}_n||_2$ for $n = 0, \ldots, N-1$ are gathered to form a vector $\hat{\mathbf{w}}$, given by

$$\hat{\mathbf{w}} = [||\tilde{\mathbf{w}}_0||_2, ||\tilde{\mathbf{w}}_1||_2, \ldots, ||\tilde{\mathbf{w}}_{N-1}||_2]^T, \tag{4.16}$$

and $\min ||\hat{\mathbf{w}}||_1$ represents the minimum number of non-zero valued $||\tilde{\mathbf{w}}_n||_2$ or the sparsest antenna array. This idea is called group sparsity [67], which is used here for finding a common set of active antenna locations for all constellation points at all Q frequencies. Moreover, DM constraints at all frequencies need to be imposed. Therefore, the following matrices are first constructed

$$\mathbf{W}(\omega_q) = [\mathbf{w}_0(\omega_q), \mathbf{w}_1(\omega_q), \ldots, \mathbf{w}_{M-1}(\omega_q)], \tag{4.17}$$

$$\mathbf{P}_{SL}(\omega_q, \theta_{SL}) = [\mathbf{p}_0(\omega_q, \theta_{SL}), \mathbf{p}_1(\omega_q, \theta_{SL}), \ldots, \mathbf{p}_{M-1}(\omega_q, \theta_{SL})]^T, \tag{4.18}$$

$$\mathbf{p}_{ML}(\omega_q, \theta_{ML}) = [\mathbf{p}_0(\omega_q, \theta_{ML}), \mathbf{p}_1(\omega_q, \theta_{ML}), \ldots, \mathbf{p}_{M-1}(\omega_q, \theta_{ML})]^T, \tag{4.19}$$

for $q = 0, 1, \ldots, Q-1$. Then, based on the above matrices, a series of block diagonal matrices are formed as follows

$$\mathbf{W} = \text{blkdiag}\{\mathbf{W}(\omega_0), \mathbf{W}(\omega_1), \ldots, \mathbf{W}(\omega_{Q-1})\}, \tag{4.20}$$

$$\mathbf{P}_{SL} = \text{blkdiag}\{\mathbf{P}_{SL}(\omega_0, \theta_{SL}), \mathbf{P}_{SL}(\omega_1, \theta_{SL}), \ldots, \mathbf{P}_{SL}(\omega_{Q-1}, \theta_{SL})\}, \tag{4.21}$$

$$\mathbf{P}_{ML} = \text{blkdiag}\{\mathbf{p}_{ML}(\omega_0, \theta_{ML}), \mathbf{p}_{ML}(\omega_1, \theta_{ML}), \ldots, \mathbf{p}_{ML}(\omega_{Q-1}, \theta_{ML})\}, \tag{4.22}$$

$$\mathbf{S}_{SL} = \text{blkdiag}\{\mathbf{S}(\omega_0, \theta_{SL}), \mathbf{S}(\omega_1, \theta_{SL}), \ldots, \mathbf{S}(\omega_{Q-1}, \theta_{SL})\}, \tag{4.23}$$

$$\mathbf{S}_{ML} = \text{blkdiag}\{\mathbf{S}(\omega_0, \theta_{ML}), \mathbf{S}(\omega_1, \theta_{ML}), \ldots, \mathbf{S}(\omega_{Q-1}, \theta_{ML})\}. \tag{4.24}$$

Then, the l_1 norm minimisation for sparse DM array design can be formulated as

$$\begin{aligned} \min_{\mathbf{W}} \ ||\hat{\mathbf{w}}||_1 \quad \text{subject to} \quad & ||\mathbf{P}_{SL} - \mathbf{W}^H \mathbf{S}_{SL}||_2 \leq \alpha \\ & \mathbf{W}^H \mathbf{S}_{ML} = \mathbf{P}_{ML} \ . \end{aligned} \tag{4.25}$$

As the reweighted l_1 norm minimisation has a closer approximation to the l_0 norm [48–50], the (4.25) can be further modified into the reweighted form in a similar way as in [28]. For the reweighted design, at the i-th iteration, the above formulations (4.25) becomes

$$\begin{aligned} \min_{\mathbf{W}} \quad & \sum_{n=0}^{N-1} \delta_n^i ||\tilde{\mathbf{w}}_n^i||_2 \\ \text{subject to} \quad & ||\mathbf{P}_{SL} - (\mathbf{W}^i)^H \mathbf{S}_{SL}||_2 \leq \alpha \\ & (\mathbf{W}^i)^H \mathbf{S}_{ML} = \mathbf{P}_{ML} \ , \end{aligned} \tag{4.26}$$

where the superscript i indicates the i-th iteration, and δ_n is the reweighting term for the n-th row of coefficients, given by $\delta_n^i = (||\tilde{\mathbf{w}}_n^{i-1}||_2 + \kappa)^{-1}$. The problem in (4.26) can be solved using cvx, a package for specifying and solving convex programs [46, 47].

4.4 Design Examples

In this section, several representative design examples are provided to show the working of the proposed multi-carrier based DM array structure and the performance of the location-optimised sparse array in comparison with a standard ULA.

Without loss of generality, the mainlobe direction is assumed to be $\theta_{ML} = 90^\circ$ and the sidelobe regions are $\theta_{SL} \in [0^\circ, 85^\circ] \cup [95^\circ, 180^\circ]$, sampled every 1° in the design. Consider a standard Wi-Fi transmission. The carrier frequency f_0 is set to 2.4GHz, with a bandwidth of 2.5MHz, split into 8 frequencies (8-point IDFT). The desired response is a value of one (magnitude) with 90° phase shift at the mainlobe (QPSK) and a value of 0.1 (magnitude) with random phase shifts over the sidelobe regions for each frequency.

To have a fair comparison, the DM result using the method in (4.8) is first obtained based on a 21-element ULA with a spacing of half-wavelength at the highest frequency.

Based on the design result, the error norm between the designed and the desired responses is then calculated and its value represented by α is then used in the sparse array design as the threshold.

4.4.1 Design Example with a Given Array Geometry

The resultant beam patterns using (4.8) at frequencies $f_0-4\triangle f$, $f_0-2\triangle f$, f_0, $f_0+2\triangle f$ are shown in Figs. 4.3, 4.4, 4.5 and 4.6, and the corresponding phase patterns are displayed in Figs. 4.7, 4.8, 4.9, 4.10. The beam and phase patterns on frequencies $f_0-3\triangle f$, $f_0-\triangle f$, $f_0+\triangle f$, $f_0+3\triangle f$ are not shown as they have the same features as the aforementioned figures, where all main beams are exactly pointed to 90° with a reasonable sidelobe level, and the designed phase at the mainlobe direction ($\theta = 90°$) for the constellation points follows the standard QPSK constellation, i.e., symbols '00', '01', '11', '10' correspond to 45°, 135°, −135° and −45°, respectively, while for the rest of the θ angles, phases of these symbols are random and their phase difference are scrambled, demonstrating that DM has been achieved effectively. The resultant weight coefficients for $m = 0$ (symbol 00) at the frequency 2.39875GHz is shown in Table 4.1.

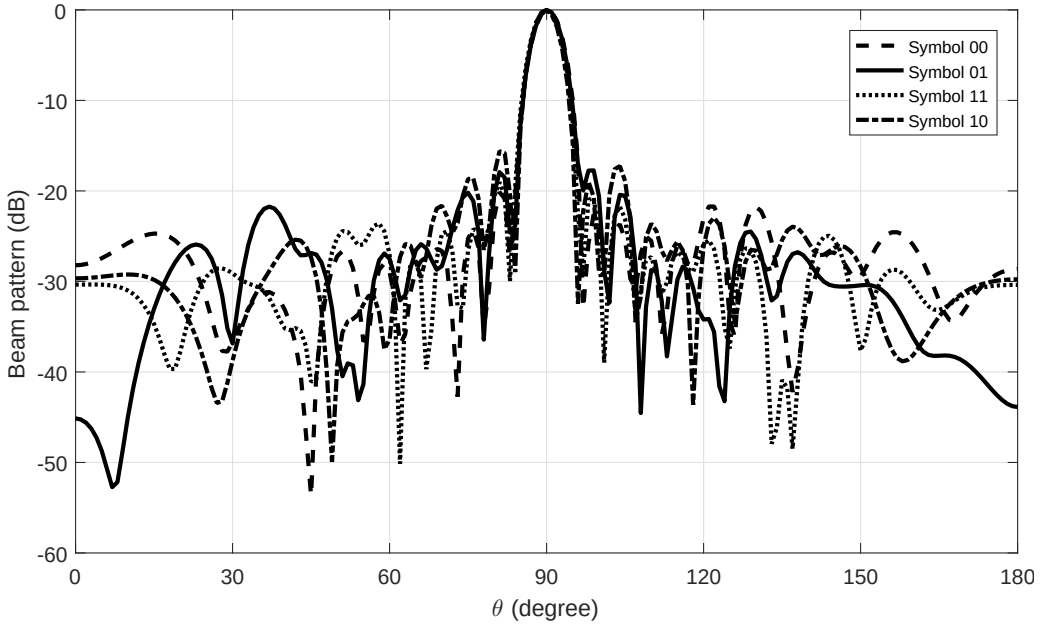

Figure 4.3: Simulated beam responses based on the multi-carrier design for ULA (4.8) at $f_0 - 4 \triangle f$.

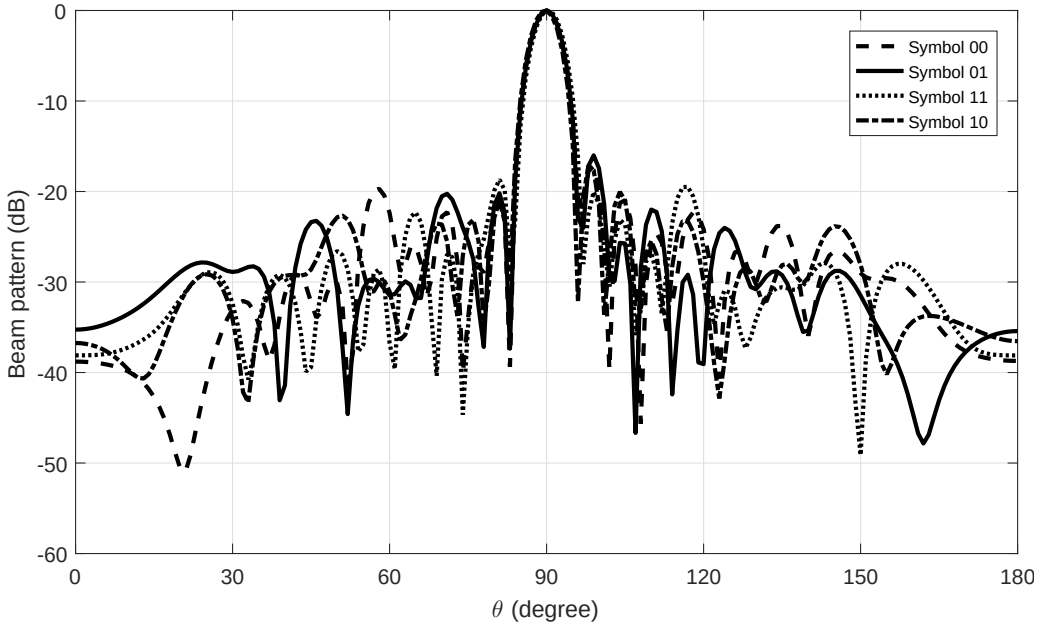

Figure 4.4: Simulated beam responses based on the multi-carrier design for ULA (4.8) at $f_0 - 2 \triangle f$.

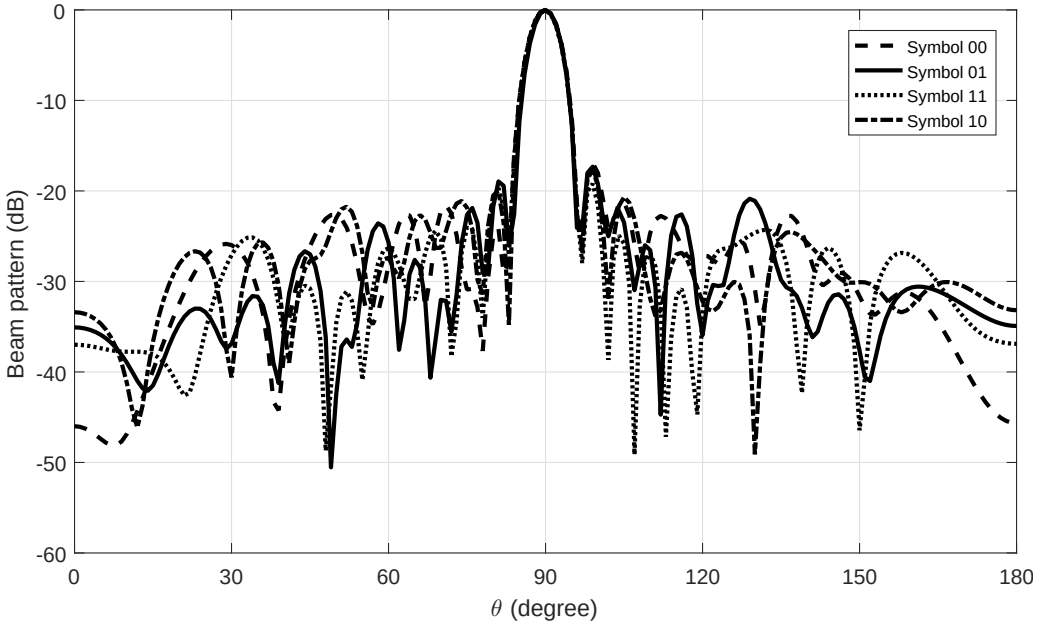

Figure 4.5: Simulated beam responses based on the multi-carrier design for ULA (4.8) at f_0.

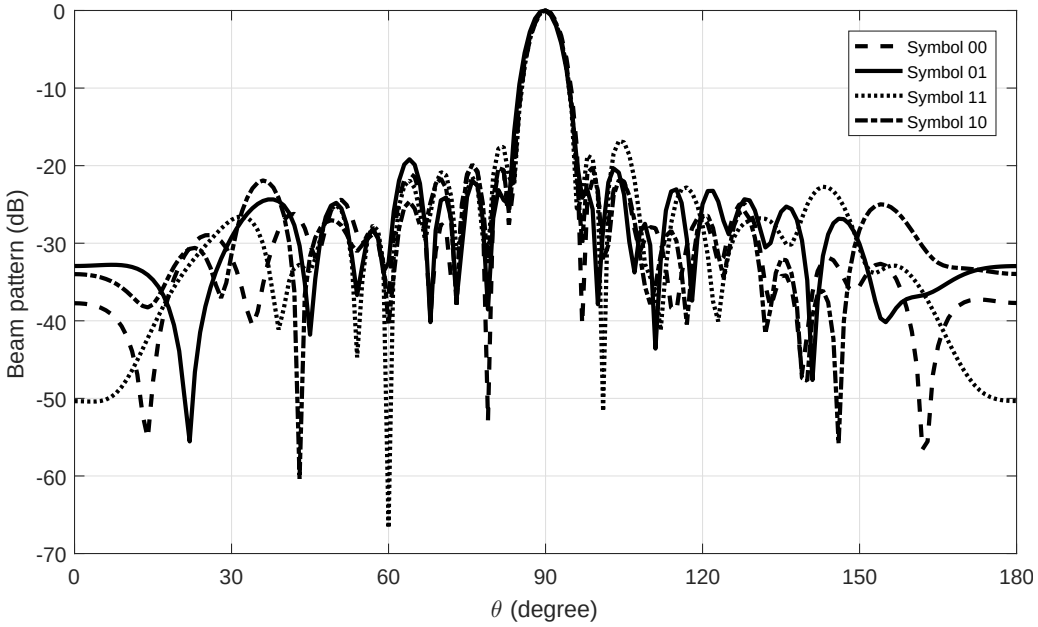

Figure 4.6: Simulated beam responses based on the multi-carrier design for ULA (4.8) at $f_0 + 2 \triangle f$.

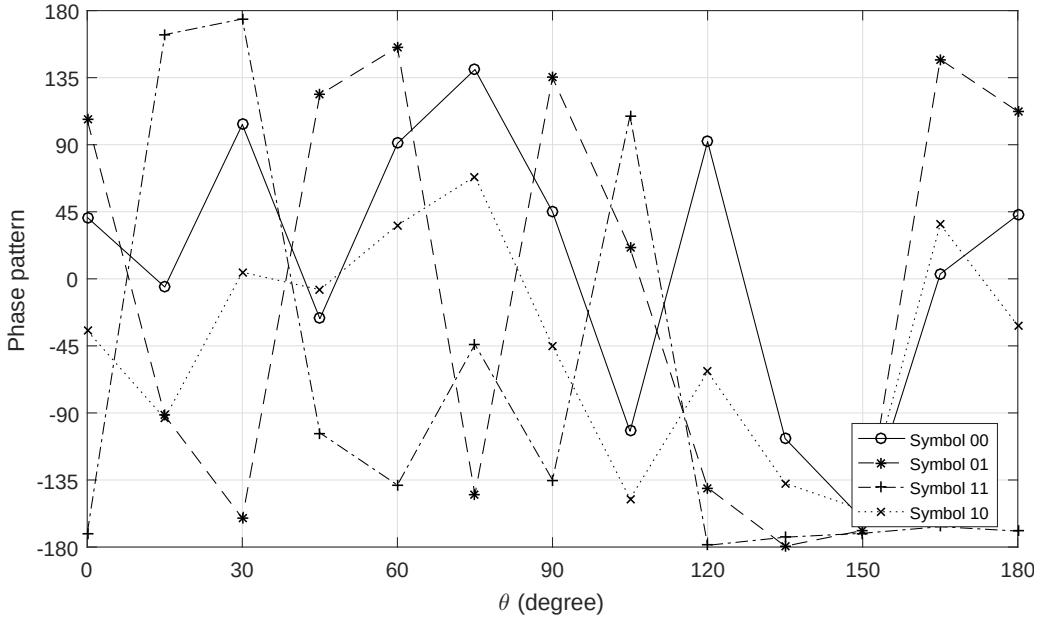

Figure 4.7: Simulated phase patterns based on the multi-carrier design for ULA (4.8) at $f_0 - 4 \triangle f$.

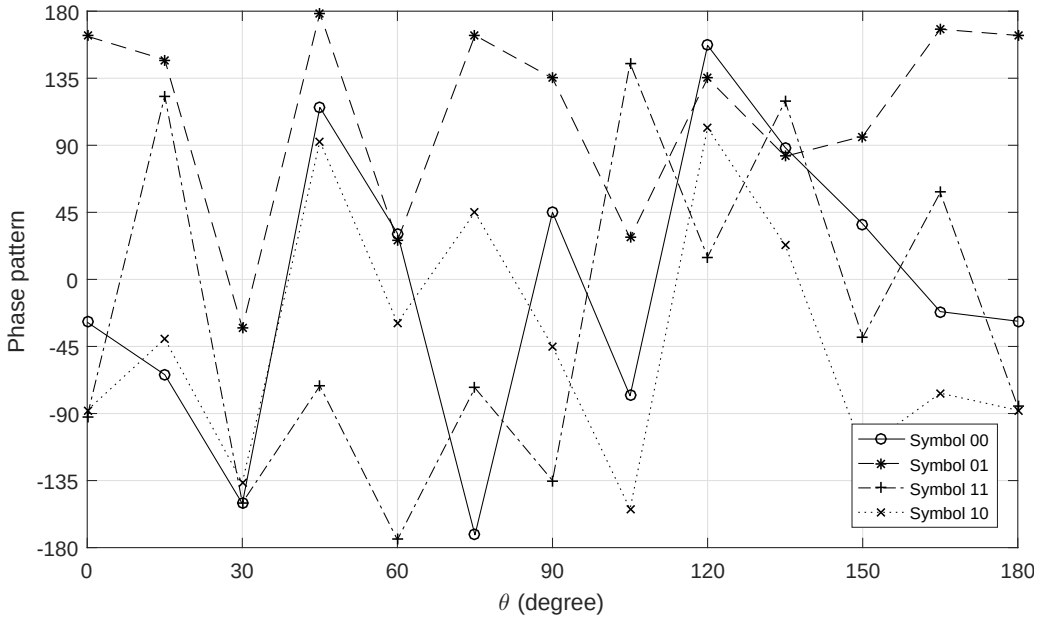

Figure 4.8: Simulated phase patterns based on the multi-carrier design for ULA (4.8) at $f_0 - 2 \triangle f$.

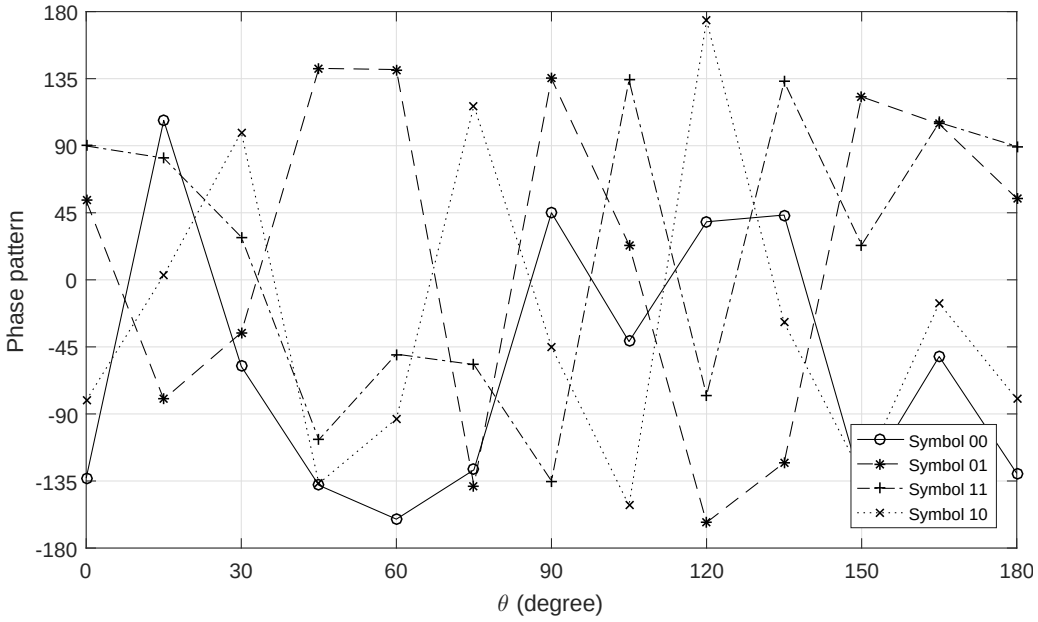

Figure 4.9: Simulated phase patterns based on the multi-carrier design for ULA (4.8) at f_0.

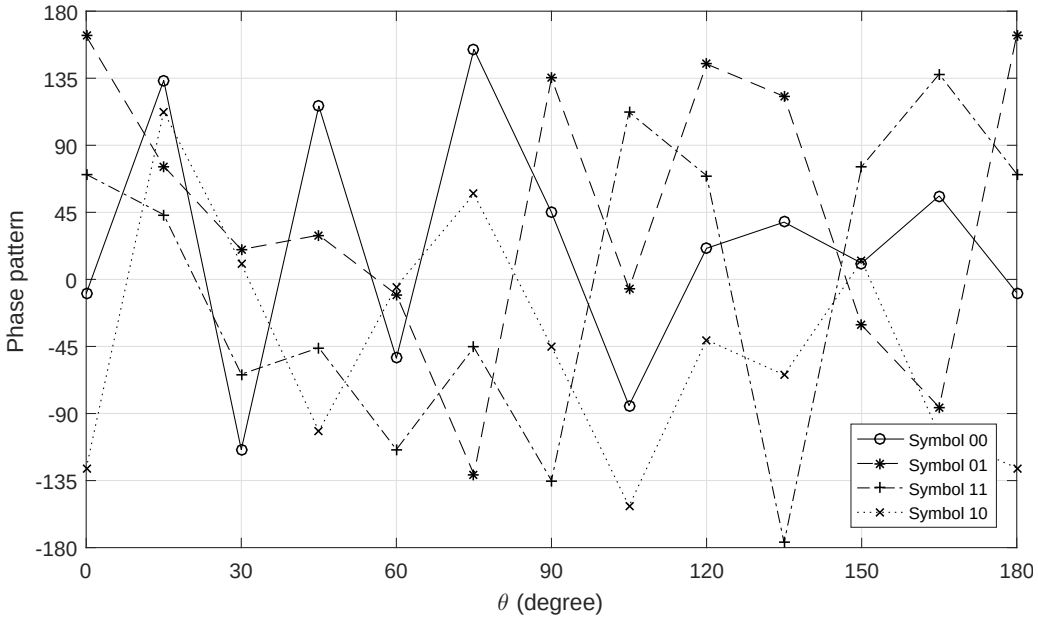

Figure 4.10: Simulated phase patterns based on the multi-carrier design for ULA (4.8) at $f_0 + 2 \triangle f$.

Table 4.1: The simulated weight coefficients for $m = 0$ (symbol 00) at the frequency 2.39875GHz based on the multi-carrier ULA design (4.8).

n	*weights*	n	*weights*
0	$0.0203 - j0.0189$	11	$0.0437 - j0.0455$
1	$0.0212 - j0.0274$	12	$0.0490 - j0.0438$
2	$0.0334 - j0.0206$	13	$0.0388 - j0.0459$
3	$0.0307 - j0.0258$	14	$0.0289 - j0.0368$
4	$0.0390 - j0.0411$	15	$0.0366 - j0.0344$
5	$0.0361 - j0.0359$	16	$0.0181 - j0.0431$
6	$0.0462 - j0.0368$	17	$0.0248 - j0.0288$
7	$0.0440 - j0.0451$	18	$0.0231 - j0.0167$
8	$0.0481 - j0.0413$	19	$0.0236 - j0.0197$
9	$0.0400 - j0.0384$	20	$0.0087 - j0.0217$
10	$0.0528 - j0.0455$		

4.4.2 Design Example with Optimised Antenna Locations

With the same value of error norm α obtained from the above ULA design case, the maximum aperture is set to be 15λ with 150 equally spaced potential antennas for the multi-carrier structure based sparse array design. Moreover, $\kappa = 0.001$ is set to indicate that antennas associated with a weight value smaller than 0.001 will be considered inactive.

For the reweighted l_1 norm minimisation method in (4.26), the resultant number of active antennas is 16, with an average spacing of $9.64cm$, as shown in Table 4.2. Figs. 4.11, 4.12, 4.13 and 4.14 show the beam patterns and Figs. 4.15, 4.16, 4.17 and 4.18 display the phase patterns at frequencies $f_0 - 4 \triangle f$, $f_0 - 2 \triangle f$, f_0 and $f_0 + 2 \triangle f$, all indicating a satisfactory design result. The beam and phase patterns for other frequencies have a similar performance to the above frequencies.

A performance comparison between the ULA design and the reweighted design is summarised in Table 4.3, where the result using direct l_1 norm minimisation in (4.25)

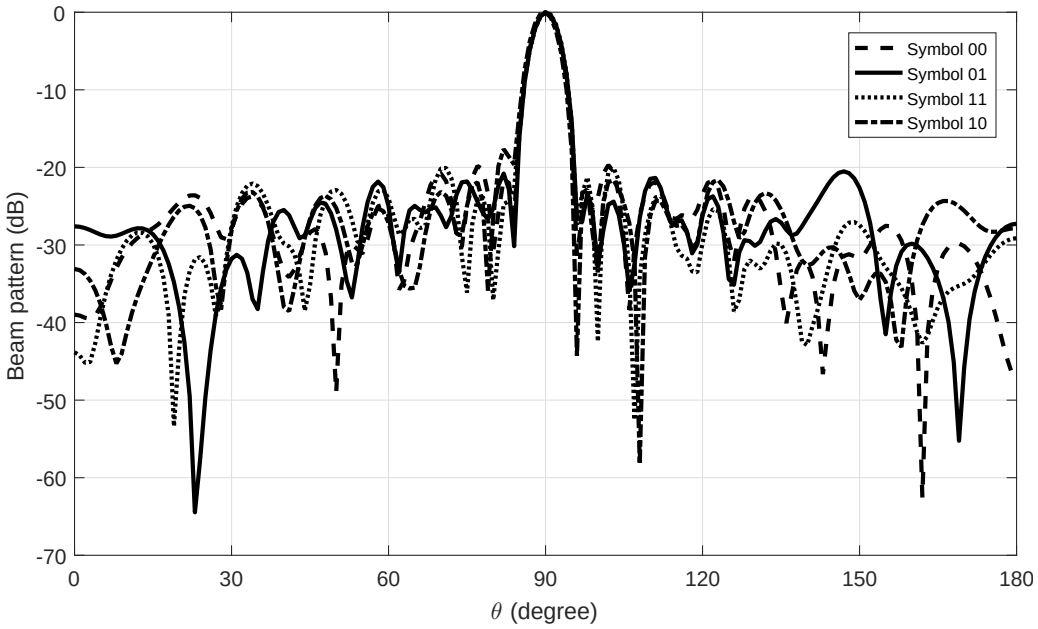

Figure 4.11: Simulated beam responses based on the multi-carrier design for sparse antenna array (4.26) at $f_0 - 4 \triangle f$.

(i.e. without reweighted iteration) is also included. As shown in the aforementioned beampatterns, they all have a very similar sidelobe level; however, the number of antennas required after location optimisation has been reduced by five using the reweighted design. Although the method in (4.25) also gives a sparse solution, with an adjacent antenna spacing larger than half wavelength, the number of antennas is increased from 21 to 24 (therefore with a much reduced sidelobe error), highlighting the need for the proposed reweighted design in (4.26).

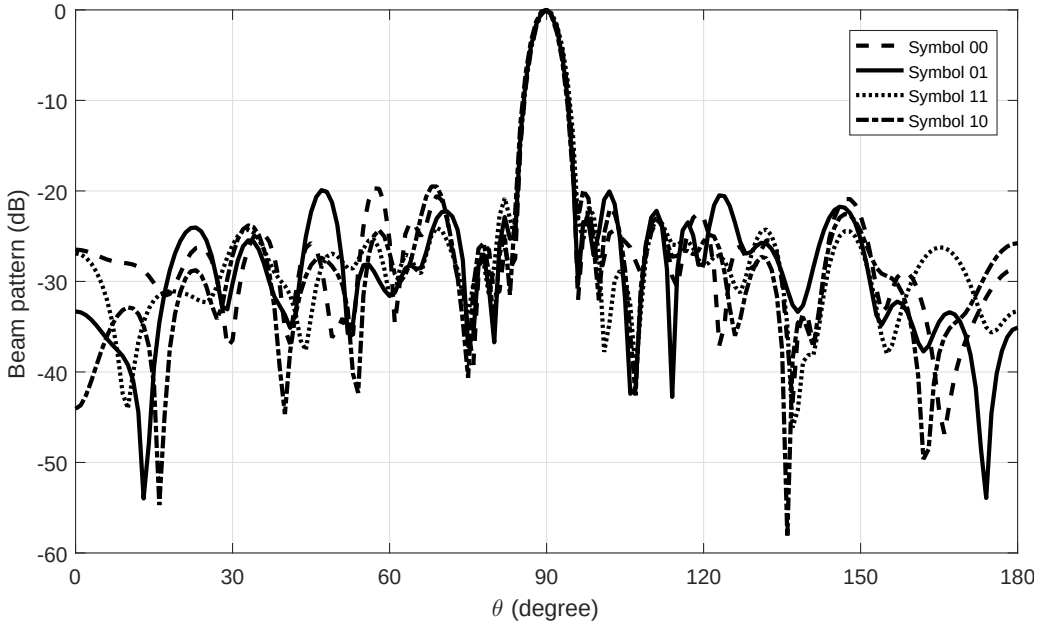

Figure 4.12: Simulated beam responses based on the multi-carrier design for sparse antenna array (4.26) at $f_0 - 2 \triangle f$.

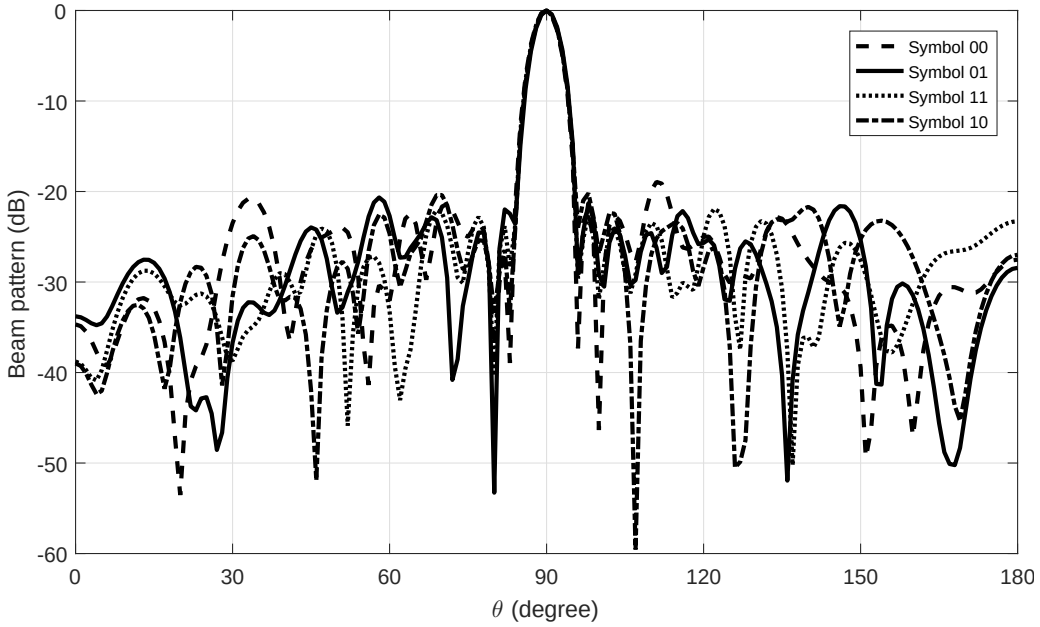

Figure 4.13: Simulated beam responses based on the multi-carrier design for sparse antenna array (4.26) at f_0.

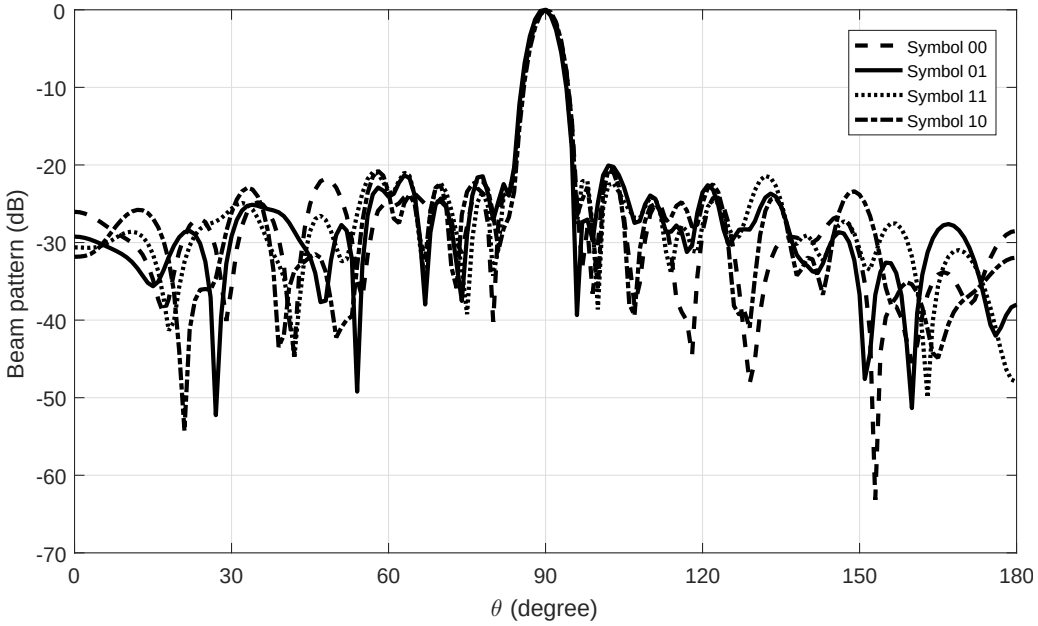

Figure 4.14: Simulated beam responses based on the multi-carrier design for sparse antenna array (4.26) at $f_0 + 2 \triangle f$.

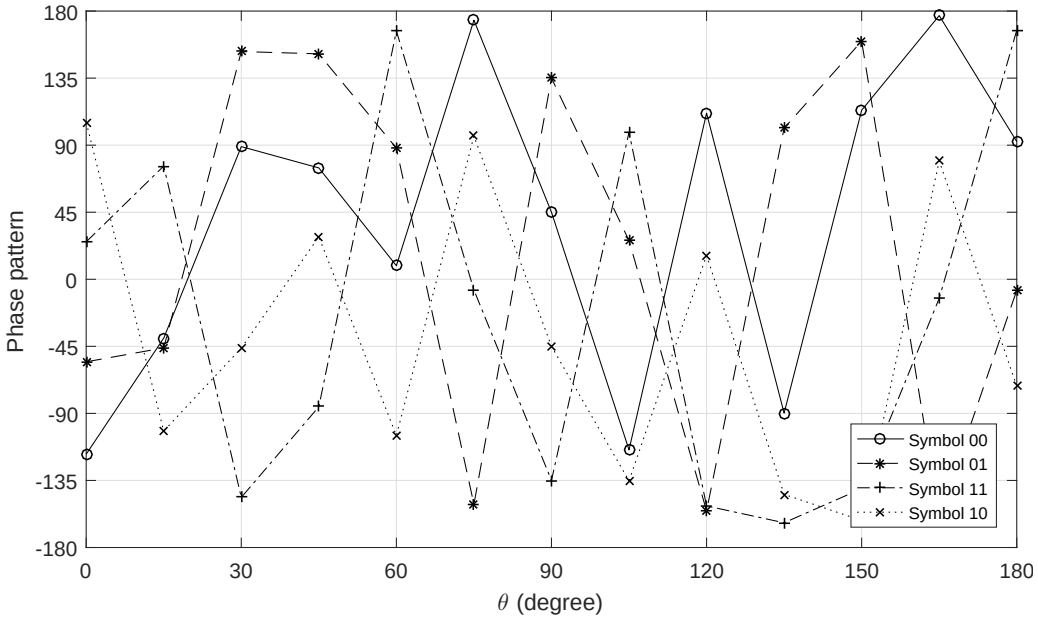

Figure 4.15: Simulated phase patterns based on the multi-carrier design for sparse antenna array (4.26) at $f_0 - 4 \triangle f$.

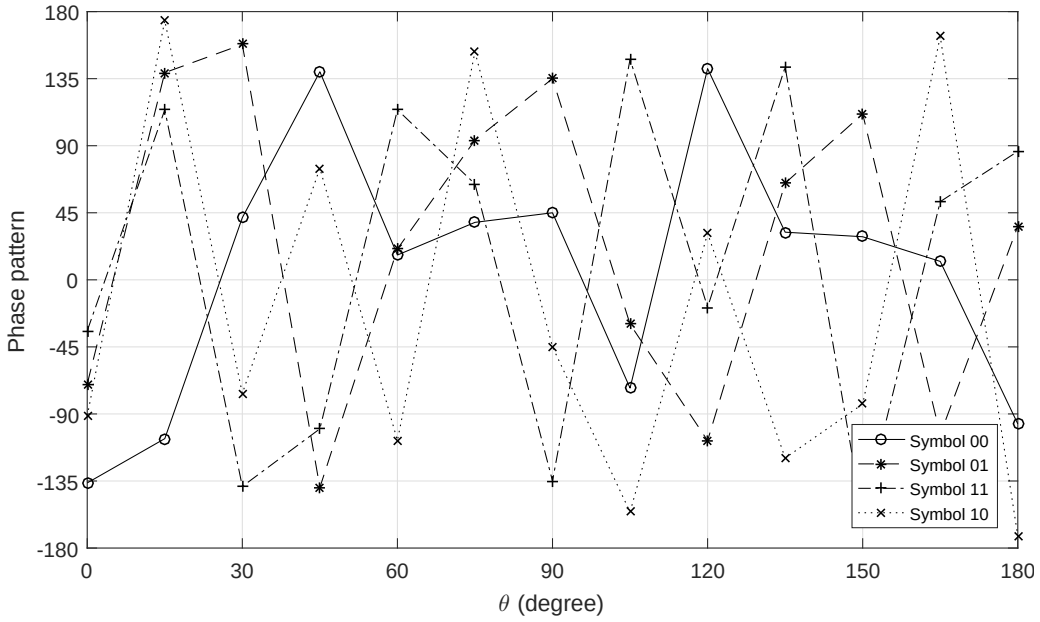

Figure 4.16: Simulated phase patterns based on the multi-carrier design for sparse antenna array (4.26) at $f_0 - 2 \triangle f$.

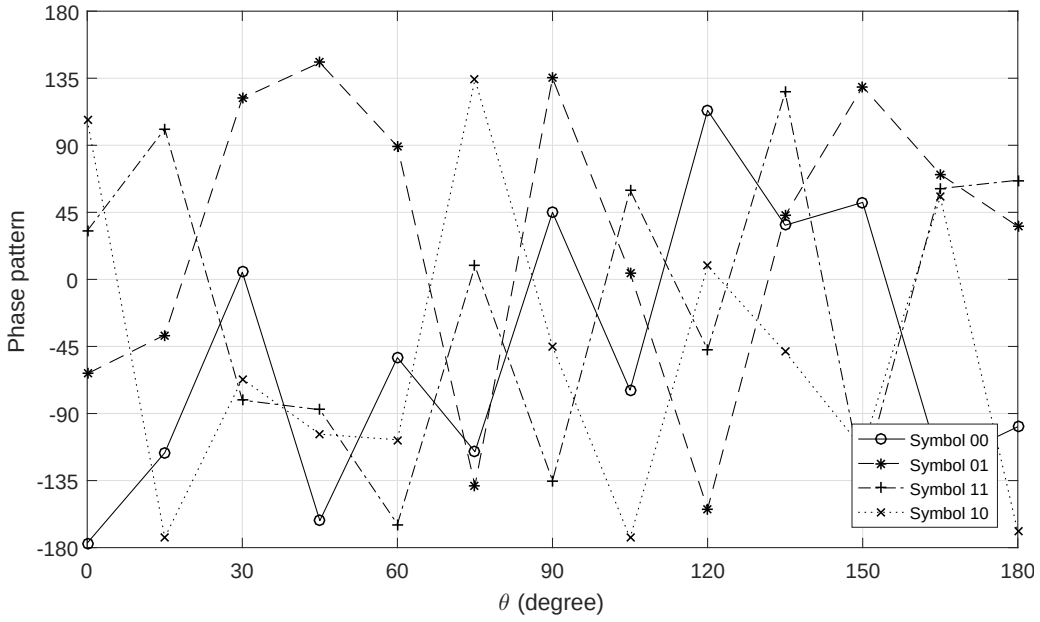

Figure 4.17: Simulated phase patterns based on the multi-carrier design for sparse antenna array (4.26) at f_0.

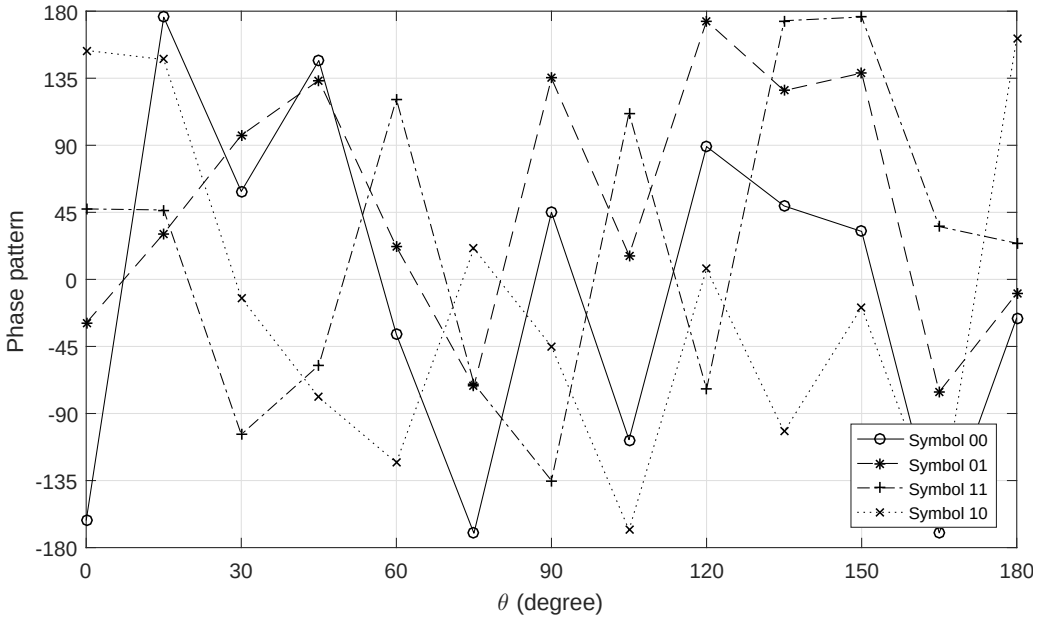

Figure 4.18: Simulated phase patterns based on the multi-carrier design for sparse antenna array (4.26) at $f_0 + 2 \triangle f$.

Table 4.2: Optimised antenna locations based on the multi-carrier design for sparse antenna array using reweighted l_1 norm minimisation.

n	$d_n(cm)$	n	$d_n(cm)$	n	$d_n(cm)$
0	33.96	6	89.31	12	145.92
1	44.03	7	100.63	13	155.98
2	55.35	8	110.70	14	167.30
3	66.67	9	119.50	15	178.62
4	75.47	10	124.53		
5	77.99	11	134.60		

Table 4.3: Summary of the design results based on the multi-carrier designs.

	ULA	l_1	Reweighted l_1
Antenna number	21	24	16
Aperture(cm)	124.95	187.43	144.66
Average spacing(cm)	6.25	8.15	9.64
$\|\|\mathbf{P}_{SL} - \mathbf{W}^H \mathbf{S}_{SL}\|\|_2$	7.631	7.088	7.6965

4.5 PAPR Constraint Based on a Given Array Geometry

Although the IDFT based DM shown in Fig. 4.2 works well in theory, in practice the Peak to Average Power Ratio (PAPR) problem needs to be considered, where due to signal envelope fluctuation, signal peaks can fall into saturation regions of an amplifier, resulting in non-linear distortion. The PAPR of the output signal $\mathbf{x}_n$ at the n-th antenna can be defined as [56–58, 68, 69]

$$\begin{aligned}\text{PAPR}(\mathbf{x}_n) =& \frac{\max\limits_{k=0,\ldots,Q-1} |x_n(k)|^2}{\frac{1}{Q}\sum_{k=0}^{Q-1} |x_n(k)|^2} \\ =& \frac{||\mathbf{x}_n||_\infty^2}{\frac{1}{Q}||\mathbf{x}_n||_2^2} \quad n \in 0, 1, \ldots, N-1,\end{aligned} \tag{4.27}$$

where $\mathbf{x}_n = [x_n(0), \ldots, x_n(Q-1)]$ and the upper bound of PAPR can be represented by ρ ($\rho \geq 1$). As the PAPR constraint is designed for all antennas and each antenna has Q frequency dependent weight coefficients, before introducing the PAPR constraint to the DM design, the formulation (4.8) designed for a particular constellation point at a particular frequency is extended to the following, where cost functions and constraints for all constellation points at all frequencies are considered together [30]

$$\begin{aligned}\min_{\mathbf{W}} \quad & ||\mathbf{P}_{SL} - \mathbf{W}^H \mathbf{S}_{SL}||_2 \\ \text{subject to} \quad & \mathbf{W}^H \mathbf{S}_{ML} = \mathbf{P}_{ML},\end{aligned} \tag{4.28}$$

where

$$\begin{aligned}&\mathbf{W} = \text{blkdiag}\{\mathbf{W}(\omega_0), \ldots, \mathbf{W}(\omega_{Q-1})\}, \\ &\mathbf{P}_{SL} = \text{blkdiag}\{\mathbf{P}_{SL}(\omega_0, \theta_{SL}), \ldots, \mathbf{P}_{SL}(\omega_{Q-1}, \theta_{SL})\}, \\ &\mathbf{P}_{ML} = \text{blkdiag}\{\mathbf{p}_{ML}(\omega_0, \theta_{ML}), \ldots, \mathbf{p}_{ML}(\omega_{Q-1}, \theta_{ML})\}, \\ &\mathbf{S}_{SL} = \text{blkdiag}\{\mathbf{S}(\omega_0, \theta_{SL}), \ldots, \mathbf{S}(\omega_{Q-1}, \theta_{SL})\}, \\ &\mathbf{S}_{ML} = \text{blkdiag}\{\mathbf{s}(\omega_0, \theta_{ML}), \ldots, \mathbf{s}(\omega_{Q-1}, \theta_{ML})\}, \\ &\mathbf{W}(\omega_q) = [\mathbf{w}_0(\omega_q), \ldots, \mathbf{w}_{M-1}(\omega_q)], \\ &\mathbf{P}_{SL}(\omega_q, \theta_{SL}) = [\mathbf{p}_0(\omega_q, \theta_{SL}), \ldots, \mathbf{p}_{M-1}(\omega_q, \theta_{SL})],^T \\ &\mathbf{p}_{ML}(\omega_q, \theta_{ML}) = [\mathbf{p}_0(\omega_q, \theta_{ML}), \ldots, \mathbf{p}_{M-1}(\omega_q, \theta_{ML})].^T\end{aligned} \tag{4.29}$$

Therefore, the formulation for DM design subject to the PAPR constraint is given by

$$\begin{aligned} \min_{\mathbf{W}} \quad & ||\mathbf{P}_{SL} - \mathbf{W}^H \mathbf{S}_{SL}||_2 \\ \text{subject to} \quad & \mathbf{W}^H \mathbf{S}_{ML} = \mathbf{P}_{ML} \\ & ||\mathbf{x}_n||_2^2 = Q \\ & \text{PAPR}(\mathbf{x}_n) \leq \rho \quad n = 0, \ldots, N-1. \end{aligned} \tag{4.30}$$

Here, an energy constraint $||\mathbf{x}_n||_2^2 = Q$ is also imposed [66] for the PAPR requirements (although Q can be any values, Q is chosen to make the denominator of the PAPR expression (4.27) equal to one for simplicity). Then, based on the constraint $||\mathbf{x}_n||_2^2 = Q$, $\text{PAPR}(\mathbf{x}_n) \leq \rho$ can be changed to $\max_{k=0,\ldots,Q-1} |x_n(k)|^2 \leq \rho$.

However, the formulation (4.30) is nonconvex because of the PAPR constraint. For example, for $\rho = 1$, each of $[x_n(0), \ldots, x_n(Q-1)]$ in $\mathbf{x}_n$ can only take values from the unit circle [66], which does not satisfy a convex set. To solve the problem, the Wideband Beampattern Formation via Iterative Techniques (WBFIT) method proposed in [66] is modified, which is formulated as

$$\begin{aligned} \min_{\mathbf{x}_n} \quad & ||\mathbf{u}_n - \mathbf{x}_n||_2 \\ \text{subject to} \quad & ||\mathbf{x}_n||_2^2 = Q \\ & \text{PAPR}(\mathbf{x}_n) \leq \rho \quad n = 0, \ldots, N-1, \end{aligned} \tag{4.31}$$

where $\mathbf{u}_n$ is a reference vector.

The difference between the problem in (4.30) and the WBFIT method in (4.31) is the additional phase requirement to the desired directions in our design. To solve the problem, the Newton's method is introduced into the optimisation process, and the modified WBFIT method is employed iteratively to find the weight coefficients until the given phase requirement in the desired directions is satisfied.

Basically, there are two stages for the proposed solution. At the first stage, the coefficients in equation (4.28) without considering the PAPR constraint is first calculated, and use them to construct a 3-D matrix. At the second stage, a set of auxiliary variables $\{\psi_q\}_{q=-Q/2}^{Q/2-1}$ is introduced and multiply them by the 3-D matrix; based on the result, new weight coefficients are obtained meeting the phase requirement with its IDFT outputs $\mathbf{x}_n$ subject to the PAPR constraint.

4.5.1 Stage One

The PAPR constraint is designed for $\mathbf{x}_n$, $n = 0, 1, \ldots, N-1$, corresponding to the n-th antenna, and as shown in Fig. 4.2, each antenna is associated with Q frequency dependent inputs (weight coefficients) $[w^*_{n,0}, w^*_{n,1}, \ldots, w^*_{n,Q-1}]$, resulting in Q outputs $[x_n(0), \ldots, x_n(Q-1)]$ by IDFT [30]. Then, in the context of M-ary signaling for each frequency, there are M^Q sets of inputs (weight coefficients) for all Q frequencies, and each set contains $N \times Q$ coefficients. Then an $N \times Q \times M^Q$ matrix $\hat{\mathbf{W}}$ can be constructed to represent all sets of inputs, with $\hat{\mathbf{W}}(n, :, u)$ representing the inputs of the IDFT structure at the n-th antenna for the u-th set of coefficients. Details of constructing the 3-D matrix are described as follows

1. Calculate the values of weight coefficients $\mathbf{w}_m(\omega_q)$ for $m = 0, \ldots, M-1$ and $q = 0, \ldots, Q-1$ in (4.28).

2. Select one set of weight coefficients (an $N \times 1$ vector) from each frequency (e.g. for the q-th sub-carrier frequency, select one column from $[\mathbf{w}_0(\omega_q), \ldots, \mathbf{w}_{M-1}(\omega_q)]$), and combine them together to form an $N \times Q$ matrix for all Q frequencies, representing one set of inputs of the IDFT. Then, with all M^Q sets of inputs, the $N \times Q \times M^Q$ matrix $\hat{\mathbf{W}}$ is constructed.

4.5.2 Stage Two

The objective of the modified WBFIT is to find new weight coefficients for each set of inputs that satisfy DM with their corresponding IDFT outputs $\mathbf{x}_n$ subject to the PAPR constraints. To achieve this, a set of auxiliary variables $\{\psi_q\}_{q=-Q/2}^{Q/2-1}$ is introduced. Details of the second stage are given below.

1. For the u-th set of inputs $\hat{\mathbf{W}}(:, :, u)$, $u = 0, \ldots, M^Q - 1$, $\{\psi_q\}_{q=-Q/2}^{Q/2-1}$ are randomly generated following a uniform distribution within [0, 2π].

2. Form the matrix $\mathbf{E} = diag\{e^{j\psi_{-Q/2}}, \ldots, e^{j\psi_{Q/2-1}}\}$ and minimise the difference be-

tween $\mathbf{E}\hat{\mathbf{W}}^H(:,:,u)$ and the DFT of $\mathbf{X}$, subject to PAPR $\leq \rho$ ($\rho \geq 1$), i.e.

$$\begin{aligned}
&\min_{\mathbf{X}} \quad ||\mathbf{E}\hat{\mathbf{W}}^H(:,:,u) - \mathbf{F}\mathbf{X}||_2 \\
&\text{subject to} \\
&angle((\mathbf{F}\mathbf{X})(q,:,u)\mathbf{S}(\omega_q,\theta_{ML})) \\
&= angle(\hat{\mathbf{W}}^H(q,:,u)\mathbf{S}(\omega_q,\theta_{ML})) \\
&||\mathbf{x}_n||_2^2 = Q \\
&\text{PAPR}(\mathbf{x}_n) \leq \rho \; for \; n = 0,\ldots,N-1,
\end{aligned} \tag{4.32}$$

where

$$\mathbf{F} = [\mathbf{dft}_{-Q/2},\ldots,\mathbf{dft}_{Q/2-1}]^T, \tag{4.33}$$

$$\begin{aligned}
\mathbf{dft}_q =&[1, e^{-j2\pi q/Q},\ldots,e^{-j2\pi\frac{(Q-1)q}{Q}}] \\
&for \quad q = -Q/2,\ldots,Q/2-1,
\end{aligned} \tag{4.34}$$

$$\mathbf{X} = [\mathbf{x}_0,\mathbf{x}_1,\ldots,\mathbf{x}_{N-1}], \tag{4.35}$$

$$\mathbf{x}_n = [x_n(0),x_n(1),\ldots,x_n(Q-1)]^T. \tag{4.36}$$

Here, the proposed phase constraint

$$\begin{aligned}
&angle((\mathbf{F}\mathbf{X})(q,:,u)\mathbf{S}(\omega_q,\theta_{ML})) \\
&= angle(\hat{\mathbf{W}}^H(q,:,u)\mathbf{S}(\omega_q,\theta_{ML}))
\end{aligned} \tag{4.37}$$

is introduced to represent a phase equalisation in the desired directions between the designed phases $angle((\mathbf{F}\mathbf{X})(q,:,u)\mathbf{S}(\omega_q,\theta_{ML}))$ and the corresponding desired phases $angle(\hat{\mathbf{W}}^H(q,:,u)\mathbf{S}(\omega_q,\theta_{ML}))$.

3. Similar to [66], the cost function in (4.32) is further changed to the following for the minimisation corresponding to the n-th antenna, $n = 0,\ldots,N-1$,

$$\begin{aligned}
&||\mathbf{E}\hat{\mathbf{W}}^H(n,:,u) - \mathbf{F}\mathbf{x}_n||_2 \\
=&||\frac{1}{Q}\mathbf{F}^H\mathbf{E}\hat{\mathbf{W}}^H(n,:,u) - \mathbf{x}_n||_2.
\end{aligned} \tag{4.38}$$

Then the formulation in (4.32) changes to

$$\begin{aligned} &\min_{\mathbf{x}_n} \quad ||\frac{1}{Q}\mathbf{F}^H\mathbf{E}\hat{\mathbf{W}}^H(n,:,u) - \mathbf{x}_n||_2 \\ &\text{subject to} \\ &angle((\mathbf{FX})(q,:,u)\mathbf{S}(\omega_q,\theta_{ML})) \\ &= angle(\hat{\mathbf{W}}^H(q,:,u)\mathbf{S}(\omega_q,\theta_{ML})) \\ &||\mathbf{x}_n||_2^2 = Q \\ &\text{PAPR}(\mathbf{x}_n) \leq \rho \; for \; n = 0,\ldots,N-1. \end{aligned} \tag{4.39}$$

4. The problem in (4.39) can be solved by the 'nearest-vector' method in [66, 70, 71] in combination with the Newton's method for the phase requirement in desired directions.

   According to the nearest-vector solution, $\mathbf{x}_n$ subject to the constraint on $||\mathbf{x}_n||_2^2 = Q$ are first obtained, which is $\mathbf{x}_n = \sqrt{Q}\frac{\frac{1}{Q}\mathbf{F}^H\mathbf{E}\hat{\mathbf{W}}^H(n,:,u)}{||\frac{1}{Q}\mathbf{F}^H\mathbf{E}\hat{\mathbf{W}}^H(n,:,u)||_2}$. With the PAPR constraint ($\max|\mathbf{x}_n| \leq \sqrt{\rho}$), if the magnitudes of all elements in $\mathbf{x}_n$ are no more than $\sqrt{\rho}$, then $\mathbf{x}_n$ is a solution; otherwise, the element in $\mathbf{x}_n$ corresponding to the largest element in magnitude in $\frac{1}{Q}\mathbf{F}^H\mathbf{E}\hat{\mathbf{W}}^H(n,:,u)$, represented by s_a, is given by $\sqrt{\rho}e^{jangle(s_a)}$ and the rest of the $Q-1$ elements in $\mathbf{x}_n$ is calculated by (4.39); in other words, step 4 for the rest of the $Q-1$ elements is re-run. Here the difference is that the size of $\mathbf{x}_n$ and $\frac{1}{Q}\mathbf{F}^H\mathbf{E}\hat{\mathbf{W}}^H(n,:,u)$ in (4.39) becomes $(Q-1)\times 1$, instead of the original $Q\times 1$, and the energy constraint changes to $||\mathbf{x}_n||_2^2 = Q-\rho$. If the PAPR constraint is still not satisfied for the new results, then the value of the largest element in $\mathbf{x}_n$ (size $(Q-1)\times 1$ in this iteration) is set, as it has been done above when the size of $\mathbf{x}_n$ is $Q\times 1$, and re-run step 4 for the rest of the $Q-2$ elements, and so on. The iterative process ends when the PAPR constraint is satisfied [70, 71].

5. Now the phase requirement at the desired directions is considered.

   Based on the new weight coefficients, which are the DFT of $\mathbf{X}$ calculated in the last step, if the phase constraint

$$\begin{aligned} &angle((\mathbf{FX})(q,:,u)\mathbf{S}(\omega_q,\theta_{ML})) \\ &- angle(\hat{\mathbf{W}}^H(q,:,u)\mathbf{S}(\omega_q,\theta_{ML})) = 0 \end{aligned} \tag{4.40}$$

is satisfied, then the desired phase pattern in the mainlobe direction based on the new coefficients subject to the PAPR constraint is achieved, and $\{\psi_q\}_{q=-Q/2}^{Q/2-1}$ is the proper set of auxiliary values, and $u = u + 1$ is set and go back to step 1 for the $(u + 1)$-th set of inputs.

If not, then

$$\{\psi_q\}_{q=-Q/2}^{Q/2-1} = \{\psi_q\}_{q=-Q/2}^{Q/2-1} - \frac{f(\{\psi_q\}_{q=-Q/2}^{Q/2-1})}{f'(\{\psi_q\}_{q=-Q/2}^{Q/2-1})}, \tag{4.41}$$

where

$$\begin{aligned} f(\{\psi_q\}_{q=-Q/2}^{Q/2-1}) =& angle((\mathbf{FX})(q,:,u)\mathbf{S}(\omega_q,\theta_{ML})) \\ & - angle(\hat{\mathbf{W}}^H(q,:,u)\mathbf{S}(\omega_q,\theta_{ML})), \end{aligned} \tag{4.42}$$

and run from steps 2 to 5 iteratively until the phase constraint in step 5 is satisfied. Here the Newton's iterative method has been used to optimise $\{\psi_q\}_{q=-Q/2}^{Q/2-1}$ to limit the corresponding phase differences which is the left side of equation (4.40) to be smaller than itself from the previous iteration. $\{\psi_q\}_{q=-Q/2}^{Q/2-1}$ on the right side of (4.41) represents the previous value and on the left side denotes the latest value. The value of the denominator $f'(\{\psi_q\}_{q=-Q/2}^{Q/2-1})$ is selected by trial and error.

4.6 Design Examples

In this section, examples based on a 20-element ULA with and without PAPR $\leq \rho$ ($\rho \geq 1$) constraints are provided to show the effectiveness of the proposed solution. Both broadside and off-broadside design examples are provided. In the broadside design example, the mainlobe direction is assumed to be $\theta_{ML} = 90°$ and the sidelobe regions are $\theta_{SL} \in [0°, 85°] \cup [95°, 180°]$, sampled every 1°. While in the off-broad design example, $\theta_{ML} = 120°$ and $\theta_{SL} \in [0°, 115°] \cup [125°, 180°]$, sampled every 1°. The carrier frequency f_0 is set to 2.4GHz, with a bandwidth of 1.25MHz split into $Q = 4$ frequencies (4-point IDFT). For each frequency, the desired response is a value of one (magnitude) with 90° phase shift at the mainlobe, i.e. QPSK where the constellation points are at $45°, 135°, -135°, -45°$ for symbols '00', '01', '11', '10', and a value of 0.1 (magnitude) with random phase over the sidelobe regions. The threshold of the PAPR is set to $\rho = 2.5$. The value of denominator

$f'(\{\psi_q\}_{q=-Q/2}^{Q/2-1})$ is set to be 4 by trial and error, and the value smaller than this cannot guarantee the convergence of (4.40).

Moreover, histograms are used to show the probability of PAPRs, where the x-axis represents bin edges, and y-axis denotes values of probability, and each bin is set to include the right edge, not including the left edge, except for the first bin $\in [1, 1.5]$.

4.6.1 Broadside Design Example without PAPR Constraint

The resultant beam patterns using (4.8) without PAPR constraint at frequencies $f_0 - 2\triangle f$, $f_0 - \triangle f$, f_0 and $f_0 + \triangle f$ are shown in Figs. 4.19, 4.20, 4.21 and 4.22 for symbols '00,01,11,00', '00,01,11,01', '00,01,11,11', '00,01,11,10', and the corresponding phase patterns are displayed in Figs. 4.23, 4.24, 4.25 and 4.26. The beam and phase patterns for other symbols are not shown as they have the same features as the aforementioned figures, where all main beams are exactly pointed to 90° with a reasonable sidelobe level, and the phase in the main beam direction follows the given QPSK constellation diagram and random over the sidelobe ranges. Moreover, as shown in Fig. 4.27, PAPRs for all sets of inputs are in the range of $[1, 4]$.

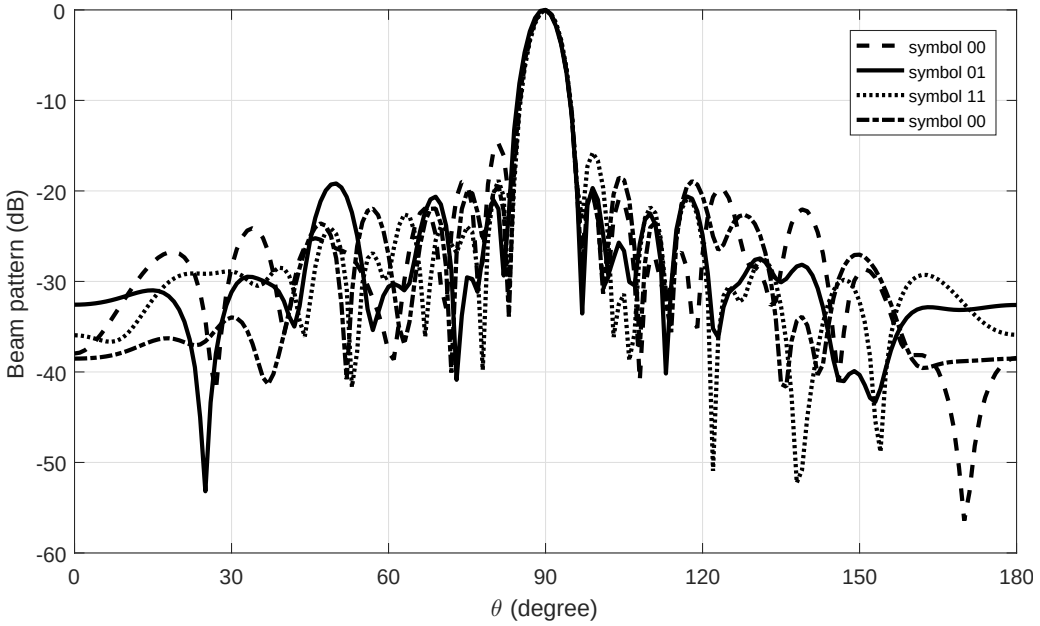

Figure 4.19: Simulated beam responses based on the broadside design using (4.8) for symbols '00, 01, 11, 00' without PAPR constraint.

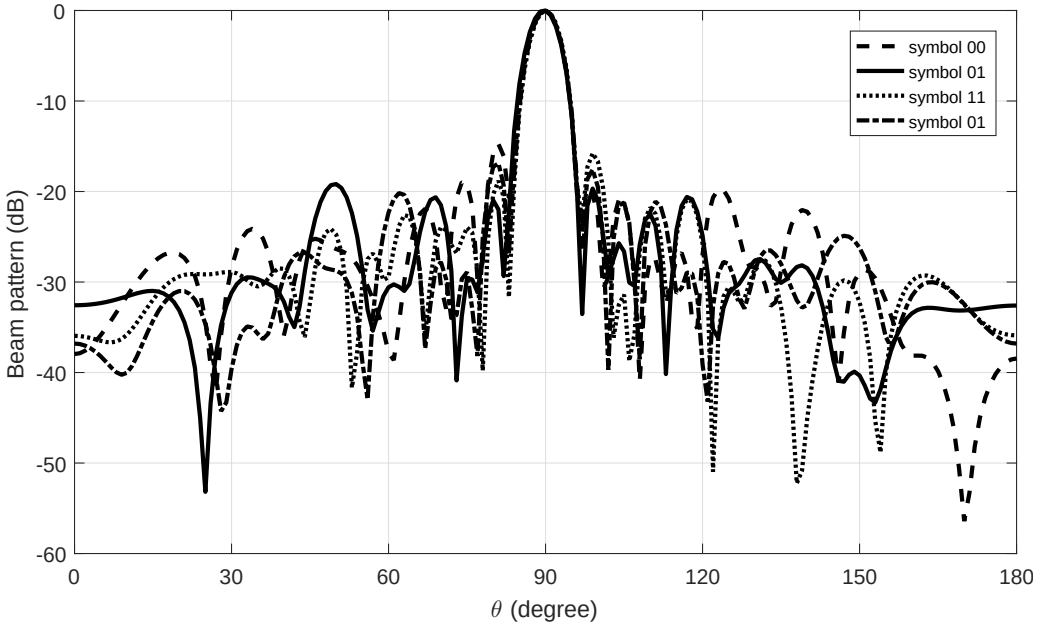

Figure 4.20: Simulated beam responses based on the broadside design using (4.8) for symbols '00, 01, 11, 01' without PAPR constraint.

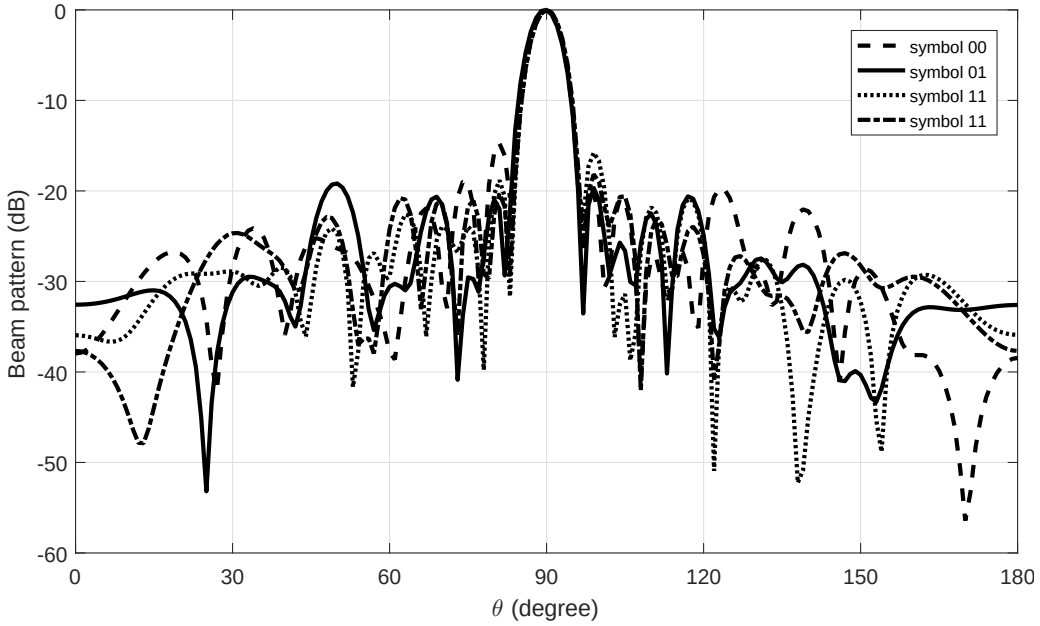

Figure 4.21: Simulated beam responses based on the broadside design using (4.8) for symbols '00, 01, 11, 11' without PAPR constraint.

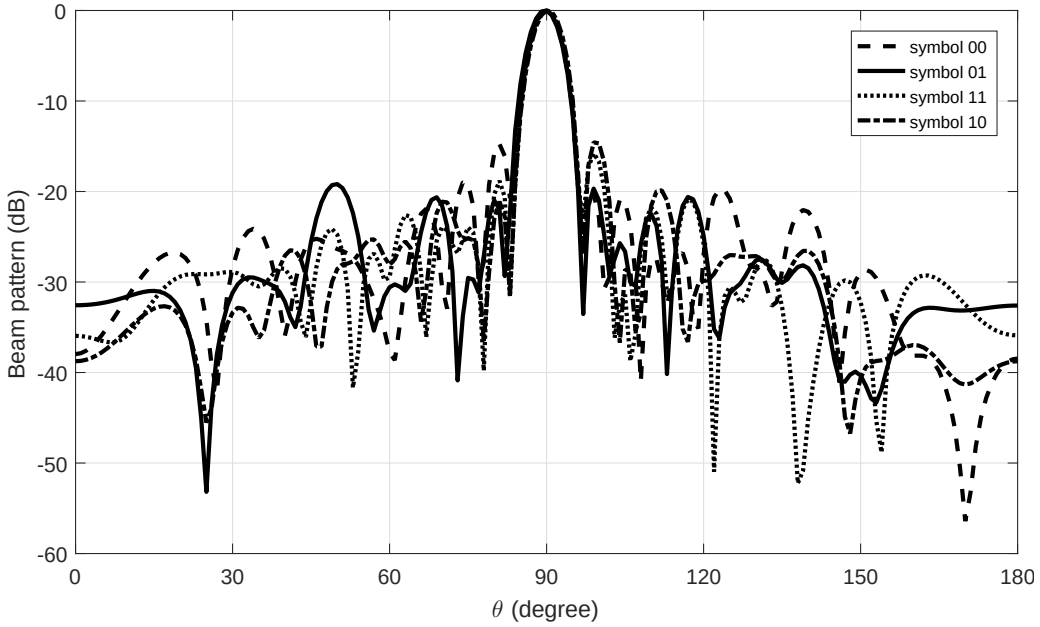

Figure 4.22: Simulated beam responses based on the broadside design using (4.8) for symbols '00, 01, 11, 10' without PAPR constraint.

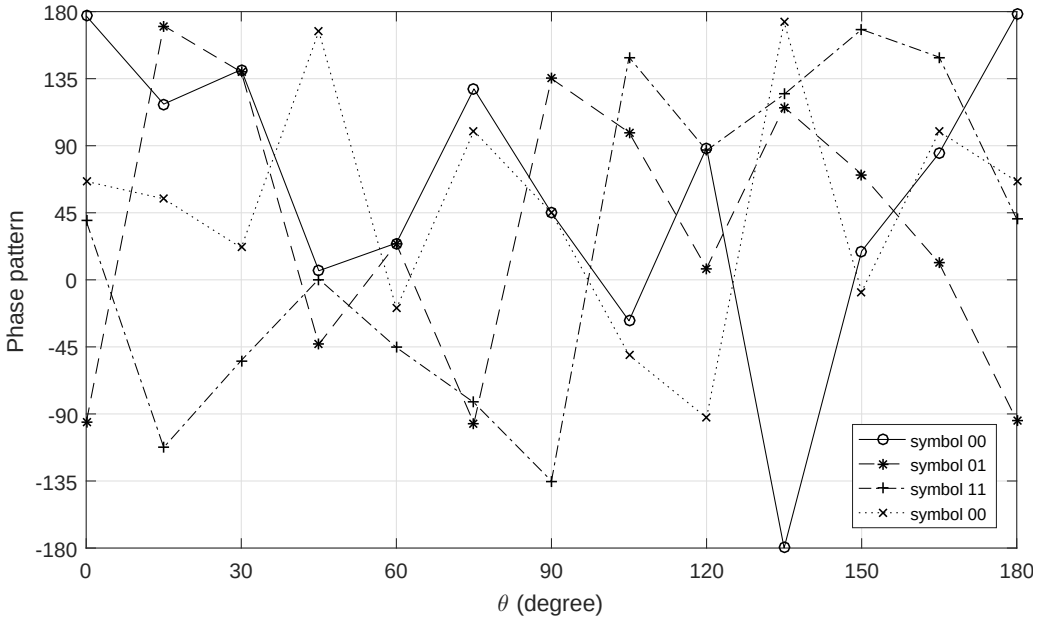

Figure 4.23: Simulated phase patterns based on the broadside design using (4.8) for symbols '00, 01, 11, 00' without PAPR constraint.

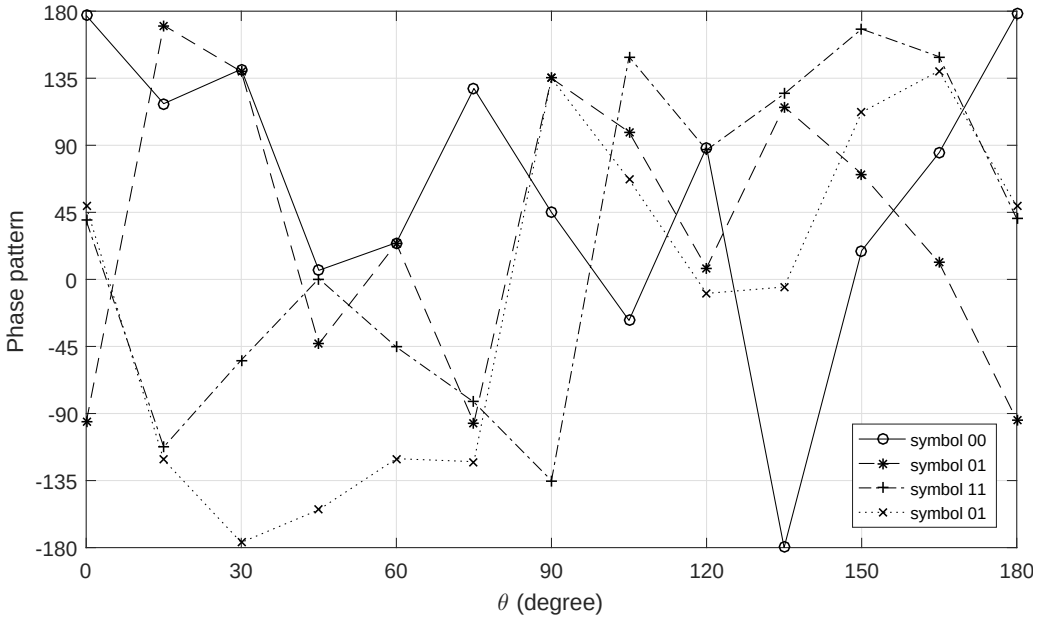

Figure 4.24: Simulated phase patterns based on the broadside design using (4.8) for symbols '00, 01, 11, 01' without PAPR constraint.

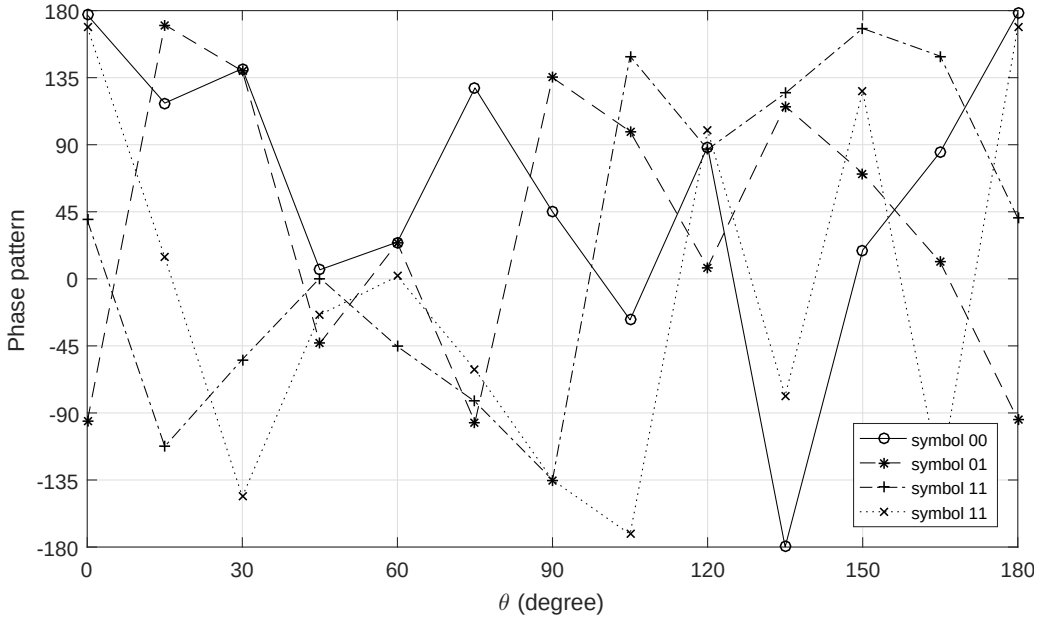

Figure 4.25: Simulated phase patterns based on the broadside design using (4.8) for symbols '00, 01, 11, 11' without PAPR constraint.

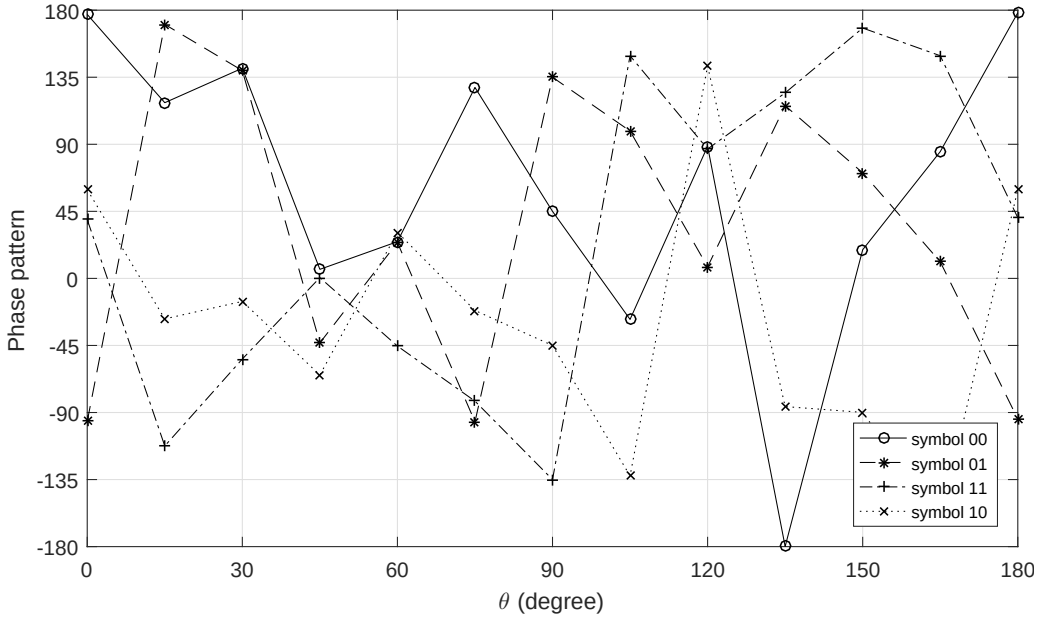

Figure 4.26: Simulated phase patterns based on the broadside design using (4.8) for symbols '00, 01, 11, 10' without PAPR constraint.

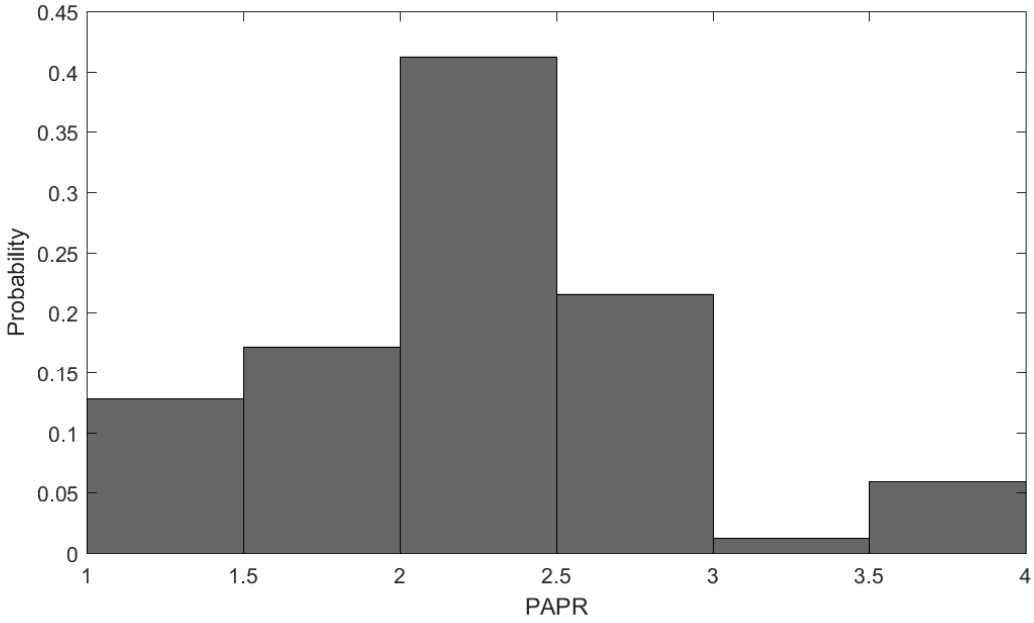

Figure 4.27: Histogram of PAPR based on design without PAPR constraint.

4.6.2 Broadside Design Example Subject to PAPR $\leq \rho$

The resultant beam and phase patterns for the symbols '00, 01, 11, 00', '00, 01, 11, 01', '00, 01, 11, 11', '00, 01, 11, 10' under PAPR ≤ 2.5 using (4.39) are shown in Figs. 4.28, 4.29, 4.30, 4.31, and Figs. 4.32, 4.33, 4.34, 4.35, demonstrating the satisfaction of the DM requirements. The beam and phase patterns for other symbols have the DM characteristics as well. The range of the PAPRs for all sets of inputs in this design are shown in Fig. 4.36, where all values are to the left of the value 2.5, which is the pre-defined PAPR threshold, representing the PAPR constraint has been satisfied in the design.

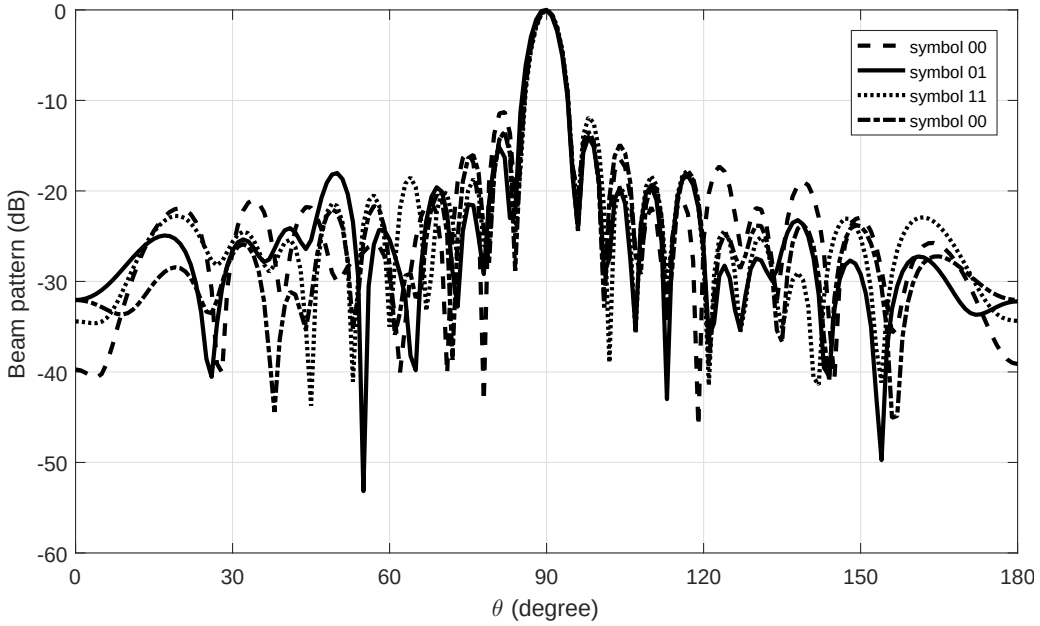

Figure 4.28: Simulated beam responses based on the broadside design using (4.32) for symbols '00, 01, 11, 00' when $\rho = 2.5$.

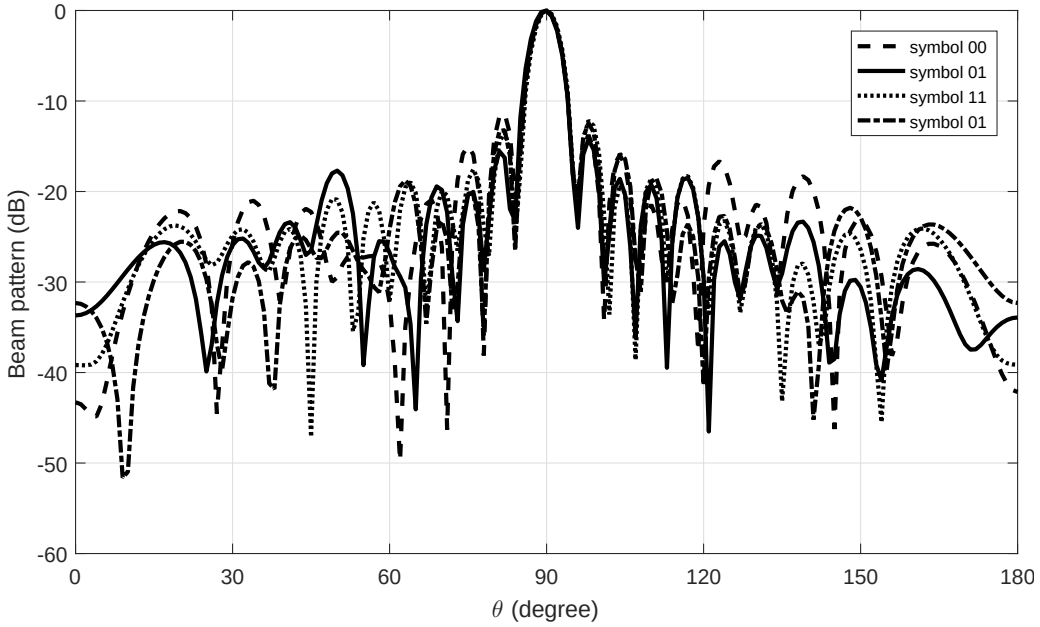

Figure 4.29: Simulated beam responses based on the broadside design using (4.32) for symbols '00, 01, 11, 01' when $\rho = 2.5$.

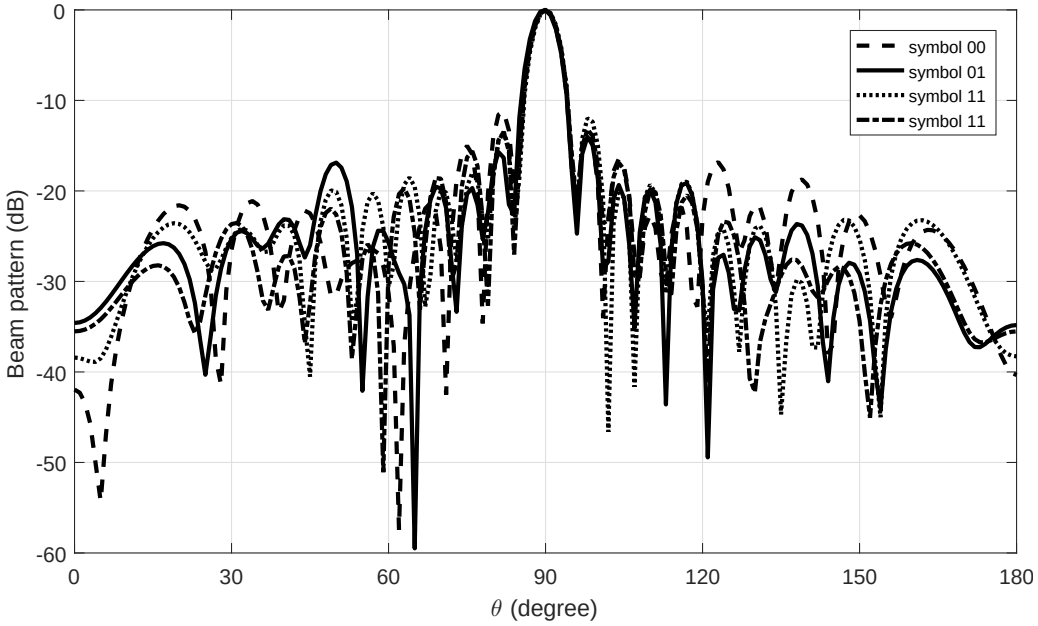

Figure 4.30: Simulated beam responses based on the broadside design using (4.32) for symbols '00, 01, 11, 11' when $\rho = 2.5$.

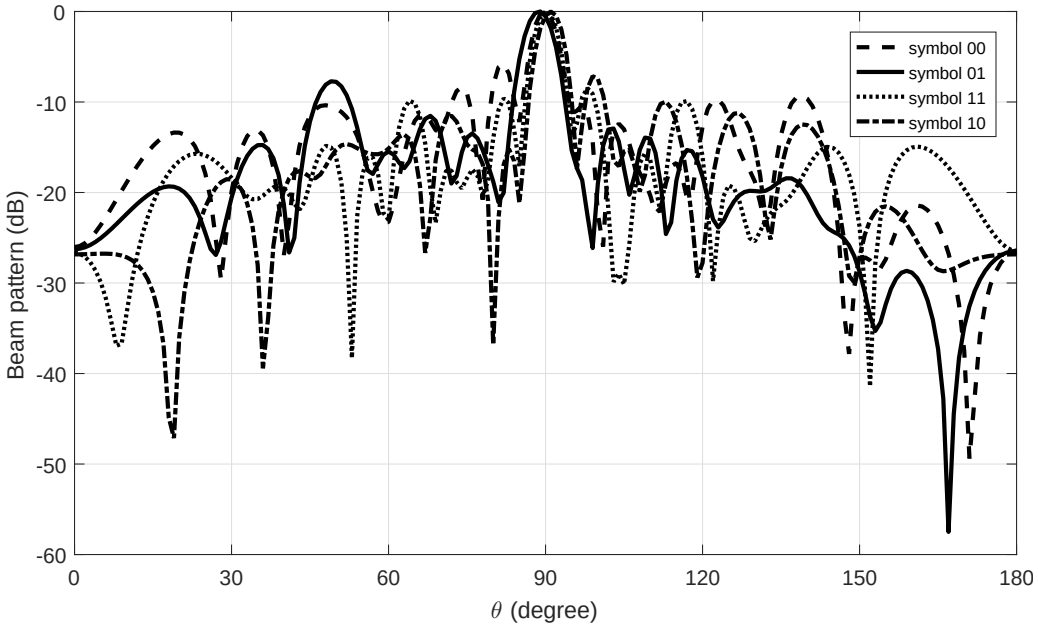

Figure 4.31: Simulated beam responses based on the broadside design using (4.32) for symbols '00, 01, 11, 10' when $\rho = 2.5$.

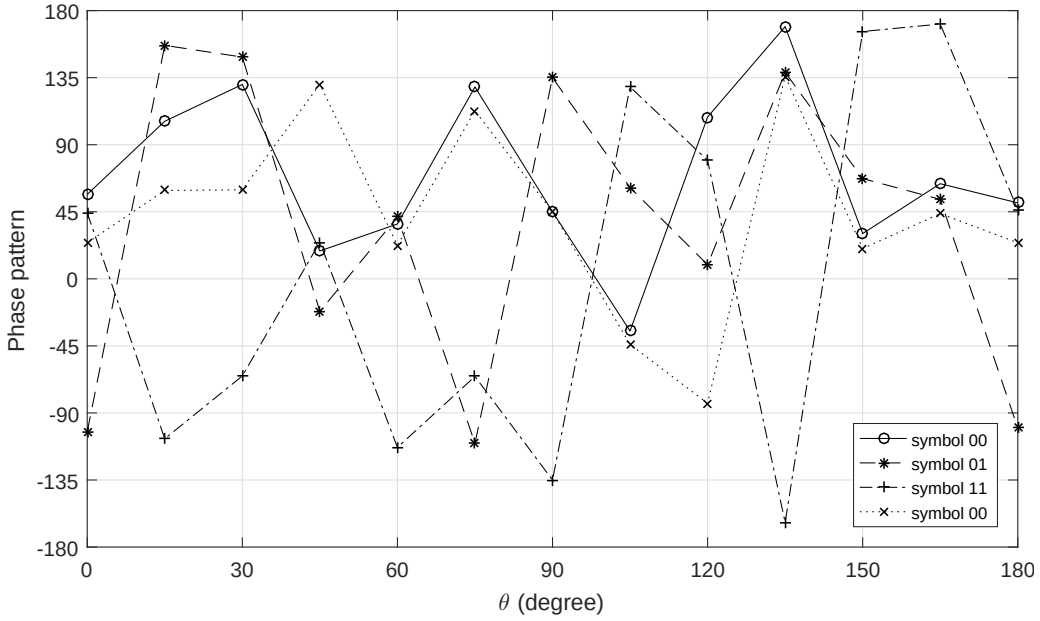

Figure 4.32: Simulated phase patterns based on the broadside design using (4.32) for symbols '00, 01, 11, 00' when $\rho = 2.5$.

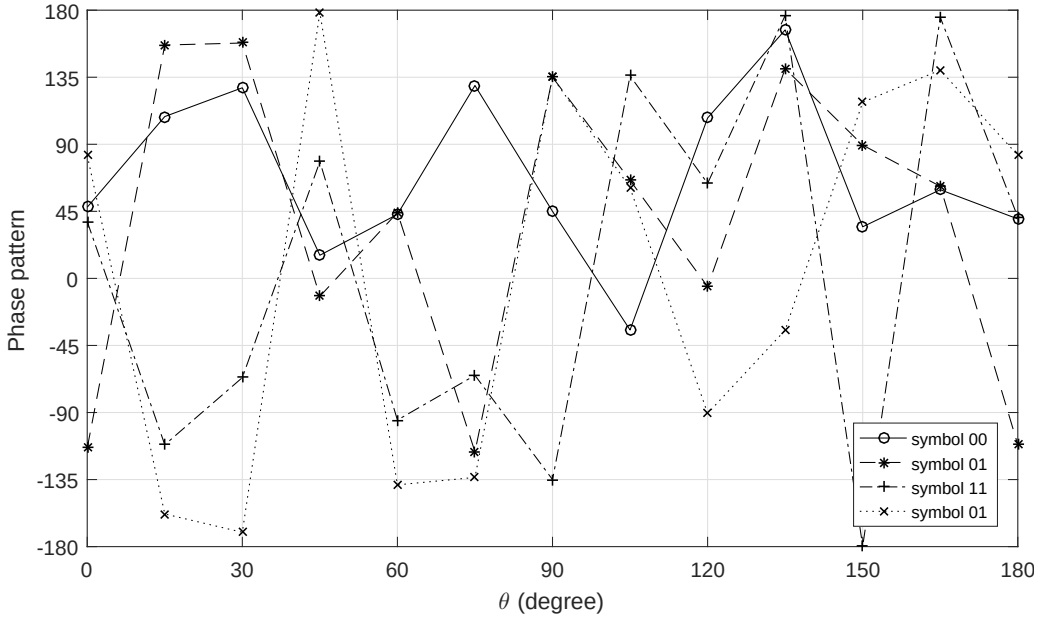

Figure 4.33: Simulated phase patterns based on the broadside design using (4.32) for symbols '00, 01, 11, 01' when $\rho = 2.5$.

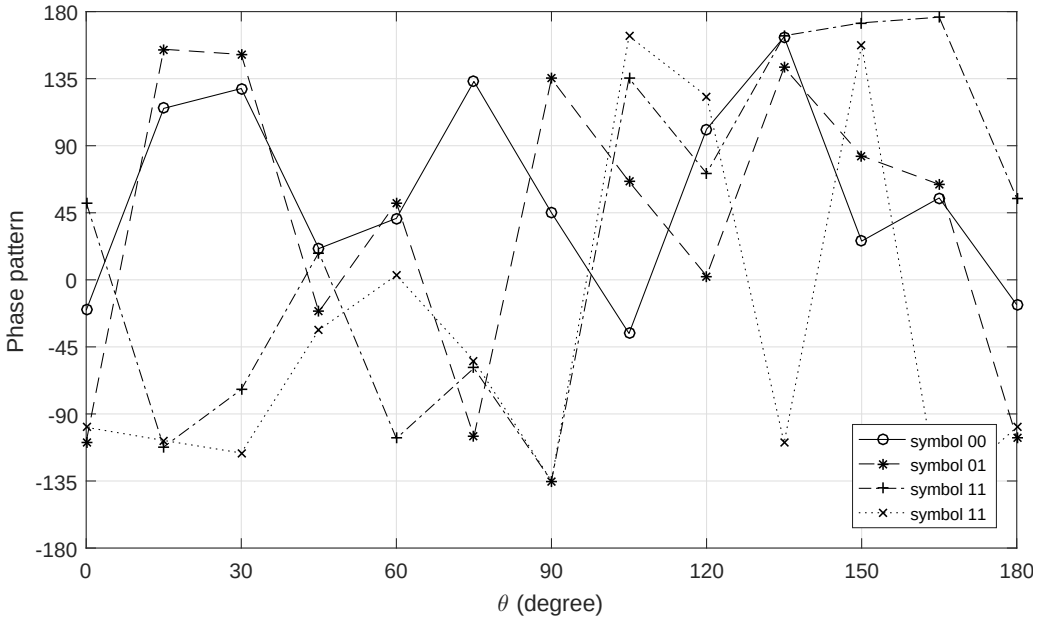

Figure 4.34: Simulated phase patterns based on the broadside design using (4.32) for symbols '00, 01, 11, 11' when $\rho = 2.5$.

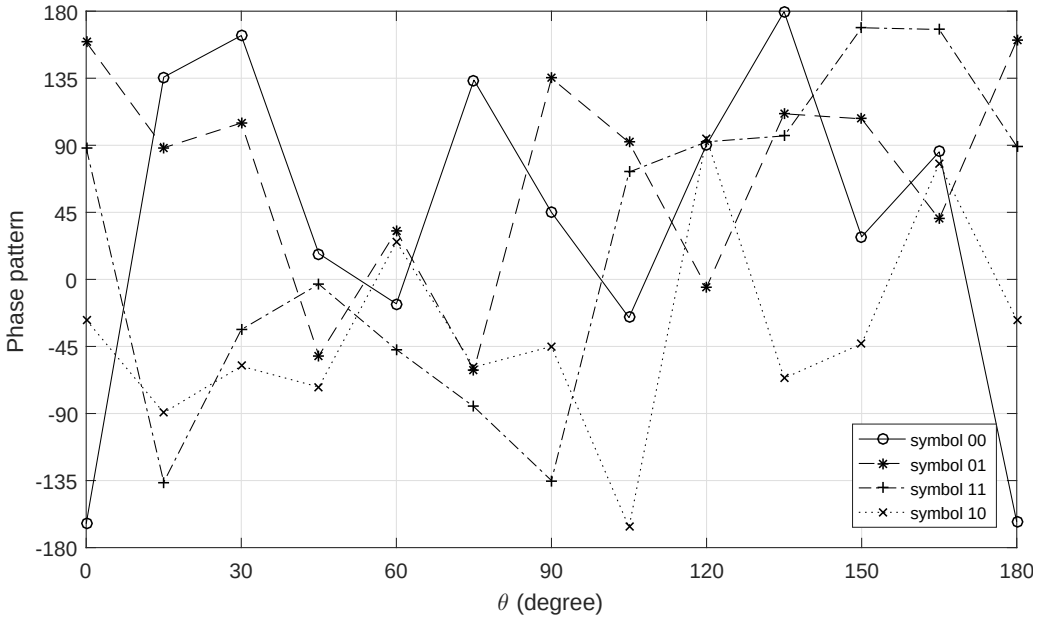

Figure 4.35: Simulated phase patterns based on the broadside design using (4.32) for symbols '00, 01, 11, 10' when $\rho = 2.5$.

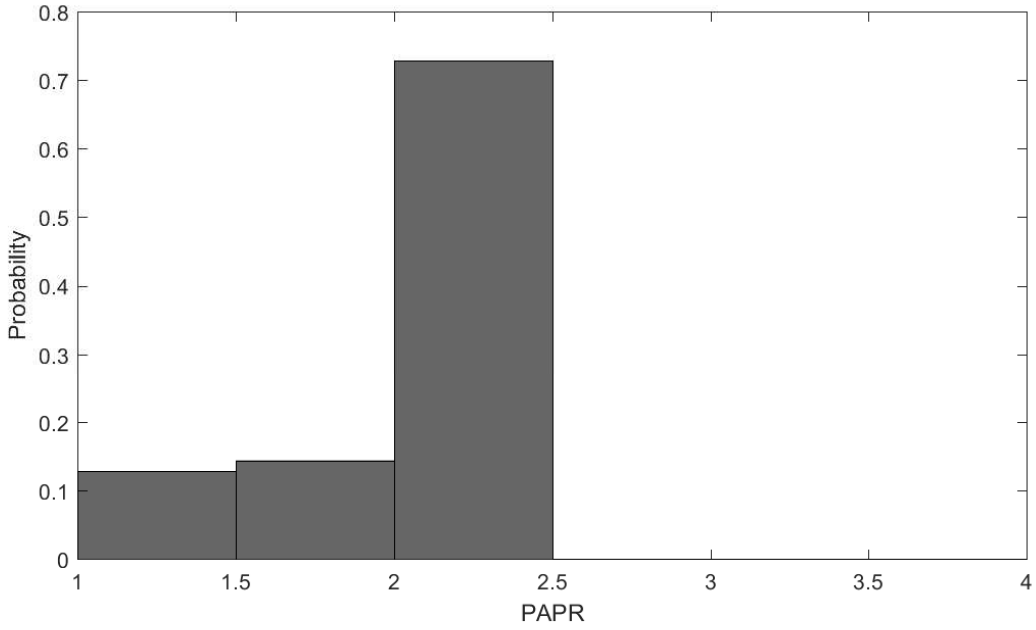

Figure 4.36: Histogram of PAPR based on broadside design using (4.32) when $\rho = 2.5$.

4.6.3 Off-Broadside Design Example Subject to PAPR $\leq \rho$

The resultant beam patterns for these four symbols are shown in Figs. 4.37, 4.38, 4.39, 4.40, where all the main beams pointed to the desired direction 120° with low sidelobe level in other directions. The corresponding phase patterns are displayed in Figs. 4.41, 4.42, 4.43, 4.44, where it can be seen that in the desired direction 120° the phases for these symbols are the same as the required QPSK modulation pattern, while in other directions the phase values are random. The beam and phase patterns for other symbols have the DM characteristics as well. Fig. 4.45 shows the histogram of PAPRs for all sets of inputs, demonstrating the PAPR constraint $\rho = 2.5$ has been satisfied in the design.

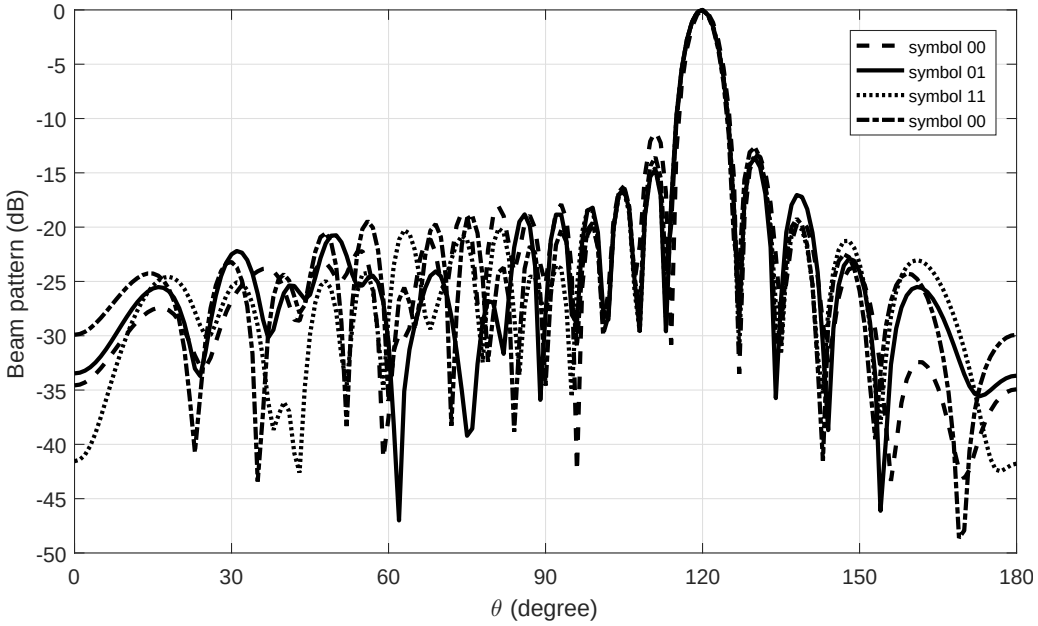

Figure 4.37: Simulated beam responses based on the off-broadside design using (4.32) for symbols '00,01,11,00' when $\rho = 2.5$.

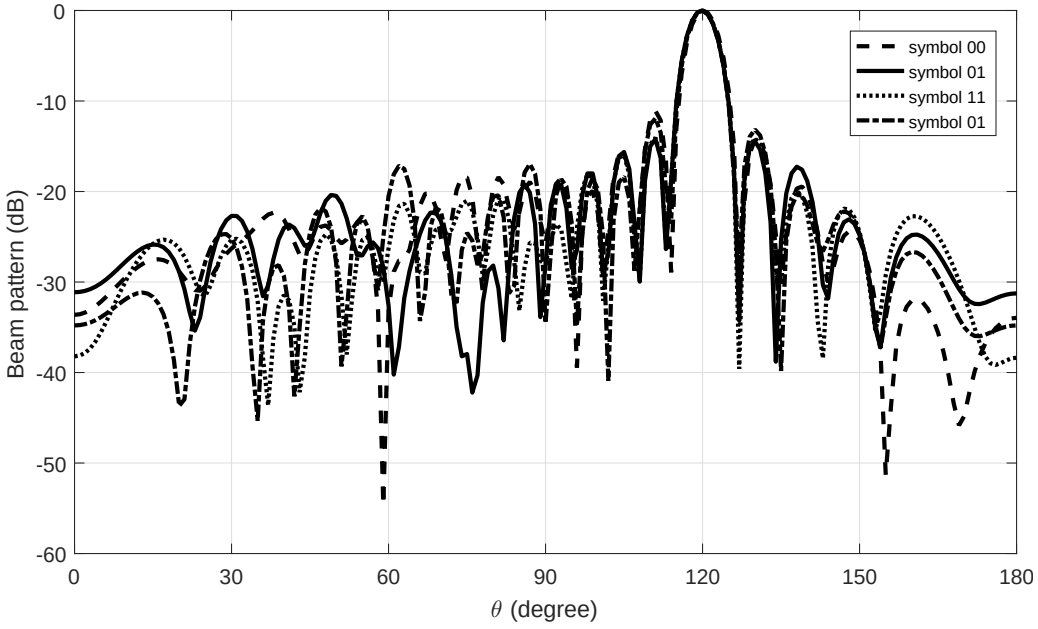

Figure 4.38: Simulated beam responses based on the off-broadside design using (4.32) for symbols '00,01,11,01' when $\rho = 2.5$.

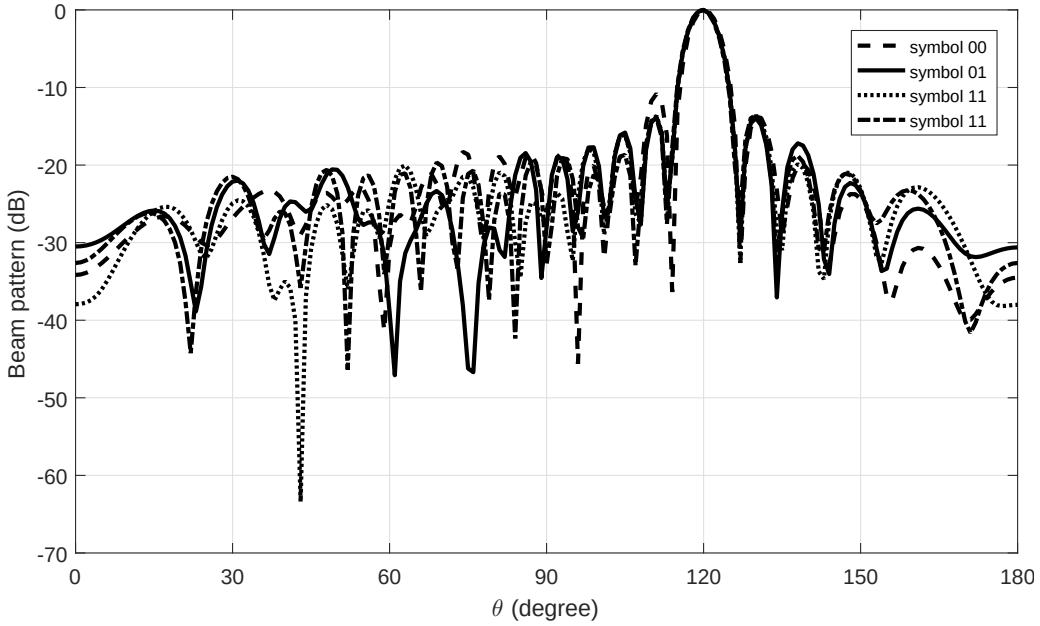

Figure 4.39: Simulated beam responses based on the off-broadside design using (4.32) for symbols '00,01,11,11' when $\rho = 2.5$.

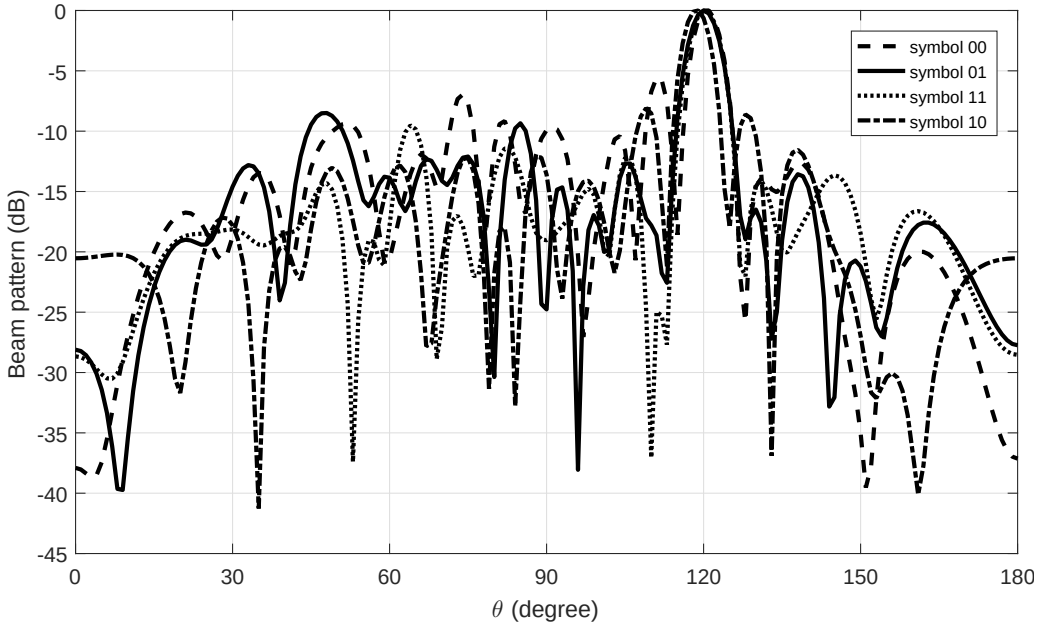

Figure 4.40: Simulated beam responses based on the off-broadside design using (4.32) for symbols '00,01,11,10' when $\rho = 2.5$.

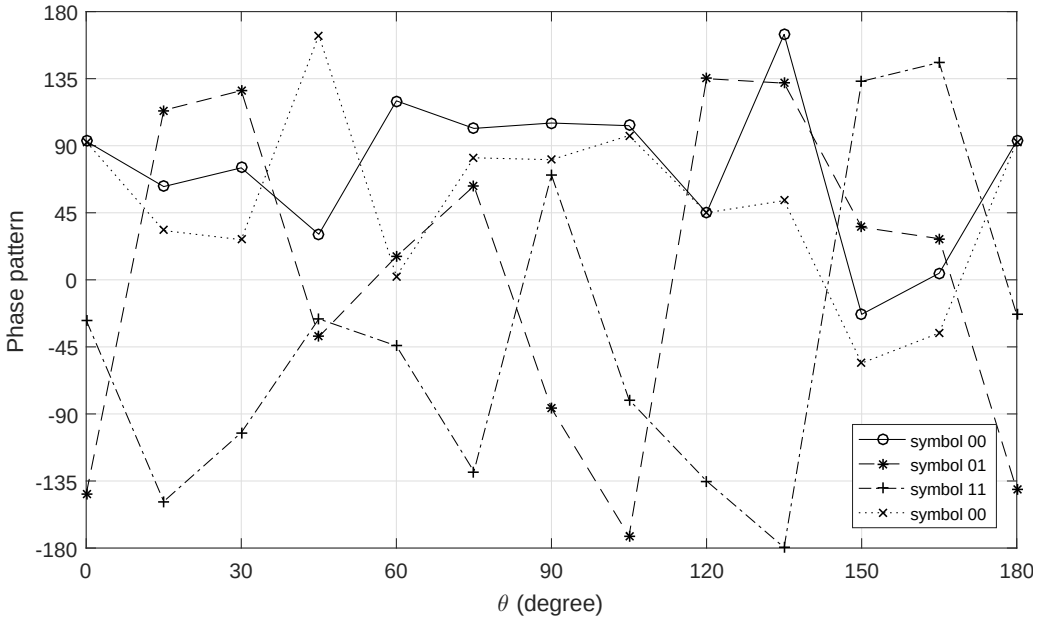

Figure 4.41: Simulated phase patterns based on the off-broadside design using (4.32) for symbols '00,01,11,00' when $\rho = 2.5$.

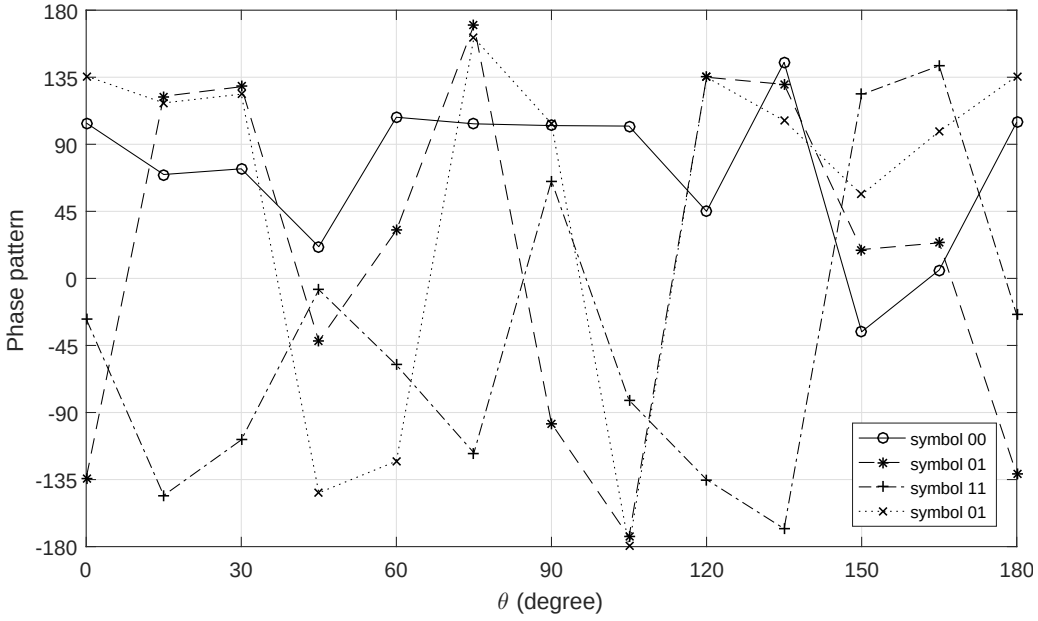

Figure 4.42: Simulated phase patterns based on the off-broadside design using (4.32) for symbols '00,01,11,01' when $\rho = 2.5$.

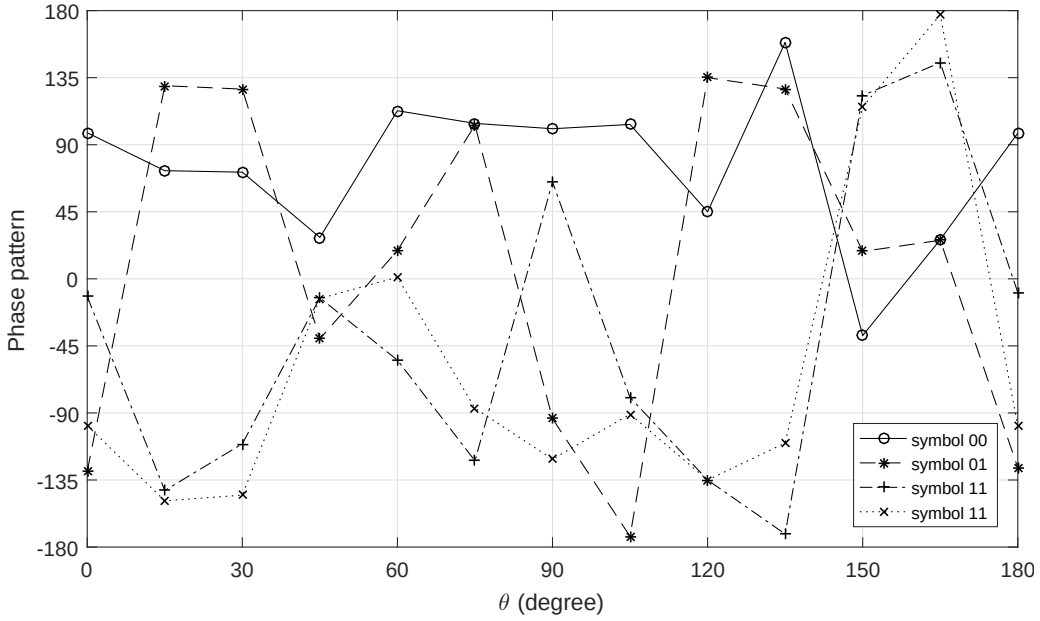

Figure 4.43: Simulated phase patterns based on the off-broadside design using (4.32) for symbols '00,01,11,11' when $\rho = 2.5$.

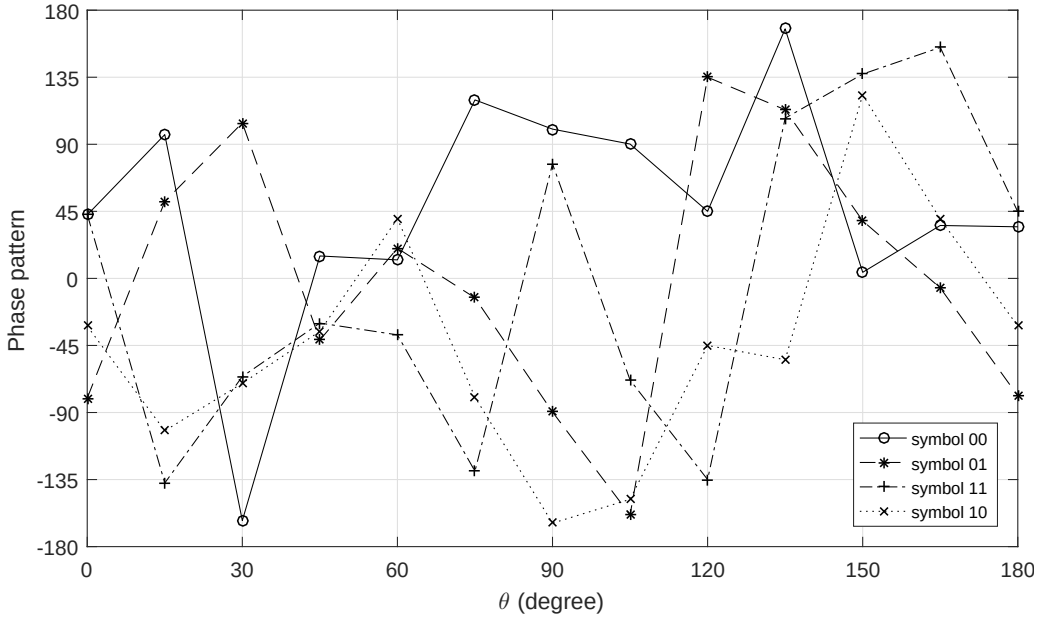

Figure 4.44: Simulated phase patterns based on the off-broadside design using (4.32) for symbols '00,01,11,10' when $\rho = 2.5$.

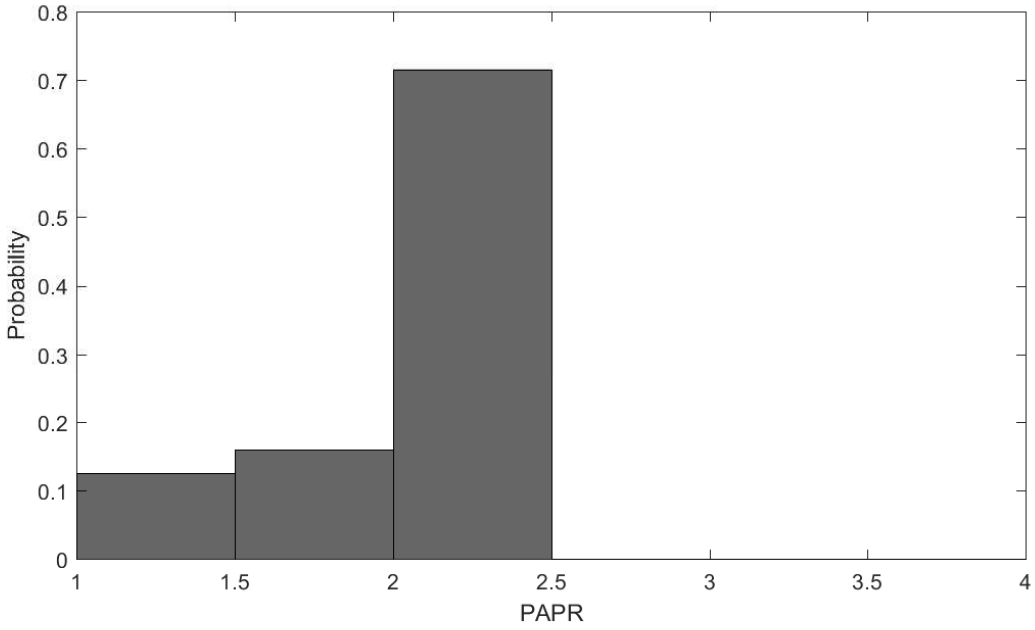

Figure 4.45: Histogram of PAPR based on the off-broadside design using (4.32) when $\rho = 2.5$.

4.7 Summary

In this chapter, a multi-carrier based antenna array structure for DM has been proposed for the first time, where a baseband implementation similar to the classic OFDM structure in wireless communications is derived. Then the antenna location optimisation problem in this context was studied and a class of CS-based design methods were developed. The key is to find a common set of sparse result for all modulation symbols at all frequencies using the concept of group sparsity. As shown in the provided design examples, in the context of DM, the sparse design has achieved a main lobe pointing to the desired direction with scrambled phases in other directions. In particular, the design can provide a sparse solution as expected, using less number of antennas with a satisfactory performance compared to the ULA design case.

Moreover, to solve the potential high peak to average power ratio problem in the antenna array design for IDFT based multi-carrier DM, a modified WBFIT method has been proposed to meet both the DM requirement and the PAPR constraint. It is a combi-

nation of the Newton's method and the existing WBFIT method in literature. As shown in the provided broadside and off-broadside design examples subject to $\rho \geq 1$, the main beams of the design results point to the desired direction and the phase responses follow the given constellation diagram in the mainlobe and random in the sidelobe, providing an effective DM performance; in the meantime, histograms show that the PAPR constraint has been met too.

Chapter 5

Orthogonally Polarised Dual-Channel Directional Modulation Based on Linear Crossed-Dipole Arrays

5.1 Introduction

In the traditional DM technique, there is only a single signal transmitted at one carrier frequency to the desired direction. To increase channel capacity in the context of one carrier frequency, in this chapter the polarisation information of the electromagnetic signal is exploited and two orthogonal polarised signals can be transmitted to the same direction at the same frequency simultaneously, as demonstrated in the recent conference publication [29]. For the electromagnetic wave the polarization is the plane in which the electric wave vibrates effectively. So for a vertical receiver antenna, it receives vertically polarised signals the best. Similarly, for a horizontal antenna, the horizontally polarised signals is received the best. Then the channel capacity is doubled compared with the design without polarisation consideration. These two signals can also be considered as one composite signal using the four dimensional (4-D) modulation scheme across the two polarisation diversity channels [72–74]. This can be achieved by employing polarisation-

sensitive arrays, such as tripole arrays and crossed-dipole arrays [72, 75–82]. To receive and separate the two orthogonally polarised signals, a crossed-dipole antenna or array is needed at the receiver side [82], and the polarisation directions of the antennas at the receiver side do not need to match those of the transmitted signals, as cross-interference due to a mismatch can be solved easily using some standard signal processing techniques, e.g. the Wiener filter based on a known reference signal [72].

Moreover, compared to the ULA design [29], to further exploit the DOFs [5, 6] in the spatial domain, the orthogonally polarised design for DM is applied to sparse antenna arrays. In this chapter, the CS-based formulation is applied to the design. In the context of M-ary signaling, assume there are M symbols for each of the two signals s_1 and s_2. Then, for the two signals transmitted simultaneously, there will be M^2 combined symbols in total. The key is to find a set of common crossed-dipole locations for all M^2 combined symbols, which can be solved using the group sparsity technique [67]; otherwise, the design would end up with different antenna locations for different symbols.

The remaining part of this chapter is structured as follows. A review of polarised beamforming based on crossed-dipole arrays is given in Sec. 5.2. DM designs for two signals transmitted to the same direction at the same frequency, but with orthogonal polarisation states, based on either a given fixed array geometry or an array with optimised crossed-dipole locations are presented in Sec. 5.3. Design examples are provided in Sec. 5.4 and conclusions drawn in Sec. 5.5.

5.2 Polarisation-Sensitive Beamforming

Fig. 5.1 shows the structure of an N-element linear crossed-dipole array. Each antenna has two orthogonally orientated dipoles, and the one parallel to the x-axis is connected to a complex-valued coefficient, represented by $w_{n,x}$, and the one parallel to the y-axis is connected to $w_{n,y}$ for $n = 0, \ldots, N-1$. The spacing between the zeroth and the n-th antenna is denoted by d_n ($n = 1, \ldots, N-1$), and the aperture of the array is d_{N-1}. The elevation angle and azimuth angle are denoted by $\theta \in [0, \pi]$ and $\phi \in [0, 2\pi]$, respectively.

For a transverse electromagnetic (TEM) wave in the far-field from the transmitter

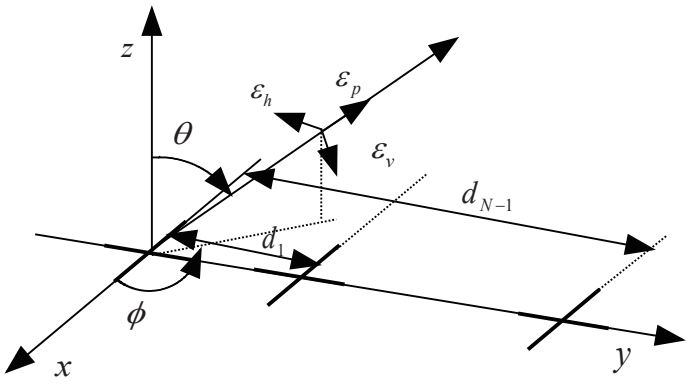

Figure 5.1: A linear crossed-dipole antenna array.

array, ε_p is considered as the unit vector of the transmission direction of the TEM wave, and ε_h and ε_v are two orthogonal unit vectors, and also at right angle to ε_p, i.e., $\varepsilon_h \cdot \varepsilon_v = 0$, $\varepsilon_h \cdot \varepsilon_p = 0$, and $\varepsilon_v \cdot \varepsilon_p = 0$. Based on the transmission direction in the transmitter coordinate system,

$$\varepsilon_p = [\sin\theta\cos\phi, \sin\theta\sin\phi, \cos\theta]^T, \tag{5.1}$$

where $\{\cdot\}^T$ is the transpose operation. The choice of ε_h and ε_v is not unique. Based on the orthogonality of these three unit vectors, normally it is assumed that

$$\begin{aligned} \varepsilon_h &= [-\sin\phi, \cos\phi, 0]^T, \\ \varepsilon_v &= [\cos\theta\cos\phi, \cos\theta\sin\phi, -\sin\theta]^T. \end{aligned} \tag{5.2}$$

Here it can be seen that ε_h is parallel to the x-y plane, due to the zero value in the z direction, then ε_h is assumed as the unit vector of the horizontal component. Since ε_v is perpendicular to ε_p ($\varepsilon_v \cdot \varepsilon_p = 0$), ε_v is considered as the unit vector of the vertical component.

Moreover, the electric field is assumed to have transverse components [75, 76],

$$E = E_h\varepsilon_h + E_v\varepsilon_v, \tag{5.3}$$

where E_h and E_v correspond to the horizontal component and the vertical component, respectively [83], given by

$$\begin{bmatrix} E_h \\ E_v \end{bmatrix} = \begin{bmatrix} He^{j\omega t} \\ Ve^{j\omega t} \end{bmatrix} = \begin{bmatrix} a_h e^{j\psi_h} e^{j\omega t} \\ a_v e^{j\psi_v} e^{j\omega t} \end{bmatrix}, \tag{5.4}$$

where ω represents carrier frequency, H and V are complex numbers, a_h and a_v are amplitudes (positive and real-valued) of the horizontal and vertical components, and ψ_h and ψ_v are the corresponding initial phases. The polarisation ratio is represented by $\frac{V}{H} = \frac{a_v e^{j\psi_v}}{a_h e^{j\psi_h}} = (\tan\gamma)e^{j\eta}$ for $\gamma \in [0, \pi/2]$ and $\eta \in (-\pi, \pi]$, where $\tan\gamma$ represents the amplitude ratio, and η is the phase difference between two components [83].

In the case of $a_h \neq 0$, $\gamma \in [0, \pi/2)$, with the amplitude A of the polarised signal given by $A = \sqrt{|H|^2 + |V|^2}$,

$$A = \sqrt{a_h^2 + a_v^2} = a_h\sqrt{1 + (\tan\gamma)^2} = a_h\frac{1}{\cos\gamma}. \tag{5.5}$$

Based on this,

$$\begin{aligned} a_h &= A\cos\gamma \\ a_h e^{j\psi_h} &= A(\cos\gamma)e^{j\psi_h} \\ H &= A(\cos\gamma)e^{j\psi_h}. \end{aligned} \tag{5.6}$$

Similarly,

$$\begin{aligned} A &= a_v\frac{1}{\sin\gamma} \\ V &= A(\sin\gamma)e^{j\psi_v}. \end{aligned} \tag{5.7}$$

For $a_h = 0$ when there is no horizontal component and $\gamma = \pi/2$,

$$\begin{aligned} \begin{bmatrix} H \\ V \end{bmatrix} &= \begin{bmatrix} 0 \\ a_v e^{j\psi_v} \end{bmatrix} \\ &= \frac{a_v e^{j\psi_v}}{e^{j\eta}} \begin{bmatrix} \cos\gamma \\ (\sin\gamma)e^{j\eta} \end{bmatrix} \\ &= a_v e^{j\psi_h} \begin{bmatrix} \cos\frac{\pi}{2} \\ (\sin\frac{\pi}{2})e^{j\eta} \end{bmatrix} \\ &= A \begin{bmatrix} (\cos\frac{\pi}{2})e^{j\psi_h} \\ (\sin\frac{\pi}{2})e^{j\psi_v} \end{bmatrix}. \end{aligned} \tag{5.8}$$

Therefore, for $\gamma \in [0, \pi/2], \eta \in (-\pi, \pi]$,

$$\begin{bmatrix} H \\ V \end{bmatrix} = A \begin{bmatrix} (\cos\gamma)e^{j\psi_h} \\ (\sin\gamma)e^{j\psi_v} \end{bmatrix}. \tag{5.9}$$

Here it is assumed that $\psi_h = 0$, which is acceptable, since what matters is the relative difference between the two phases. Therefore

$$\begin{bmatrix} H \\ V \end{bmatrix} = A \begin{bmatrix} \cos\gamma \\ (\sin\gamma)e^{j\eta} \end{bmatrix}. \tag{5.10}$$

Then the electric field can be given by

$$\begin{aligned} E =& E_h\varepsilon_h + E_v\varepsilon_v \\ =& A((\cos\gamma)\varepsilon_h + (\sin\gamma)e^{j\eta}\varepsilon_v) \\ =& A(\cos\gamma[-\sin\phi, \cos\phi, 0]^T \\ &+ (\sin\gamma)e^{j\eta}[\cos\theta\cos\phi, \cos\theta\sin\phi, -\sin\theta]^T) \\ =& A((-\cos\gamma\sin\phi + (\sin\gamma)e^{j\eta}\cos\theta\cos\phi)\hat{x} \\ &+ (\cos\gamma\cos\phi + (\sin\gamma)e^{j\eta}\cos\theta\sin\phi)\hat{y} \\ &- ((\sin\gamma)e^{j\eta}\sin\theta)\hat{z}), \end{aligned} \tag{5.11}$$

where the carrier wave $e^{j\omega t}$ is ignored. Considering the x- and y-axes where these dipoles are placed, a spatial-polarisation coherent vector $\mathbf{s}_p$ [82, 84] can be given by

$$\begin{aligned} \mathbf{s}_p(\theta, \phi, \gamma, \eta) &= \begin{bmatrix} s_{px}(\theta, \phi, \gamma, \eta) \\ s_{py}(\theta, \phi, \gamma, \eta) \end{bmatrix} \\ &= \begin{bmatrix} -\cos\gamma\sin\phi + (\sin\gamma)e^{j\eta}\cos\theta\cos\phi \\ \cos\gamma\cos\phi + (\sin\gamma)e^{j\eta}\cos\theta\sin\phi \end{bmatrix}. \end{aligned} \tag{5.12}$$

Here, the zeroth antenna located at the transmitter coordinate origin is assumed as the reference point, then the spatial steering vector of the array for transmission is a function of elevation angle θ and azimuth angle ϕ, given by

$$\mathbf{s}_s(\theta, \phi) = [1, e^{-j\omega d_1 \sin\theta\sin\phi/c}, \ldots, e^{-j\omega d_{N-1}\sin\theta\sin\phi/c}]^T, \tag{5.13}$$

where c is the propagation speed. For a ULA with a half-wavelength spacing ($d = \lambda/2$), the spatial steering vector can be simplified to

$$\mathbf{s}_s(\theta, \phi) = [1, e^{-j\pi\sin\theta\sin\phi}, \ldots, e^{-j\pi(N-1)\sin\theta\sin\phi}]^T. \tag{5.14}$$

For convenience, the array structure is split into two sub-arrays: one is parallel to the x-axis and the other is parallel to the y-axis. Then, the steering vectors of the two sub-arrays can be given by

$$\begin{aligned}\mathbf{s}_x(\theta,\phi,\gamma,\eta) =& s_{px}(\theta,\phi,\gamma,\eta)\mathbf{s}_s(\theta,\phi),\\ \mathbf{s}_y(\theta,\phi,\gamma,\eta) =& s_{py}(\theta,\phi,\gamma,\eta)\mathbf{s}_s(\theta,\phi).\end{aligned} \tag{5.15}$$

The beam response of the array is [85]

$$p(\theta,\phi,\gamma,\eta) = \mathbf{w}^H\mathbf{s}(\theta,\phi,\gamma,\eta), \tag{5.16}$$

where $\{\cdot\}^H$ represents the Hermitian transpose, $\mathbf{s}(\theta,\phi,\gamma,\eta)$ is the $2N\times 1$ steering vector of the array

$$\begin{aligned}\mathbf{s}(\theta,\phi,\gamma,\eta) =& [\mathbf{s}_x(\theta,\phi,\gamma,\eta),\mathbf{s}_y(\theta,\phi,\gamma,\eta)]^T,\\ \mathbf{s}_x(\theta,\phi,\gamma,\eta) =& [s_{0,x}(\theta,\phi,\gamma,\eta),\ldots,s_{N-1,x}(\theta,\phi,\gamma,\eta)]^T,\\ \mathbf{s}_y(\theta,\phi,\gamma,\eta) =& [s_{0,y}(\theta,\phi,\gamma,\eta),\ldots,s_{N-1,y}(\theta,\phi,\gamma,\eta)]^T,\end{aligned} \tag{5.17}$$

and $\mathbf{w}$ is the complex-valued weight vector

$$\mathbf{w} = [w_{0,x},\ldots,w_{N-1,x},w_{0,y},\ldots,w_{N-1,y}]^T. \tag{5.18}$$

5.3 Directional Modulation Design

5.3.1 Design with a Fixed Crossed-Dipole Array

In traditional DM, there is only one signal transmitted at one carrier frequency to the desired direction, and the weight coefficients are thus designed for one single signal. To increase channel capacity, in this section, a set of common weight coefficients is designed for two signals (s_1 and s_2) with orthogonal polarisation states transmitted to the same direction at the same frequency simultaneously. $\mathbf{s}(\theta,\phi,\gamma_1,\eta_1)$, $\mathbf{s}(\theta,\phi,\gamma_2,\eta_2)$, $p(\theta,\phi,\gamma_1,\eta_1)$, and $p(\theta,\phi,\gamma_2,\eta_2)$ are used to represent the steering vectors for s_1 and s_2, and beam responses for s_1 and s_2, respectively.

Here, it is assumed that ϕ is fixed, and r sampling points in the mainlobe and $\Theta - r$ points in the sidelobe for both s_1 and s_2 are sampled. Then, a $2N\times 2r$ matrix $\mathbf{S}_{ML}$ can

be constructed for steering vectors of two signals in the mainlobe, and a $2N \times 2(\Theta - r)$ matrix $\mathbf{S}_{SL}$ includes all steering vectors over the sidelobe range [30],

$$\begin{aligned}\mathbf{S}_{SL} = [&\mathbf{s}(\theta_0, \phi, \gamma_1, \eta_1), \ldots, \mathbf{s}(\theta_{\Theta-r-1}, \phi, \gamma_1, \eta_1) \\ &\mathbf{s}(\theta_0, \phi, \gamma_2, \eta_2), \ldots, \mathbf{s}(\theta_{\Theta-r-1}, \phi, \gamma_2, \eta_2)], \\ \mathbf{S}_{ML} = [&\mathbf{s}(\theta_{\Theta-r}, \phi, \gamma_1, \eta_1), \ldots, \mathbf{s}(\theta_{\Theta-1}, \phi, \gamma_1, \eta_1) \\ &\mathbf{s}(\theta_{\Theta-r}, \phi, \gamma_2, \eta_2), \ldots, \mathbf{s}(\theta_{\Theta-1}, \phi, \gamma_2, \eta_2)].\end{aligned} \tag{5.19}$$

Moreover, for M-ary signaling, each of s_1 and s_2 can create M constellation points (M symbols), leading to M desired responses. Then, for both signals transmitted simultaneously, there are M^2 different symbols and M^2 sets of response pairs. According to the direction of the elevation angle θ, $\mathbf{p}_{SL,m}$ and $\mathbf{p}_{ML,m}$ can be defined as beam responses over the sidelobe and mainlobe directions for the m-th symbol, where $m = 0, \ldots, M^2 - 1$,

$$\begin{aligned}\mathbf{p}_{SL,m} = [&p_m(\theta_0, \phi, \gamma_1, \eta_1), \ldots, p_m(\theta_{\Theta-r-1}, \phi, \gamma_1, \eta_1) \\ &p_m(\theta_0, \phi, \gamma_2, \eta_2), \ldots, p_m(\theta_{\Theta-r-1}, \phi, \gamma_2, \eta_2)], \\ \mathbf{p}_{ML,m} = [&p_m(\theta_{R-r}, \phi, \gamma_1, \eta_1), \ldots, p_m(\theta_{\Theta-1}, \phi, \gamma_1, \eta_1) \\ &p_m(\theta_{R-r}, \phi, \gamma_2, \eta_2), \ldots, p_m(\theta_{\Theta-1}, \phi, \gamma_2, \eta_2)] \ .\end{aligned} \tag{5.20}$$

Then, the weight coefficients for the m-th symbol can be solved by

$$\begin{aligned}\min_{\mathbf{w}_m} \quad & ||\mathbf{p}_{SL,m} - \mathbf{w}_m^H \mathbf{S}_{SL}||_2 \\ \text{subject to} \quad & \mathbf{w}_m^H \mathbf{S}_{ML} = \mathbf{p}_{ML,m},\end{aligned} \tag{5.21}$$

where $\mathbf{w}_m = [w_{0,x,m}, \ldots, w_{N-1,x,m}, w_{0,y,m}, \ldots, w_{N-1,y,m}]^T$ corresponds to the m-th response pair $\mathbf{p}_m(\theta, \phi, \gamma, \eta) = [\mathbf{p}_{SL,m}, \mathbf{p}_{ML,m}]$, and $||\cdot||_2$ denotes the l_2 norm. The problem in (5.21) can be solved by the method of Lagrange multipliers and the optimum value for the coefficients $\mathbf{w}_m$ can be found in the earlier conference publication [29], which is given by

$$\begin{aligned}\mathbf{w}_m = &\mathbf{R}^{-1}(\mathbf{S}_{SL}\mathbf{p}_{SL,m}^H - \mathbf{S}_{ML}((\mathbf{S}_{ML}^H \mathbf{R}^{-1} \mathbf{S}_{ML})^{-1} \\ &\times (\mathbf{S}_{ML}^H \mathbf{R}^{-1} \mathbf{S}_{SL} \mathbf{p}_{SL,m}^H - \mathbf{p}_{ML,m}^H))),\end{aligned} \tag{5.22}$$

where $\mathbf{R} = \mathbf{S}_{SL}\mathbf{S}_{SL}^H$.

5.3.2 Sparse Array Design

The intention of sparse array design using CS-based methods is to find the minimum number of non-zero valued weight coefficients from a large number of potential antennas to generate a response close to the desired one. As antennas with zero-valued coefficients are removed, the objective function for finding the minimum number of weight coefficients can be given by $\min ||\mathbf{w}||_1$, where the l_1 norm $||\cdot||_1$ is used as an approximation to the l_0 norm $||\cdot||_0$, and the constraint for keeping the difference between desired and designed responses under a given threshold value can be written as $||\mathbf{p} - \mathbf{w}^H\mathbf{S}||_2 \leq \alpha$, where α represents the allowed difference. Based on this idea of sparse array design, weight vector $\mathbf{w}_m$ for the m-th constellation points in (5.21) can be adjusted to

$$\begin{aligned} \min_{\mathbf{w}_m} \quad & ||\mathbf{w}_m||_1 \\ \text{subject to} \quad & ||\mathbf{p}_{SL,m} - \mathbf{w}_m^H\mathbf{S}_{SL}||_2 \leq \alpha \\ & \mathbf{w}_m^H\mathbf{S}_{ML} = \mathbf{p}_{ML,m}. \end{aligned} \tag{5.23}$$

As the location optimisation in (5.23) is calculated individually for each constellation point, the same set of active crossed-dipole positions cannot be guaranteed for all symbols; in other words, the antenna with weight coefficients which are zero-valued for some symbols but non-zero-valued for others, cannot be removed. To solve the problem, group sparsity is introduced [67] to find a common set of active antenna locations for all constellation points. In this design, group sparsity is applied to allow all elements in the vector $\tilde{\mathbf{w}}_n$ to be minimised simultaneously, e.g. to remove the n-th antenna, the vector $\tilde{\mathbf{w}}_n$ needs to be zero-valued

$$\tilde{\mathbf{w}}_n = [w_{n,x,0}, \ldots, w_{n,x,M^2-1}, w_{n,y,0}, \ldots, w_{n,y,M^2-1}]. \tag{5.24}$$

Then, the cost function for finding the minimum number of antenna locations can be considered as finding $\min ||\hat{\mathbf{w}}||_1$, where $\hat{\mathbf{w}}$ gathers all $||\tilde{\mathbf{w}}_n||_2$ for $n = 0, \ldots, N-1$,

$$\hat{\mathbf{w}} = [||\tilde{\mathbf{w}}_0||_2, ||\tilde{\mathbf{w}}_1||_2, \ldots, ||\tilde{\mathbf{w}}_{N-1}||_2]^T. \tag{5.25}$$

Moreover, to impose DM constraints on all constellation points, the following matrices

are first constructed

$$\begin{aligned}
\mathbf{W} &= [\mathbf{w}_0, \mathbf{w}_1, \ldots, \mathbf{w}_{M^2-1}], && (5.26)\\
\mathbf{P}_{SL} &= [\mathbf{p}_{SL,0}, \mathbf{p}_{SL,1}, \ldots, \mathbf{p}_{SL,M^2-1}]^T, && (5.27)\\
\mathbf{P}_{ML} &= [\mathbf{p}_{ML,0}, \mathbf{p}_{ML,1}, \ldots, \mathbf{p}_{ML,M^2-1}]^T \ . && (5.28)
\end{aligned}$$

Then, the sparse crossed-dipole antenna array design with group sparsity for all constellation points can be formulated as

$$\begin{aligned}
\min_{\mathbf{W}} \quad & ||\hat{\mathbf{w}}||_1 \\
\text{subject to} \quad & ||\mathbf{P}_{SL} - \mathbf{W}^H \mathbf{S}_{SL}||_2 \leq \alpha \\
& \mathbf{W}^H \mathbf{S}_{ML} = \mathbf{P}_{ML} \ .
\end{aligned} \tag{5.29}$$

The above problem can be solved using cvx, a package for specifying and solving convex problems [46, 47].

As the reweighted l_1 norm minimisation has a closer approximation to the l_0 norm [48–50], (5.29) can be further modified into the reweighted form in a similar way as in [28]. For the reweighted design, at the i-th iteration, the above formulations (5.29) becomes

$$\begin{aligned}
\min_{\mathbf{W}} \quad & \sum_{n=0}^{N-1} \delta_n^i ||\tilde{\mathbf{w}}_n^i||_2 \\
\text{subject to} \quad & ||\mathbf{P}_{SL} - (\mathbf{W}^i)^H \mathbf{S}_{SL}||_2 \leq \alpha \\
& (\mathbf{W}^i)^H \mathbf{S}_{ML} = \mathbf{P}_{ML} \ ,
\end{aligned} \tag{5.30}$$

where the superscript i indicates the value of the corresponding parameters at the i-th iteration, and δ_n is the reweighting term for the n-th row of coefficients, given by $\delta_n^i = (||\tilde{\mathbf{w}}_n^{i-1}||_2 + \kappa)^{-1}$. The iteration process is the same as in [28].

To receive and separate two orthogonally polarised signals, a crossed-dipole antenna or array is needed [82], and the polarisation directions of the antennas at the receiver side in the desired direction do not need to match those of the transmitted signals, as cross-interference due to a polarisation direction mismatch can be solved easily using some standard signal processing techniques, e.g. the Wiener filter based on a known reference signal [72].

5.4 Design Examples

In this section, design examples are provided to show the performance of the proposed design methods for both ULAs and sparse antenna arrays. For each of s_1 and s_2, the desired response is a value of one (magnitude) with a given phase at the mainlobe (QPSK), i.e., symbols '00', '01', '11', '10' correspond to 45°, 135°, −135° and −45°, respectively, and a value of 0.1 (magnitude) with random phase over the sidelobe regions. Therefore, for signals s_1 and s_2 transmitted simultaneously, 16 different symbols can be constructed. The polarisation states for s_1 are defined by $(\gamma_1, \eta_1) = (0°, 0°)$ for a horizontal polarisation, and $(\gamma_2, \eta_2) = (90°, 0°)$ for s_2 for a vertical polarisation. Moreover, without loss of generality, the mainlobe direction is assumed to be $\theta_{ML} = 0°$ for $\phi = 90°$ and the sidelobe regions are $\theta_{SL} \in [5°, 90°]$ for $\phi = \pm 90°$, sampled every 1°, representing two signals are transmitted through the y-z plane.

To have a fair comparison, the DM result by (5.21) is first obtained based on a 9λ aperture ULA with a half wavelength spacing between adjacent antennas. Then the error norm between the desired and designed responses from (5.21) is set as the allowed difference α in (5.29) and (5.30) for sparse array designs.

To verify the performance of each design, beam and phase patterns are provided for each set of constellation points to demonstrate DM has been achieved. Moreover, bit error rate (BER) is also presented. Here the signal to noise ratio (SNR) is set at 12 dB in the mainlobe direction, and assuming the additive white Gaussian noise (AWGN) level is the same for all directions, then the SNR value at the sidelobe directions will be much smaller.

5.4.1 Design Example with a Given Array Geometry

With the above parameters and design formulations in (5.21), Figs. 5.2, 5.3, 5.4 and 5.5 show the beam responses for symbols '00,00', '00,01', '00,11' and '00,10', and their corresponding phase patterns are displayed in Figs. 5.6, 5.7, 5.8, 5.9. It can be observed that all main beams are exactly pointed to 0° (the desired direction) with a low sidelobe level. The mainlobe power level for the composite signal s_{Re} is 3.01dB ($\sqrt{2}$ magnitude),

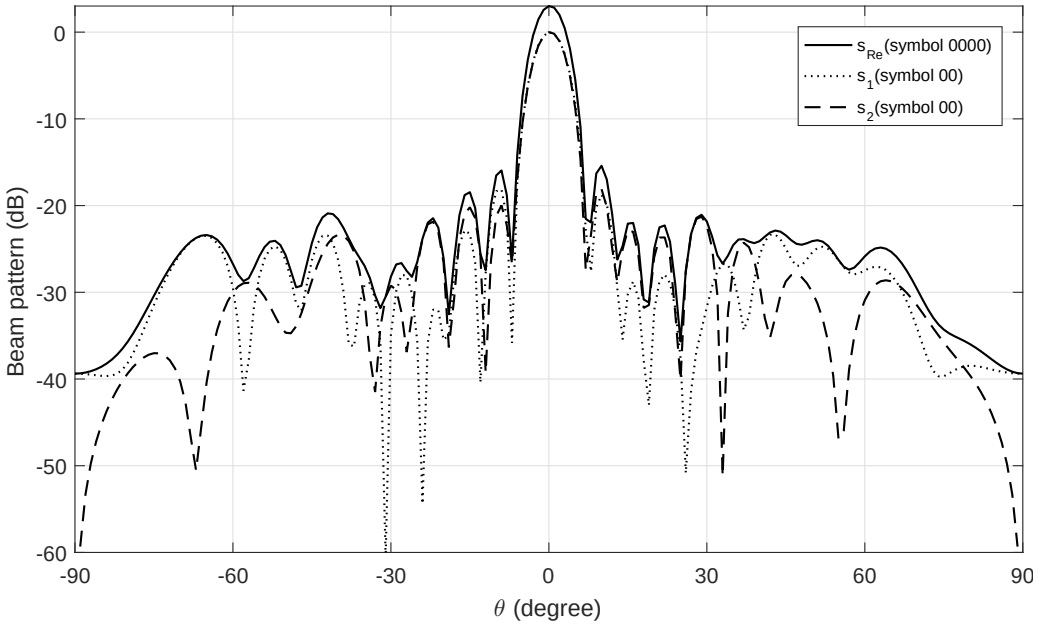

Figure 5.2: Simulated beam responses based on the crossed-dipole ULA (5.21) for symbols '00,00'.

and its corresponding components for s_1 and s_2 coincide in the mainlobe direction with 0dB power level, representing that a value of one for magnitude of the desired signals s_1 and s_2 has been satisfied. The phases of s_1 and s_2 in the desired direction are in accordance with the standard QPSK constellation, while they are random for the rest of the directions, demonstrating that DM has been achieved. The beam and phase patterns for the other symbols are not shown as they have the same features as the above.

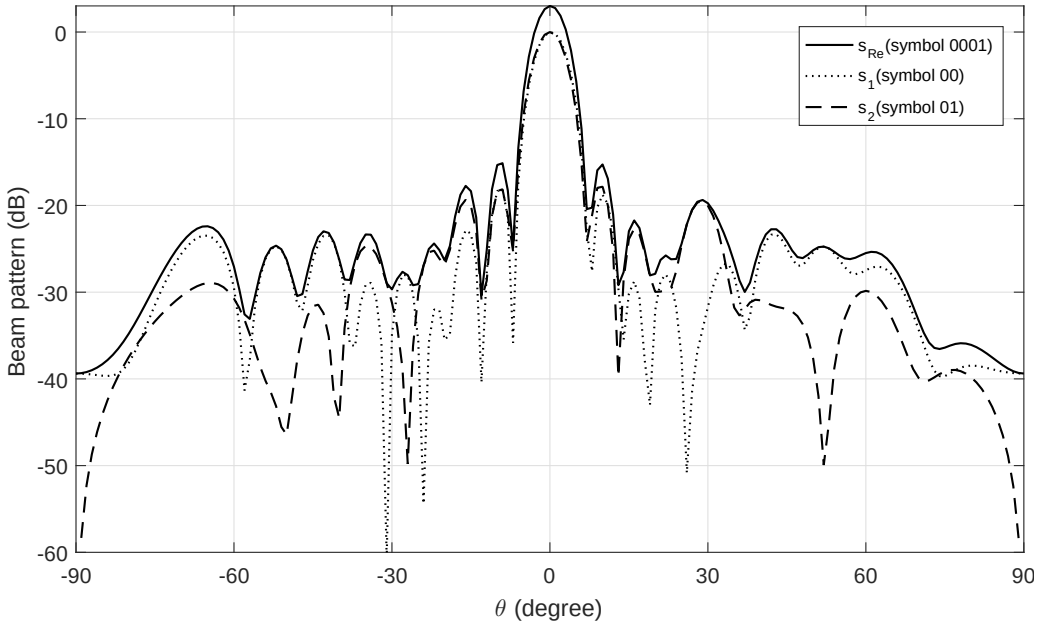

Figure 5.3: Simulated beam responses based on the crossed-dipole ULA (5.21) for symbols '00,01'.

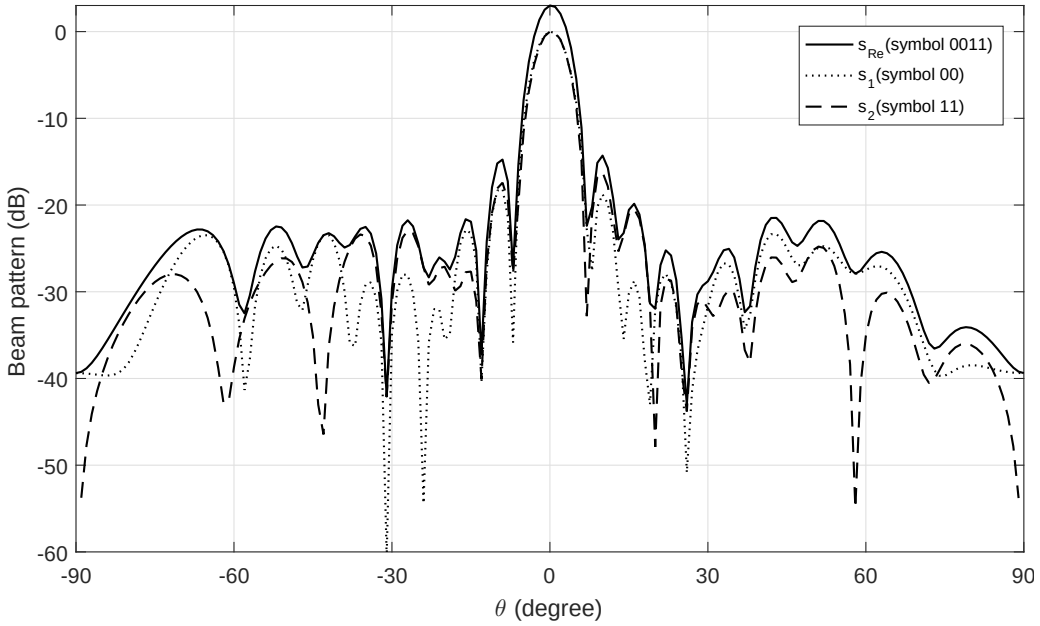

Figure 5.4: Simulated beam responses based on the crossed-dipole ULA (5.21) for symbols '00,11'.

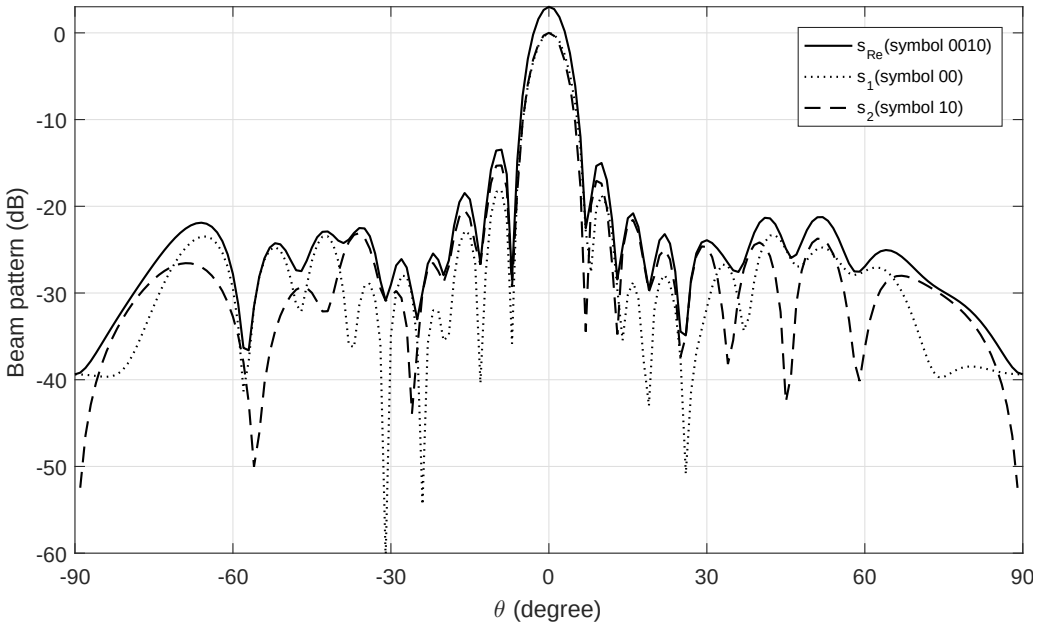

Figure 5.5: Simulated beam responses based on the crossed-dipole ULA (5.21) for symbols '00,10'.

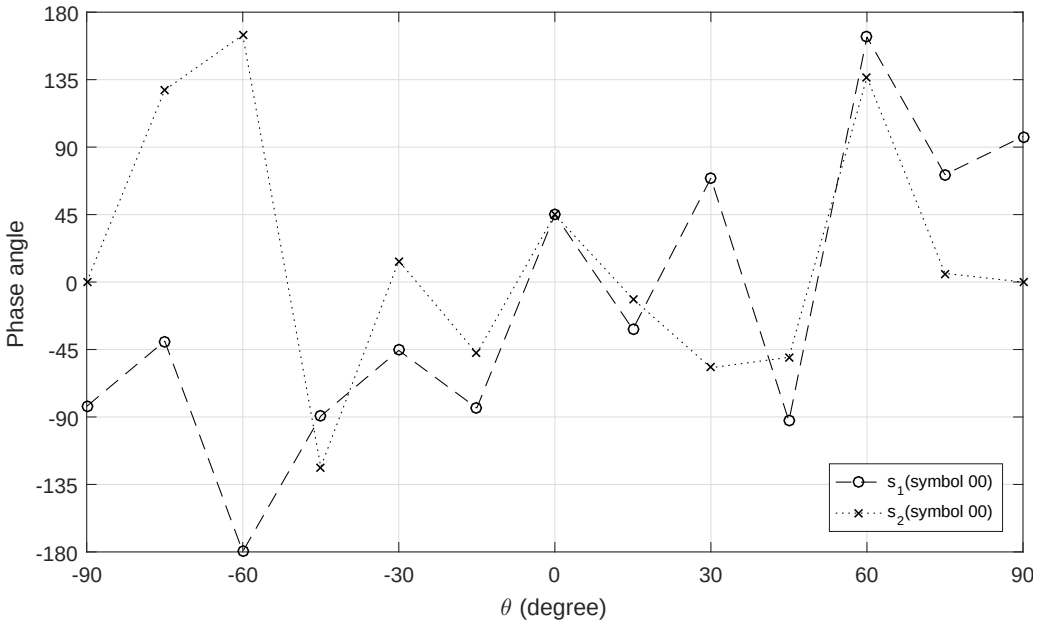

Figure 5.6: Simulated phase responses based on the crossed-dipole ULA (5.21) for symbols '00,00'.

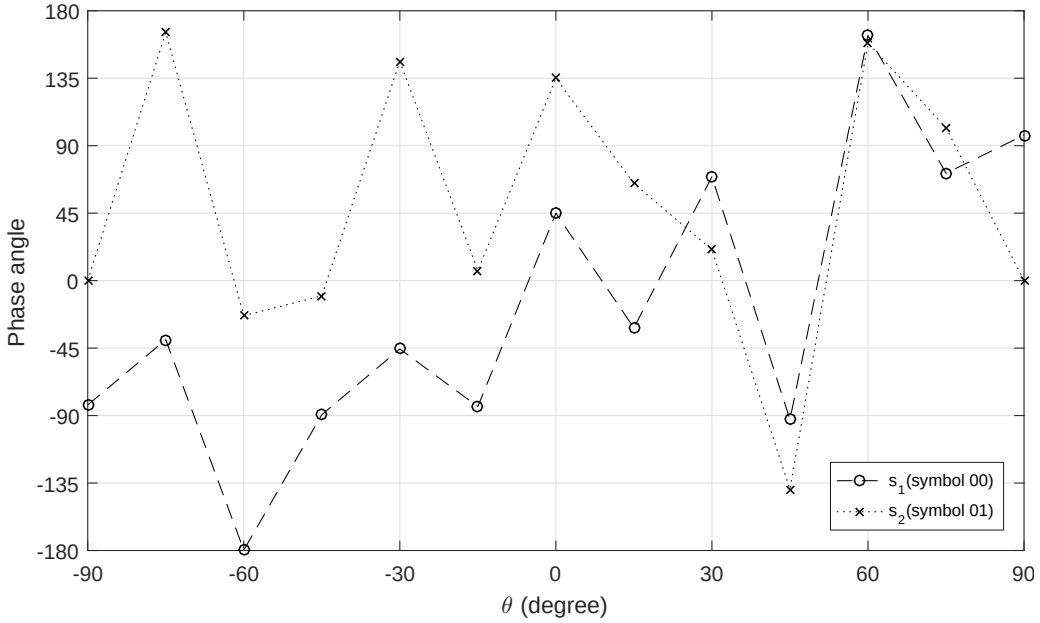

Figure 5.7: Simulated phase responses based on the crossed-dipole ULA (5.21) for symbols '00,01'.

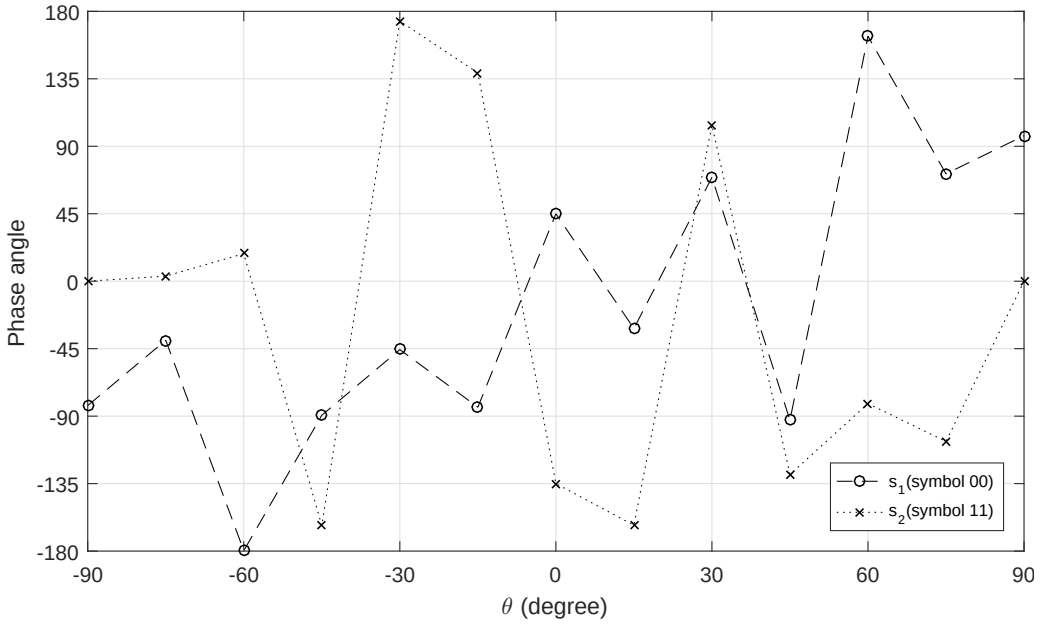

Figure 5.8: Simulated phase responses based on the crossed-dipole ULA (5.21) for symbols '00,11'.

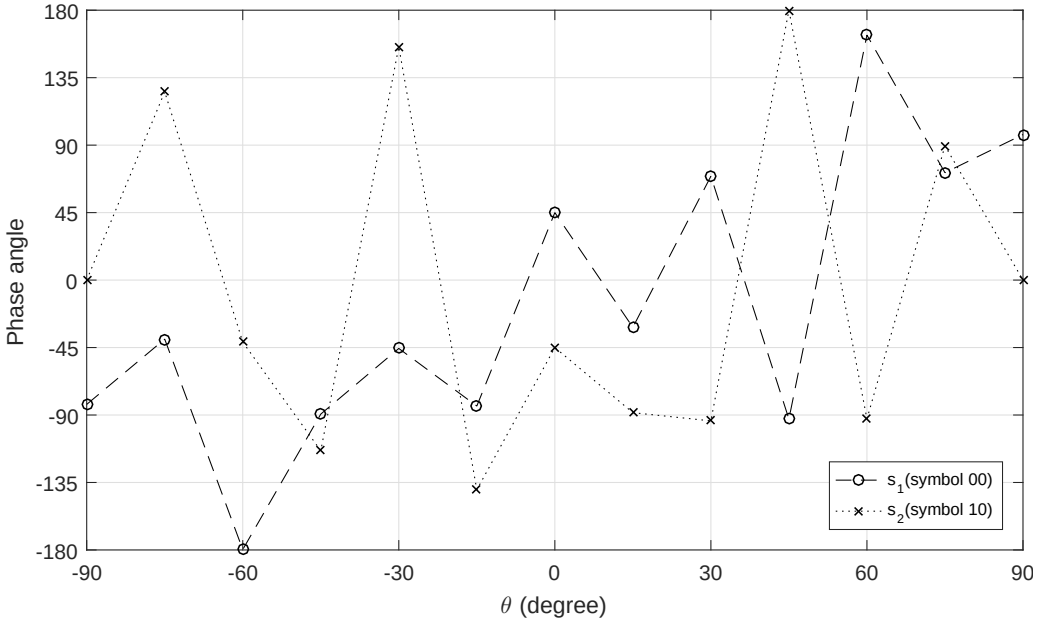

Figure 5.9: Simulated phase responses based on the crossed-dipole ULA (5.21) for symbols '00,10'.

5.4.2 Design Example with Optimised Antenna Locations

Based on the value of error norm α from the above ULA design result, the maximum aperture of the designed crossed-dipole array is set to be 20λ with 201 equally spaced potential antennas. Moreover, $\kappa = 0.001$ indicates that antennas associated with a coefficient value smaller than 0.001 will be considered inactive and thus can be removed.

For the reweighted l_1 norm minimisation method in (5.30), the number of active antennas is 14, with an average spacing of 0.9231λ, where the antenna locations are given in Table 5.1. The beam patterns for symbols '00,00', '00,01', '00,11' and '00,10' are shown in Figs. 5.10, 5.11, 5.12 and 5.13, and phase patterns are shown in Figs. 5.14, 5.15, 5.16 and 5.17, all indicating a satisfactory design result. The beam and phase patterns for other symbols have a similar performance to the above symbols.

Patterns for the usual l_1 norm minimisation in (5.29) are similar to the figures calculated by reweighted l_1 norm minimisation method, and the value of $||\mathbf{P}_{SL} - \mathbf{W}^H\mathbf{S}_{SL}||_2$ is the lowest, as shown in Table 5.2. However, the resultant number of antennas by this method is the largest (201 active antennas) due to the value of α (too small), highlighting the need for the proposed reweighted design in (5.30).

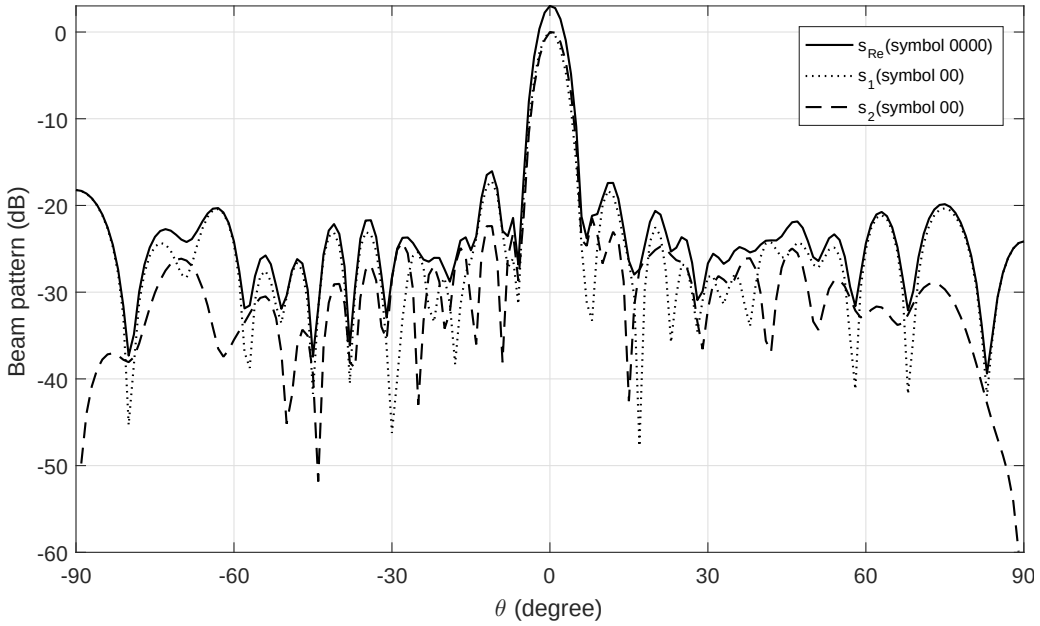

Figure 5.10: Simulated beam responses based on the sparse crossed-dipole array design with optimised locations (5.30) for symbols '00,00'.

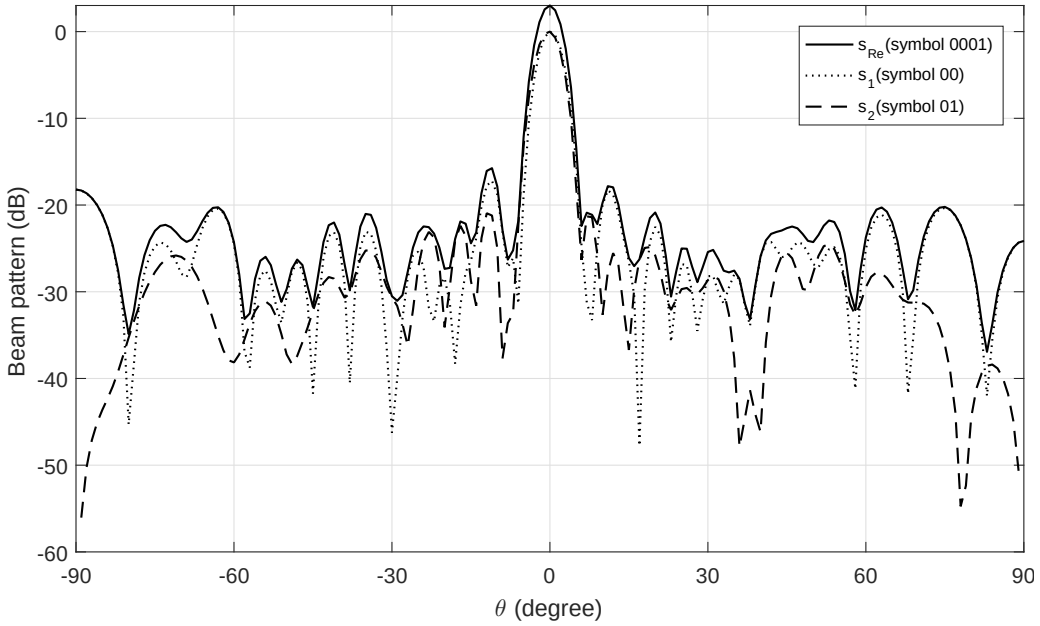

Figure 5.11: Simulated beam responses based on the sparse crossed-dipole array design with optimised locations (5.30) for symbols '00,01'.

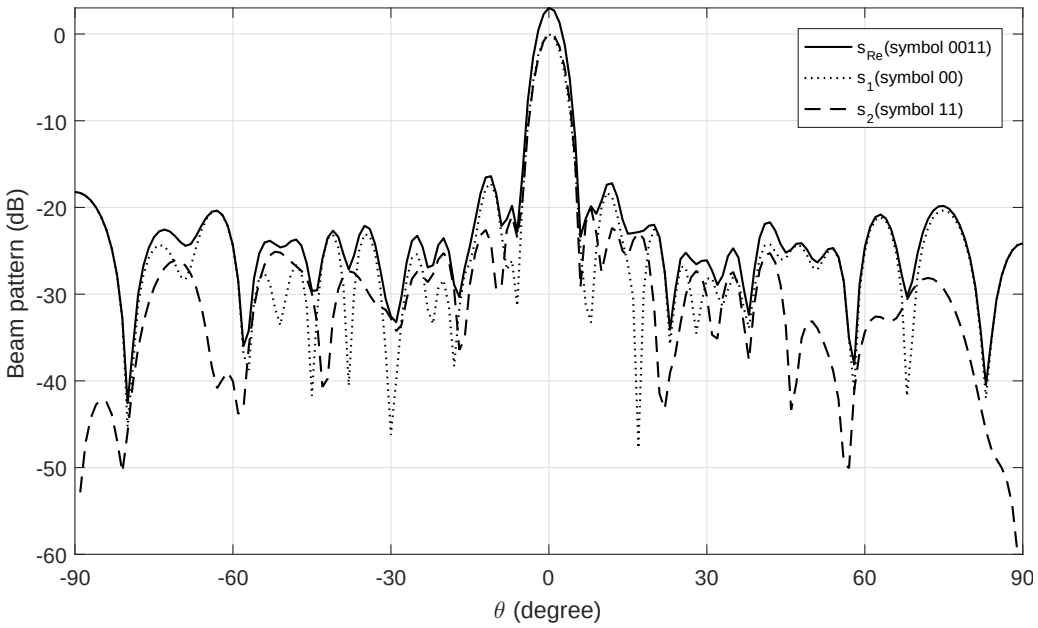

Figure 5.12: Simulated beam responses based on the sparse crossed-dipole array design with optimised locations (5.30) for symbols '00,11'.

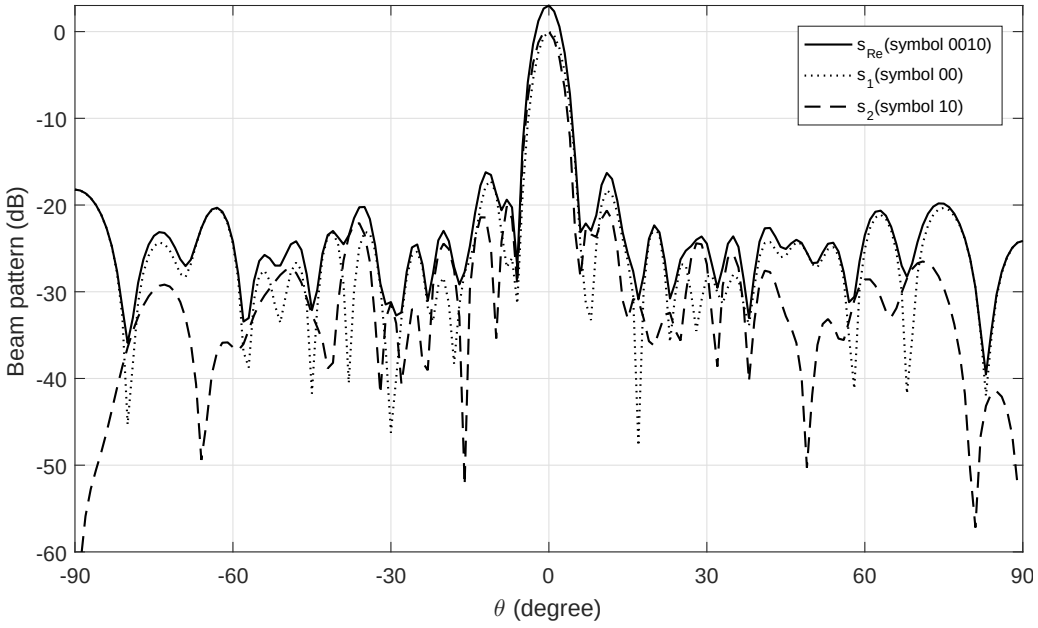

Figure 5.13: Simulated beam responses based on the sparse crossed-dipole array design with optimised locations (5.30) for symbols '00,10'.

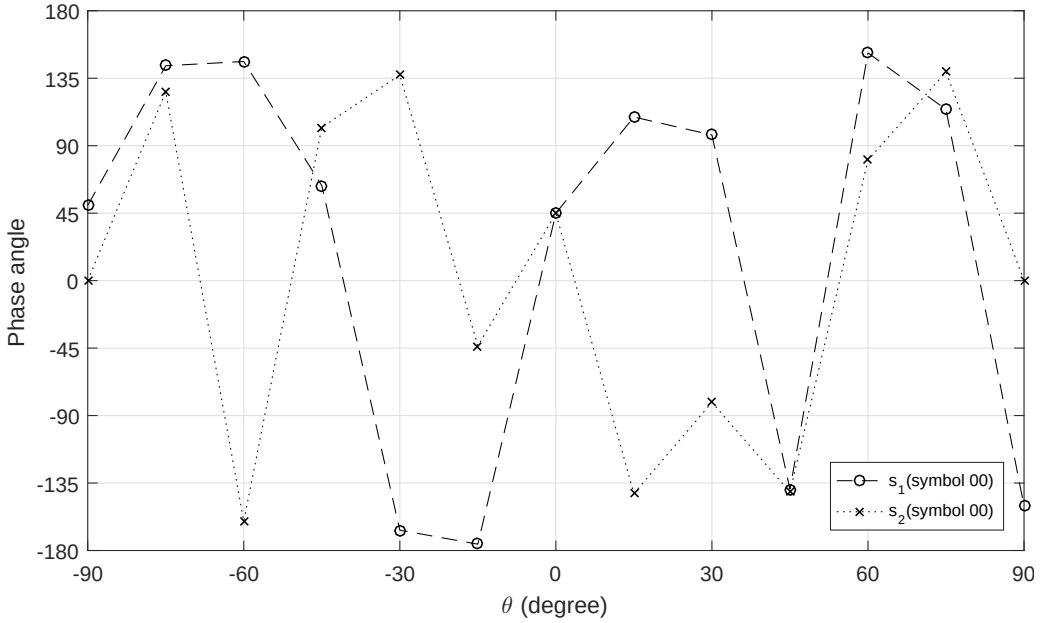

Figure 5.14: Simulated phase responses based on the sparse crossed-dipole array design with optimised locations (5.30) for symbols '00,00'.

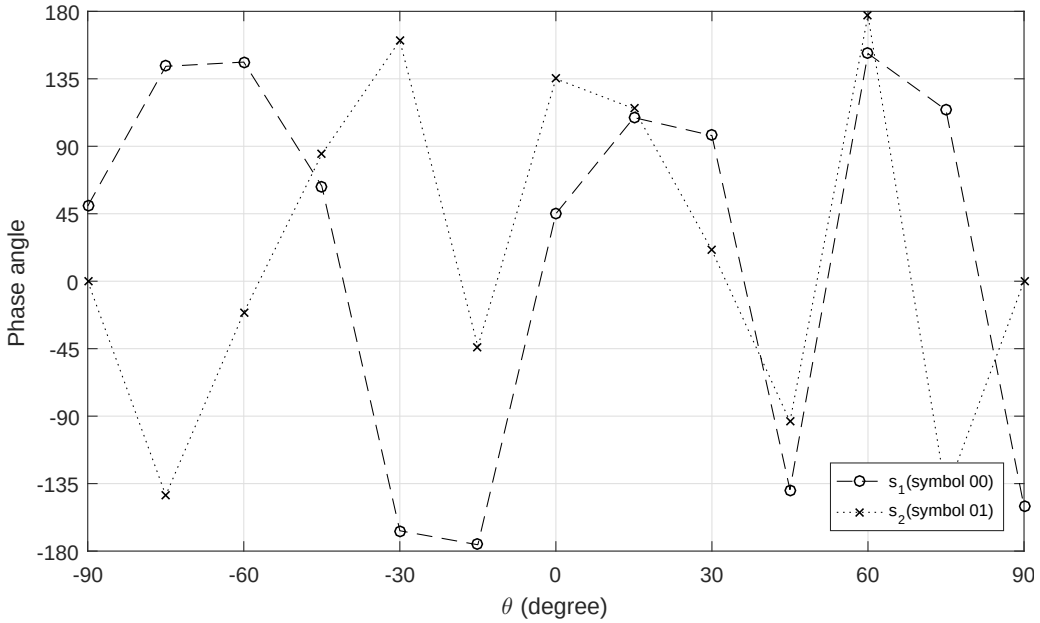

Figure 5.15: Simulated phase responses based on the sparse crossed-dipole array design with optimised locations (5.30) for symbols '00,01'.

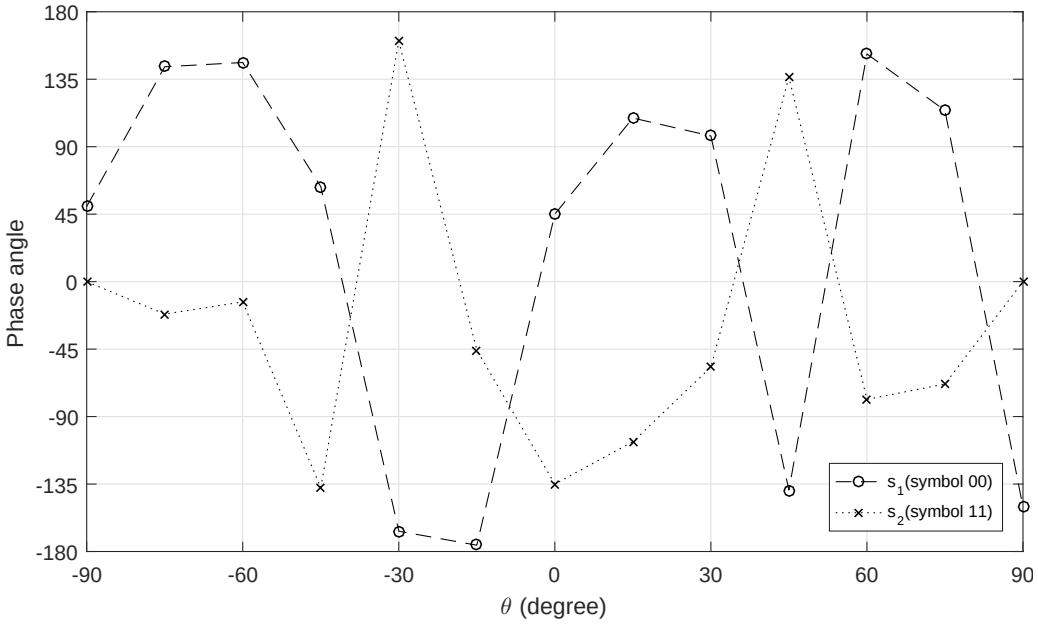

Figure 5.16: Simulated phase responses based on the sparse crossed-dipole array design with optimised locations (5.30) for symbols '00,11'.

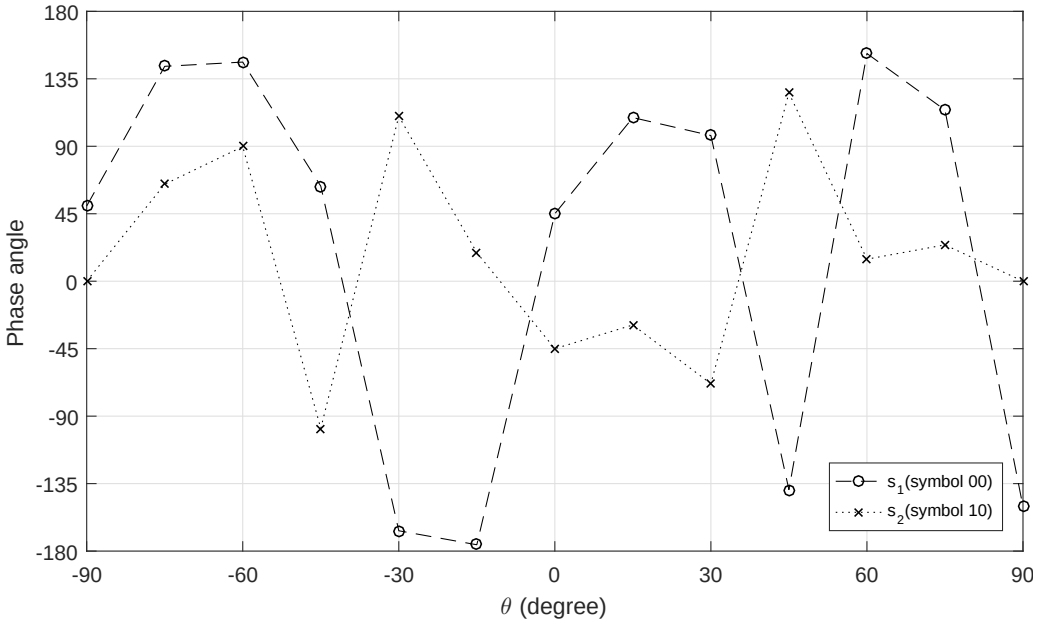

Figure 5.17: Simulated phase responses based on the sparse crossed-dipole array design with optimised locations (5.30) for symbols '00,10'.

Table 5.1: Optimised antenna locations based on the sparse crossed-dipole array design using reweighted l_1 norm minimisation method.

n	d_n/λ	n	d_n/λ	n	d_n/λ
0	4	5	8.7	10	13.2
1	5	6	9.6	11	14.2
2	5.9	7	10.5	12	15.1
3	6.8	8	11.4	13	16
4	7.7	9	12.3		

Table 5.2: Summary of the design results based on the crossed-dipole arrays.

	ULA	Usual l_1	Reweighted l_1
Antenna number	19	201	14
Aperture/λ	9	20	12
Average spacing/λ	0.5	0.1	0.9231
$\|\|\mathbf{P}_{SL} - \mathbf{W}^H\mathbf{S}_{SL}\|\|_2$	7.9968	6.2217	7.8547

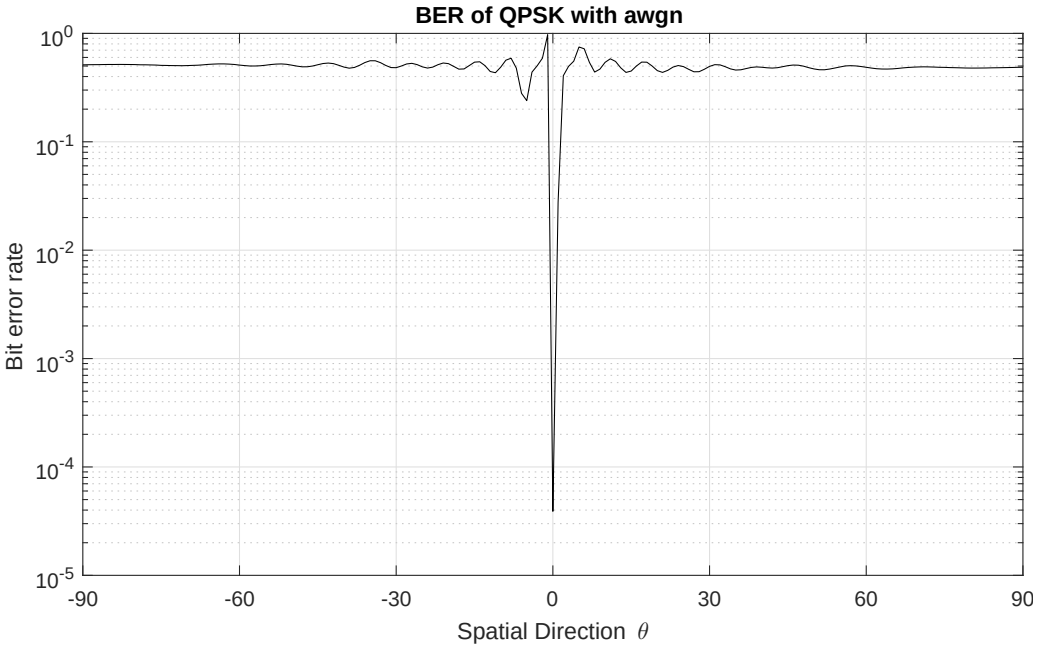

Figure 5.18: BER performance based on the ULA design.

5.4.3 BER for ULA and Sparse Array

The BER for ULA and reweighted l_1 norm sparse antenna array designs are shown in Figs. 5.18 and 5.19. It can be observed that for both designs, the BER values are down to 10^{-5} in the mainlobe, while at other directions the BER is fluctuated around 0.5, further demonstrating the effectiveness of the designs.

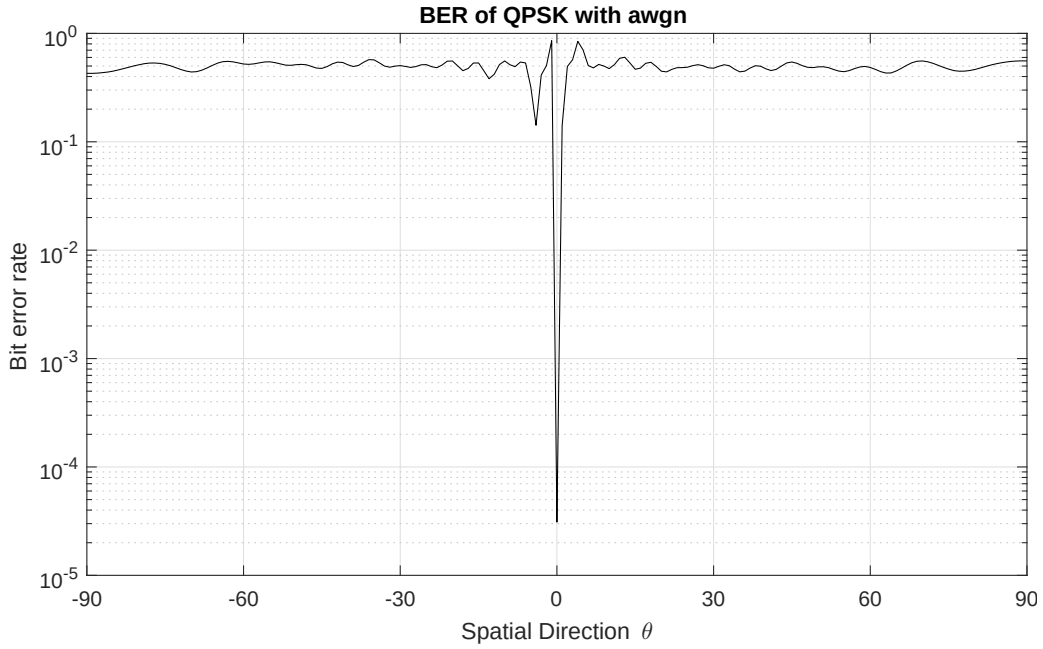

Figure 5.19: BER performance based on the sparse array design using reweighted l_1 norm minimisation.

5.5 Summary

A crossed-dipole antenna array for DM has been proposed for the first time, and array designs for two signals s_1 and s_2 with orthogonal polarisation states transmitted to the same direction at the same frequency, based on a given antenna array geometry and arrays with optimised antenna locations are studied. With such a structure, channel capacity is doubled compared with a single signal transmitted through the propagation channel. For sparse array designs, compressive sensing based formulations were introduced, including the usual l_1 norm minimisation and the reweighted l_1 norm minimisation, and the reweighted approach can provide a sparser solution than the former one, and also offer less number of antennas with a better performance (in terms of the value of $||\mathbf{P}_{SL}-\mathbf{W}^H\mathbf{S}_{SL}||_2$) than the ULA. As shown in the provided design examples, for both signals, the resultant main beams point to the desired direction with desired constellation points, in addition to a low sidelobe level and scrambled phases in other directions.

Chapter 6

Positional Modulation Design in Multi-Path Model

6.1 Introduction

All the above DM designs are based on one assumption that there is no multi-path effect between transmitters and receivers; in other words, there is only a line of sight (LOS) path. However, eavesdroppers aligned with or very close to the desired direction/directions will be a problem for secure signal transmission, as their received modulation patterns are similar to the given one. To make sure that a given modulation pattern can only be received at certain desired positions, one solution is adopting a multi-path model, as shown in shown in Fig. 6.1, where signals via both LOS and reflected paths are combined at the receiver side [32, 86–89]. In this chapter, the typical two-ray multi-path model is studied based on an antenna array and a closed-form solution is provided. Such a two-ray model is more realistic in the millimetre wave band given the more directional propagation model in this frequency band. Furthermore, the antenna location optimisation problem is investigated in the context of positional modulation and a compressive-sensing based design is proposed.

The remaining part of this chapter is structured as follows. A review of the two-ray model is given in Sec. 6.2. Positional modulation design based on a given array geometry and an array with optimised antenna locations are presented in Sec. 6.3. Design examples

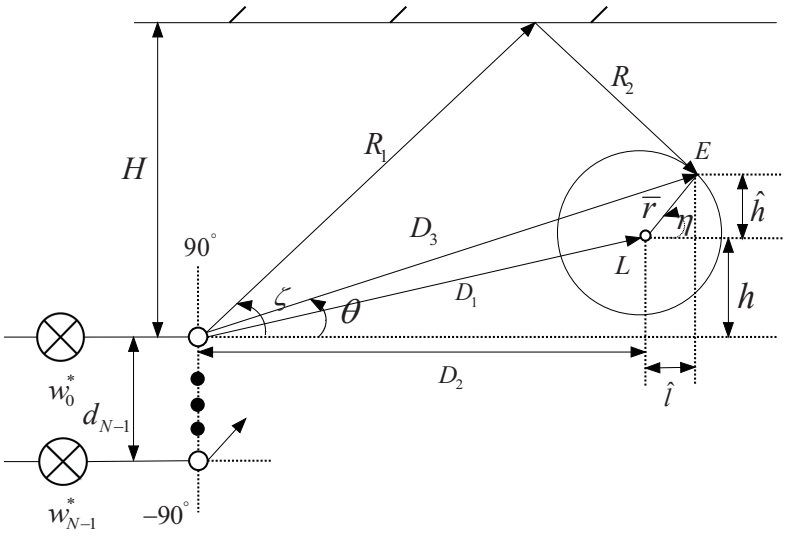

Figure 6.1: Multi-path signal transmission to the desired receiver L and eavesdroppers E.

are provided in Sec. 6.4, followed by conclusions in Sec. 6.5.

6.2 Review of Two-Path Model

An N-element omni-directional linear antenna array, represented by $\circ$, for transmit beamforming [86] is shown in Fig. 6.1, where the spacing between the zeroth and the n-th antennas is represented by d_n for $n = 1, \ldots, N-1$, with the transmission angle $\theta \in [-90°, 90°]$. The weight coefficient of each antenna is denoted by w_n, for $n = 0, \ldots, N-1$. The desired position is represented by L with a distance D_1 to the transmit array and a vertical distance h to the broadside direction where h is positive for L above the broadside direction and negative for the opposite. The projection of D_1 onto the broadside direction is represented by D_2. The positions of eavesdroppers E are shown on the circumference of the circle, with the radius $\bar{r}$ and angle $\eta \in [0°, 360°)$ to the circle centre L. For eavesdroppers in the direction η, the corresponding $\hat{h}$ and $\hat{l}$ are given, representing the vertical height and horizontal length relative to the centre point L, with $\bar{r} = \sqrt{\hat{h}^2 + \hat{l}^2}$, and the distance to transmitters is represented by D_3. To produce the required reflected path, a reflecting surface with a distance H above and perpendicular to the antenna array is created to form the two-ray model. The reflected distances R_1 and R_2 represent the path length before

and after reflection, and the transmission angle for the reflected path is determined by $\zeta \in (0°, 90°]$.

For signals transmitted to the desired location L, as shown in Fig. 6.1,

$$\begin{aligned} D_2 &= \sqrt{D_1^2 - h^2}, \quad \theta = \tan^{-1}(h/D_2), \\ \zeta &= \tan^{-1}((2H - h)/D_2). \end{aligned} \tag{6.1}$$

For signals transmitted to the eavesdroppers,

$$\begin{aligned} \hat{h}(\eta) &= \bar{r}\sin\eta, \quad \hat{l}(\eta) = \bar{r}\cos\eta, \\ D_3 &= \sqrt{(D_2 + \hat{l})^2 + (h + \hat{h})^2}. \end{aligned} \tag{6.2}$$

The corresponding $\theta(\eta)$ and $\zeta(\eta)$ for the LOS and reflected paths can be formulated as

$$\begin{aligned} \theta(\eta) &= \tan^{-1}((h + \hat{h})/(D_2 + \hat{l})), \\ \zeta(\eta) &= \tan^{-1}((2H - \hat{h} - h)/(D_2 + \hat{l})). \end{aligned} \tag{6.3}$$

Then, for the reflected path, $R_1(\zeta)$ and $R_2(\zeta)$ are given by

$$R_1(\zeta) = H/\sin\zeta, \quad R_2(\zeta) = (H - h - \hat{h})/\sin\zeta. \tag{6.4}$$

The steering vector for the LOS path and the reflected path in two-ray model are, respectively, given by

$$\begin{aligned} \mathbf{s}(\omega, \theta) &= [1, e^{j\omega d_1 \sin\theta/c}, \ldots, e^{j\omega d_{N-1}\sin\theta/c}]^T, \\ \hat{\mathbf{s}}(\omega, \zeta) &= [1, e^{j\omega d_1 \sin\zeta/c}, \ldots, e^{j\omega d_{N-1}\sin\zeta/c}]^T. \end{aligned} \tag{6.5}$$

Moreover, phase shift and power attenuation caused by these multiple paths need to be considered [86]. When $\hat{h}$ and $\hat{l}$ are both zero-valued, as shown in (6.2), $D_3 = D_1$. Therefore, the length D_1 can be considered as a special case of the length D_3. Then the phase shifts for LOS paths is given by

$$\psi(\theta) = 2\pi \times rem(D_3(\theta), \lambda), \tag{6.6}$$

where $rem(A, \lambda)$ represents the remainder of A divided by λ. The phase shift for the reflected path is determined by $R_1(\zeta) + R_2(\zeta)$ and given by

$$\phi(\zeta) = \pi + 2\pi \times rem(R_1(\zeta) + R_2(\zeta), \lambda), \tag{6.7}$$

where π is caused by the reflecting surface. The attenuation ratio for a LOS is given by [86]

$$\nu(\theta) = D/D_3(\theta). \tag{6.8}$$

Here D is assumed to be the distance where the received signal has unity power. Similarly, the attenuation ratio for the signal received via the reflected path is given by

$$\xi(\zeta) = D/(R_1(\zeta) + R_2(\zeta)). \tag{6.9}$$

Then, in the two-ray model, the beam response of the array, represented by $p(\theta, \zeta)$, is a combination of signals through the LOS path and the reflected path,

$$\begin{aligned} &p(\theta, \zeta) = \\ &\nu(\theta)e^{j\psi(\theta)}(\mathbf{w}^H\mathbf{s}(\omega, \theta)) + \xi(\zeta)e^{j\phi(\zeta)}(\mathbf{w}^H\hat{\mathbf{s}}(\omega, \zeta)), \end{aligned} \tag{6.10}$$

with the weight vector $\mathbf{w} = [w_0, w_1, \ldots, w_{N-1}]^T$.

6.3 Proposed Design for Positional Modulation

6.3.1 Positional Modulation Design for a Given Array Geometry

The objective of positional modulation design is to find a set of weight coefficients creating signals with a given modulation pattern to desired locations, while the modulations of the signals received around them are distorted. For M-ary modulations schemes, such as multiple phase shift keying (MPSK), there are M sets of desired array responses $p_m(\theta, \zeta)$, with a corresponding weight vector $\mathbf{w}_m = [w_{0,m}, \ldots, w_{N-1,m}]^T$, $m = 0, \ldots, M-1$. Assuming in total R locations in the design (r desired locations and $R - r$ eavesdropper locations) with the corresponding transmission angles θ_k for LOS and ζ_k for the reflected path to the k-th position, $k = 0, \ldots, R-1$, then an $N \times r$ matrix $\mathbf{S}_L$ is constructed as the set of steering vectors for the LOS path to desired receivers, and similarly $\mathbf{S}_E = [\mathbf{s}(\omega, \theta_0), \mathbf{s}(\omega, \theta_1), \ldots, \mathbf{s}(\omega, \theta_{R-r-1})]$ is an $N \times (R - r)$ matrix for steering vectors to eavesdroppers. The corresponding steering vectors for the reflected path to desired receivers and eavesdroppers are given by $\hat{\mathbf{S}}_L$ and $\hat{\mathbf{S}}_E$, respectively. $\mathbf{p}_{m,L}$ ($1 \times r$ vector)

and $\mathbf{p}_{m,E}$ ($1 \times (R-r)$ vector) are required responses for the desired locations and the eavesdroppers for the m-th constellation point.

Moreover, the phase shifts for the LOS and reflected paths to both eavesdroppers and desired receivers, and their corresponding attenuation ratios are given by

$$\begin{aligned}
\boldsymbol{\psi}_E &= [\psi(\theta_0), \psi(\theta_1), \ldots, \psi(\theta_{R-r-1})], \\
\boldsymbol{\psi}_L &= [\psi(\theta_{R-r}), \psi(\theta_{R-r+1}), \ldots, \psi(\theta_{R-1})], \\
\boldsymbol{\phi}_E &= [\phi(\zeta_0), \phi(\zeta_1), \ldots, \phi(\zeta_{R-r-1})], \\
\boldsymbol{\phi}_L &= [\phi(\zeta_{R-r}), \phi(\zeta_{R-r+1}), \ldots, \phi(\zeta_{R-1})], \\
\boldsymbol{\nu}_E &= [\nu(\theta_0), \nu(\theta_1), \ldots, \nu(\theta_{R-r-1})], \\
\boldsymbol{\nu}_L &= [\nu(\theta_{R-r}), \nu(\theta_{R-r+1}), \ldots, \nu(\theta_{R-1})], \\
\boldsymbol{\xi}_E &= [\xi(\zeta_0), \xi(\zeta_1), \ldots, \xi(\zeta_{R-r-1})], \\
\boldsymbol{\xi}_L &= [\xi(\zeta_{R-r}), \xi(\zeta_{R-r+1}), \ldots, \xi(\zeta_{R-1})].
\end{aligned} \tag{6.11}$$

Then, for the m-th constellation point, the coefficients can be formulated as

$$\begin{aligned}
\min_{\mathbf{w}_m} \quad & ||\mathbf{p}_{m,E} - (\boldsymbol{\nu}_E \cdot e^{j\boldsymbol{\psi}_E} \cdot (\mathbf{w}_m^H \mathbf{S}_E) + \boldsymbol{\xi}_E \cdot e^{j\boldsymbol{\phi}_E} \cdot (\mathbf{w}_m^H \hat{\mathbf{S}}_E))||_2 \\
\text{subject to} \quad & \boldsymbol{\nu}_L \cdot e^{j\boldsymbol{\psi}_L} \cdot (\mathbf{w}_m^H \mathbf{S}_L) + \boldsymbol{\xi}_L \cdot e^{j\boldsymbol{\phi}_L} \cdot (\mathbf{w}_m^H \hat{\mathbf{S}}_L) = \mathbf{p}_{m,L},
\end{aligned} \tag{6.12}$$

where $\cdot$ is the dot product. Its solution can be solved by the method of Lagrange multipliers, and the optimum value for the weight vector $\mathbf{w}_m$ is given by

$$\mathbf{w}_m = \mathbf{K}_5^{-1}(\hat{\mathbf{S}}_E \mathbf{K}_2 \mathbf{p}_{m,E}^H - \mathbf{S}_E \mathbf{K}_1 \mathbf{p}_{m,E}^H - \mathbf{K}_6^H \mathbf{S}_L \mathbf{K}_3 - \mathbf{K}_6^H \hat{\mathbf{S}}_L \mathbf{K}_4), \tag{6.13}$$

where

$$\begin{aligned}
\mathbf{K}_1 &= diag(\boldsymbol{\nu}_E diag(e^{j\boldsymbol{\psi}_E})), \quad \mathbf{K}_2 = diag(\boldsymbol{\xi}_E diag(e^{j\boldsymbol{\phi}_E})), \\
\mathbf{K}_3 &= diag(\boldsymbol{\nu}_L diag(e^{j\boldsymbol{\psi}_L})), \quad \mathbf{K}_4 = diag(\boldsymbol{\xi}_L diag(e^{j\boldsymbol{\phi}_L})), \\
\mathbf{K}_5 &= \mathbf{S}_E \mathbf{K}_1 \mathbf{K}_1^H \mathbf{S}_E^H + \mathbf{S}_E \mathbf{K}_1 \mathbf{K}_2^H \mathbf{S}_E^H + \hat{\mathbf{S}}_E \mathbf{K}_2 \mathbf{K}_1^H \mathbf{S}_E^H + \hat{\mathbf{S}}_E \mathbf{K}_2 \mathbf{K}_2^H \hat{\mathbf{S}}_E^H, \\
\mathbf{K}_6 &= (\mathbf{p}_{m,E} \mathbf{K}_2^H \hat{\mathbf{S}}_E^H \mathbf{K}_5^{-H} \mathbf{S}_L \mathbf{K}_3 - \mathbf{p}_{m,E} \mathbf{K}_1^H \mathbf{S}_E^H \mathbf{K}_5^{-H} \mathbf{S}_L \mathbf{K}_3 \\
&\quad - \mathbf{p}_{m,E} \mathbf{K}_2^H \hat{\mathbf{S}}_E^H \mathbf{K}_5^{-H} \hat{\mathbf{S}}_L \mathbf{K}_4 - \mathbf{p}_{m,E} \mathbf{K}_1^H \mathbf{S}_E^H \mathbf{K}_5^{-H} \hat{\mathbf{S}}_L \mathbf{K}_4 - \mathbf{p}_{m,L}) \\
&\quad \times (\mathbf{K}_3^H \mathbf{S}_L^H \mathbf{K}_5^{-H} \mathbf{S}_L \mathbf{K}_3 + \mathbf{K}_4^H \hat{\mathbf{S}}_L^H \mathbf{K}_5^{-H} \mathbf{S}_L \mathbf{K}_3 \\
&\quad + \mathbf{K}_3^H \mathbf{S}_L^H \mathbf{K}_5^{-H} \hat{\mathbf{S}}_L \mathbf{K}_4 + \mathbf{K}_4^H \hat{\mathbf{S}}_L^H \mathbf{K}_5^{-H} \hat{\mathbf{S}}_L \mathbf{K}_4)^{-1}.
\end{aligned} \tag{6.14}$$

6.3.2 Positional Modulation Design for an Optimised Locations Array

Equation (6.12) is for designing the positional modulation coefficients for a given set of antenna locations. In practice, optimised locations may need to find to construct an array for an improved performance, which can be considered as a sparse antenna array design problem [5, 6]. In this section, CS-based methods is studied.

For CS-based sparse array design for positional modulation, a given aperture is densely sampled with a large number (N) of potential antennas, as shown in Fig. 6.1, and the values of d_n, for $n = 1, 2, \ldots, N-1$, are selected to give a uniform grid. Through selecting the minimum number of non-zero valued weight coefficients, where the corresponding antennas are kept, and the rest of the antennas with zero-valued coefficients are removed, to generate a response close to the desired one, sparseness of the design is acquired [28, 30]. Then for the m-th constellation point, the set of weight coefficients is given by

$$\begin{aligned} \min_{\mathbf{w}_m} \quad & ||\mathbf{w}_m||_1 \\ \text{subject to} \quad & ||\mathbf{p}_{m,E} - (\boldsymbol{\nu}_E \cdot e^{j\boldsymbol{\psi}_E} \cdot (\mathbf{w}_m^H \mathbf{S}_E) + \boldsymbol{\xi}_E \cdot e^{j\boldsymbol{\phi}_E} \cdot (\mathbf{w}_m^H \hat{\mathbf{S}}_E))||_2 \leq \alpha \\ & \boldsymbol{\nu}_L \cdot e^{j\boldsymbol{\psi}_L} \cdot (\mathbf{w}_m^H \mathbf{S}_L) + \boldsymbol{\xi}_L \cdot e^{j\boldsymbol{\phi}_L} \cdot (\mathbf{w}_m^H \hat{\mathbf{S}}_L) = \mathbf{p}_{m,L}, \end{aligned} \tag{6.15}$$

where $||\cdot||_1$ is the l_1 norm, used as an approximation to the l_0 norm and α is the allowed difference between the desired and designed responses. As each antenna element corresponds to M weight coefficients and these M coefficients correspond to M symbols, to remove the n-th antenna, all coefficients in the following vector $\tilde{\mathbf{w}}_n$ need to be zero-valued or $||\tilde{\mathbf{w}}_n||_2 = 0$ [28, 30],

$$\tilde{\mathbf{w}}_n = [w_{n,0}, \ldots, w_{n,M-1}], \tag{6.16}$$

where $w_{n,m}$ represents the coefficients on the n-th antenna for the m-th symbol. Then, to calculate the minimum number of antenna elements, all $||\tilde{\mathbf{w}}_n||_2$ for $n = 0, \ldots, N-1$ are gathered to form a new vector $\hat{\mathbf{w}}$,

$$\hat{\mathbf{w}} = [||\tilde{\mathbf{w}}_0||_2, ||\tilde{\mathbf{w}}_1||_2, \ldots, ||\tilde{\mathbf{w}}_{N-1}||_2]^T. \tag{6.17}$$

Moreover, positional modulation constraints need to be imposed including

$$\begin{aligned}
\mathbf{W} &= [\mathbf{w}_0, \mathbf{w}_1, \ldots, \mathbf{w}_{M-1}], \\
\mathbf{P}_E &= [\mathbf{p}_{0,E}, \mathbf{p}_{1,E}, \ldots, \mathbf{p}_{M-1,E}]^T, \\
\mathbf{P}_L &= [\mathbf{p}_{0,L}, \mathbf{p}_{1,L}, \ldots, \mathbf{p}_{M-1,L}]^T, \\
\tilde{\boldsymbol{\nu}}_E &= \boldsymbol{\nu}_E \otimes \text{ones}(M,1),\ \tilde{\boldsymbol{\nu}}_L = \boldsymbol{\nu}_L \otimes \text{ones}(M,1), \\
\tilde{\boldsymbol{\xi}}_E &= \boldsymbol{\xi}_E \otimes \text{ones}(M,1),\ \tilde{\boldsymbol{\xi}}_L = \boldsymbol{\xi}_L \otimes \text{ones}(M,1), \\
\tilde{\boldsymbol{\psi}}_E &= \boldsymbol{\psi}_E \otimes \text{ones}(M,1),\ \tilde{\boldsymbol{\psi}}_L = \boldsymbol{\psi}_L \otimes \text{ones}(M,1), \\
\tilde{\boldsymbol{\phi}}_E &= \boldsymbol{\phi}_E \otimes \text{ones}(M,1),\ \tilde{\boldsymbol{\phi}}_L = \boldsymbol{\phi}_L \otimes \text{ones}(M,1),
\end{aligned} \tag{6.18}$$

where $\otimes$ stands for the Kronecker product, and $\text{ones}(M,1)$ is an $M \times 1$ matrix of ones. $\tilde{\boldsymbol{\nu}}_E$, $\tilde{\boldsymbol{\xi}}_E$, $\tilde{\boldsymbol{\psi}}_E$ and $\tilde{\boldsymbol{\phi}}_E$ are $M \times (R-r)$ matrix and $\tilde{\boldsymbol{\nu}}_L$, $\tilde{\boldsymbol{\xi}}_L$, $\tilde{\boldsymbol{\psi}}_L$ and $\tilde{\boldsymbol{\phi}}_L$ are $M \times r$ matrix. Then the group sparsity based sparse array design for DM [28, 30] can be formulated as

$$\begin{aligned}
\min_{\mathbf{W}} \quad & ||\hat{\mathbf{w}}||_1 \\
\text{subject to} \quad & ||\mathbf{P}_E - (\tilde{\boldsymbol{\nu}}_E \cdot e^{j\tilde{\boldsymbol{\psi}}_E} \cdot (\mathbf{W}^H \mathbf{S}_E) + \tilde{\boldsymbol{\xi}}_E \cdot e^{j\tilde{\boldsymbol{\phi}}_E} \cdot (\mathbf{W}^H \hat{\mathbf{S}}_E))||_2 \leq \alpha \\
& \tilde{\boldsymbol{\nu}}_L \cdot e^{j\tilde{\boldsymbol{\psi}}_L} \cdot (\mathbf{W}^H \mathbf{S}_L) + \tilde{\boldsymbol{\xi}}_L \cdot e^{j\tilde{\boldsymbol{\phi}}_L} \cdot (\mathbf{W}^H \hat{\mathbf{S}}_L) = \mathbf{P}_L.
\end{aligned} \tag{6.19}$$

As the reweighted l_1 norm minimisation has a closer approximation to the l_0 norm [48–50], formulation (6.19) can be further modified into the reweighted form in a similar way as in [28], where at the i-th iteration,

$$\begin{aligned}
\min_{\mathbf{W}} \quad & \sum_{n=0}^{N-1} \delta_n^i ||\tilde{\mathbf{w}}_n^i||_2 \\
\text{subject to} \quad & ||\mathbf{P}_E - (\tilde{\boldsymbol{\nu}}_E \cdot e^{j\tilde{\boldsymbol{\psi}}_E} \cdot ((\mathbf{W}^i)^H \mathbf{S}_E) + \tilde{\boldsymbol{\xi}}_E \cdot e^{j\tilde{\boldsymbol{\phi}}_E} \cdot ((\mathbf{W}^i)^H \hat{\mathbf{S}}_E))||_2 \leq \alpha \\
& \tilde{\boldsymbol{\nu}}_L \cdot e^{j\tilde{\boldsymbol{\psi}}_L} \cdot ((\mathbf{W}^i)^H \mathbf{S}_L) + \tilde{\boldsymbol{\xi}}_L \cdot e^{j\tilde{\boldsymbol{\phi}}_L} \cdot ((\mathbf{W}^i)^H \hat{\mathbf{S}}_L) = \mathbf{P}_L.
\end{aligned} \tag{6.20}$$

Here the superscript i indicates the i-th iteration, and δ_n is the reweighting term for the n-th row of coefficients, given by $\delta_n^u = (||\tilde{\mathbf{w}}_n^{u-1}||_2 + \kappa)^{-1}$. ($\gamma > 0$ is required to provide numerical stability and the iteration process is described as in [28].) The problem in (6.19) and (6.20) can be solved by cvx [46, 47].

6.4 Design Examples

In this section, several representative design examples are provided to show the performance of the proposed formulations in the two-ray model. Without loss of generality, one desired location is assumed at the circle centre with $\theta = 0°$, and $H = 500\lambda$, $D_1 = D = 1000\lambda$. Eavesdroppers are located at the circumference of the circle with $\bar{r} = 8.4\lambda$ and $\eta \in [0°, 360°)$, sampled every 1°. With the radius $\bar{r}$ and the angle η based on (6.3), it can be seen that all eavesdroppers are in the directions of $\theta \in (-0.5°, 0.5°)$, i.e. aligned with or very close to the desired user. The desired response is a value of one magnitude (the gain is 0dB) with 90° phase shift at the desired location (QPSK), i.e. symbols '00', '01', '11', '10' correspond to 45°, 135°, −135° and −45°, respectively, and a value of 0.1 (magnitude) with random phase shifts at eavesdroppers. Moreover the bit error rate (BER) result is also presented. Here the signal to noise ratio (SNR) is set at 12 dB at the desired location, and the additive white Gaussian noise (AWGN) level is assumed at the same level for all eavesdroppers.

The number of antenna elements for the ULA design is $N = 30$, while for the sparse array design, the maximum aperture of the array is set to 20λ with 401 equally spaced potential antennas. To make a fair comparison, the value of error norm between desired and designed array responses calculated from the ULA design (6.12) is used as the threshold α for the sparse array design. $\kappa = 0.001$ used in the reweighted l_1 norm minimisation (6.20) indicates that antennas associated with a weight value smaller than 0.001 will be removed.

The resultant beam and phase patterns for the eavesdroppers based on the ULA design (6.12) are shown in Figs. 6.2 and 6.3, where the beam response level at all locations of the eavesdroppers ($\eta \in [0°, 360°)$) is lower than 0dB which is the beam response for the desired locations. The phase of signal at these eavesdroppers are random while the desired phase for these four symbols should be QPSK modulation, as mentioned before. The beam and phase patterns for the sparse array design in (6.20) are not shown as they have similar characteristics to ULA's beam and phase responses. As shown in Table 6.1, with a fewer number of antennas, the sparse array design results provide a better match to the desired

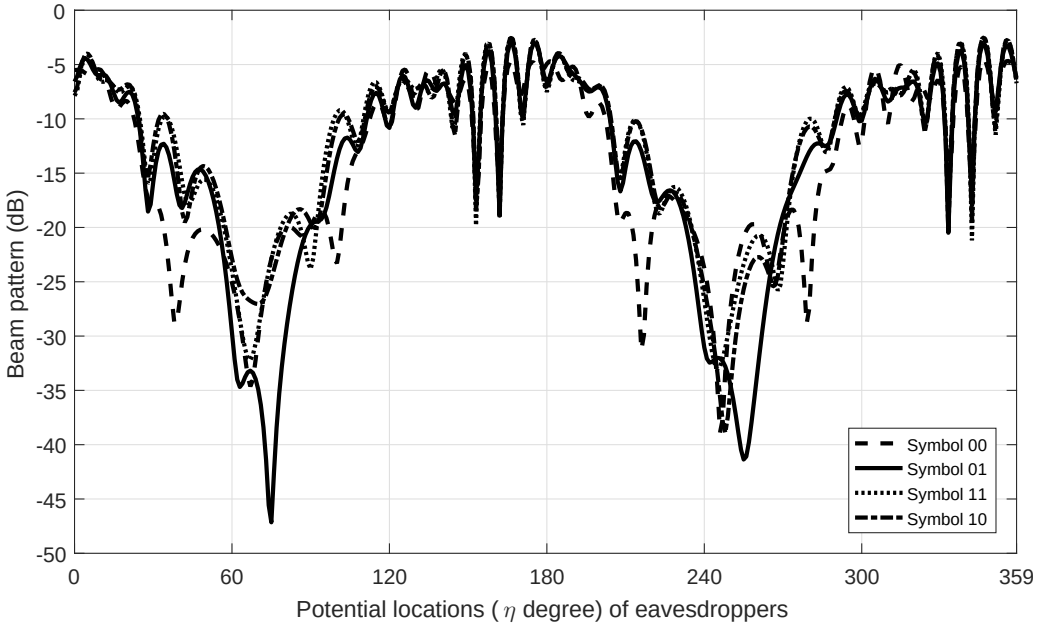

Figure 6.2: Simulated beam pattern based on the ULA design in multi-path model (6.12) for eavesdroppers.

responses based on the error norm of array responses.

Considering the imperfect knowledge of the geometry, e.g. the locations of eavesdroppers are not exactly the same as the locations that are considered in the design. Here eavesdroppers are assumed to be distributed on the circumferences of the circles with $\bar{r} = 8\lambda$ and $\bar{r} = 8.8\lambda$, while the set of weight coefficients are designed for $\bar{r} = 8.4\lambda$. Fig. 6.4 shows the BERs based on the ULA design (6.12) in the multi-path model, where BERs at these eavesdroppers in these cases are still much higher than the rate in the desired location (10^{-5}). While in LOS model, as shown in Fig. 6.5, BERs based on $\bar{r} = 8.4\lambda$ at some positions of the eavesdroppers are close to 10^{-3}, lower than the counterpart (10^{-1}) in the multi-path model, indicated by dash line in Fig. 6.4, demonstrating the effectiveness of the multi-path scheme. Moreover, for eavesdroppers close to the desired direction and also integer wavelengths away from the desired location, e.g. $\bar{r} = 8\lambda$, $\eta = 0^\circ$ and $\eta = 180^\circ$, the BERs reach 10^{-5}, same as in desired locations, much lower than the BERs at these positions in the multi-path model, further demonstrating the effectiveness of the proposed positional modulation designs. The BERs for the sparse array design (6.20) are not shown as they have similar features to the ULA designs.

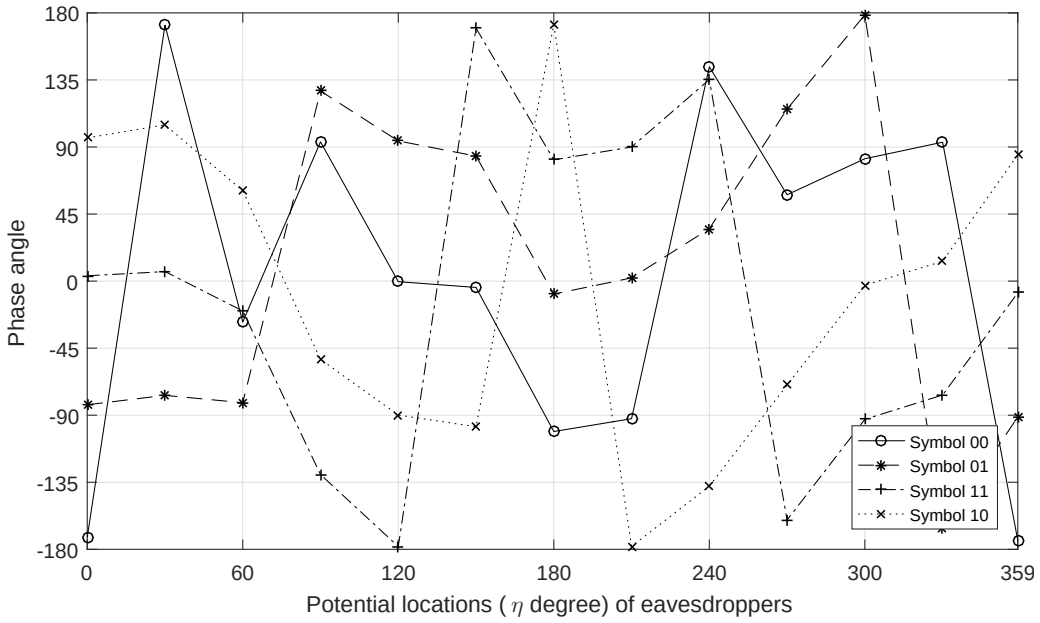

Figure 6.3: Simulated phase pattern based on the ULA design in multi-path model (6.12) for eavesdroppers.

Table 6.1: Summary of the design results in multi-path model.

	ULA	Usual l_1	Reweighted
Antenna number	30	117	8
Aperture/λ	14.5	20	19.8
Average spacing/λ	0.5	0.1724	2.8286
$\|\|\mathbf{p}_{m,E} - (\boldsymbol{\nu}_E \cdot e^{j\boldsymbol{\psi}_E} \cdot (\mathbf{w}_m^H \mathbf{S}_E)$ $+\boldsymbol{\xi}_E \cdot e^{j\boldsymbol{\phi}_E} \cdot (\mathbf{w}_m^H \hat{\mathbf{S}}_E))\|\|_2$			
(Error norm of array responses)	14.0707	13.1773	13.9028

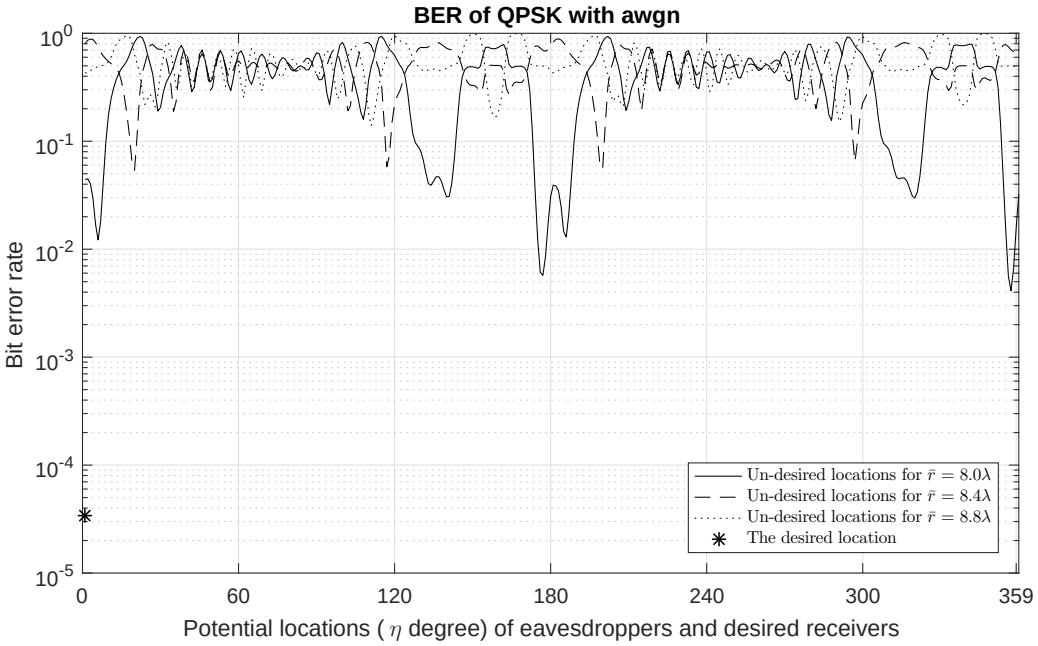

Figure 6.4: BER pattern for the eavesdroppers and desired receiver based on the ULA design (6.12) in multi-path model.

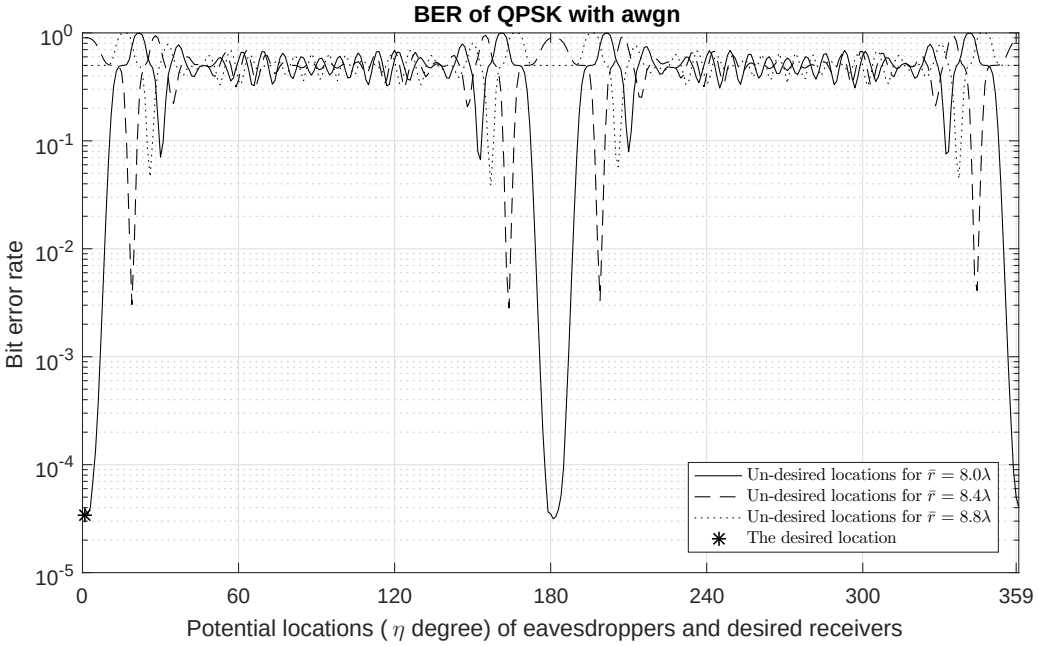

Figure 6.5: BER pattern for the eavesdroppers and desired receiver based on the ULA design in LOS model.

6.5 Summary

In this chapter, a two-ray transmission model has been studied for positional modulation, where signals via LOS and reflected paths are combined at the receiver side. With the positional modulation technique, signals with a given modulation pattern can only be received at desired locations, but scrambled for positions around them. By the proposed designs, the multi-path effect is exploited to overcome the drawback of traditional DM design when eavesdroppers are aligned with or very close to the desired users. Examples for a given array geometry and an optimised sparse array have been provided to verify the effectiveness of the proposed designs.

Chapter 7

Conclusions and Future Plan

7.1 Conclusions

DM as a physical layer security technique in signal transmission to keep known constellation points in desired directions while scrambling them for the remaining directions has been studied based on ULAs. However, one problem of the design is the heavy weight and high cost when a large number of antenna elements is used in the array. To solve the problem, the sparse array design in the context of DM has been studied for the first time, allowing the sparse array achieve a similar performance to the ULA with a fewer number of antenna elements. The main contribution of the design is to formulate the problem from the viewpoint of compressive sensing (CS) so that it can be solved using standard convex optimisation toolboxes in the CS area. In detail, a common set of active antennas for all modulation symbols needs to be found generating a response close to the desired one, and the key to the solution is to realise the the group sparsity concept needs to be employed, as a common antenna set cannot be guaranteed if antenna locations for each modulation symbol are optimised individually. The methods to achieve the sparse array design include the usual l_1 norm minimisation and the reweighted l_1 norm minimisation. Two practical scenarios are also analysed where steering vector error exists and optimised locations are too close to each other. As shown in the provided design examples, in the context of DM, all sparse designs satisfy the mainlobe pointing to the desired direction with scrambled phases in other directions. In particular, the reweighted l_1 norm minimi-

sation method can provide a sparer solution as expected, achieving a similar performance as the ULA but with less number of antennas.

To use the wider frequency spectrum, a multi-carrier based antenna array structure for DM has been proposed, where a baseband implementation similar to the classic OFDM structure in wireless communications is derived, so that a much higher data rate can be obtained. In addition, such a framework allows possible frequency division based multi-user access to the system and also provides the flexibility of using different modulation schemes at different frequencies. Based on the antenna array design in a single carrier frequency, the given antenna array design and sparse array design with antenna location optimisation problem in multi-carrier frequencies are both studied and a class of CS-based design methods (l_1 norm minimisation and reweighted l_1 norm minimisation) is developed. The key is to find a common set of sparse result for all modulation symbols at all frequencies using the concept of group sparsity. As shown in the provided design examples, the given antenna array design and the sparse array design have achieved mainlobes pointing to the desired direction with scrambled phases in other directions for all symbols. In particular, the sparse array design can provide a sparse solution as expected, using less number of antennas with a satisfactory performance compared to the ULA design case. However, the problem of multi-carrier design is the high peak to average power ratio (PAPR) of the resultant signals, leading to non-linear distortion when signal peaks pass through saturation regions of a power amplifier. To solve the problem, the PAPR $\leq \rho$ ($\rho \geq 1$) constraint is considered in the design and a solution based on a modified wideband beampattern formation via iterative techniques (modified WBFIT) method is proposed. As shown in the provided design examples subject to both DM requirement and PAPR constraint, the main beams point to the desired direction and the phase follows the given constellation diagram in the mainlobe and random in sidelobe ranges, satisfying DM; in the meantime, histograms of PAPR probability are presented to demonstrate the effectiveness of the proposed design.

Moreover, in the case of a single carrier frequency, to increase channel capacity, the polarisation information of signals is exploited and a crossed-dipole antenna array for DM has been proposed for the first time, where two signals s_1 and s_2 with orthogonal

polarisation states can be transmitted to the same direction at the same frequency, based on a given array geometry and arrays with optimised antenna locations. These two signals can also be considered as one composite signal using a four dimensional (4-D) modulation scheme across the two polarisation diversity channels, and a set of common weight coefficients can be designed to achieve DM for the two signals based on crossed-dipole arrays. As these two signals will combine into a composite signal s_{Re} at receiver side, to receive and separate the corresponding components, a crossed-dipole antenna or array is needed, and the polarisation directions of the antennas at the receiver side do not need to match those of the transmitted signals, as cross-interference due to a mismatch can be solved easily using some standard signal processing techniques, e.g. the Wiener filter based on a known reference signal. For DM design based on a given array geometry, the method of Lagrange multipliers can be used to solve the problem. For sparse array designs, CS-based formulations are also introduced, including usual l_1 norm minimisation and reweighted l_1 norm minimisation with the concept of group sparsity for finding a set of common antenna locations for all symbols. Through comparison, the reweighted approach can provide a sparser solution than the former one, and also offer less number of antennas with a satisfied performance (error norm of array responses) than the ULA. As shown in the provided design examples, for both signals, the main beams point to the desired direction with desired constellation points, following a low sidelobe level and scrambled phases in other directions.

Although DM can make the symbol pattern the same as the given one in the desired directions, with scrambled phase and magnitude as low as possible in sidelobe directions, for eavesdroppers aligned with or very close to the desired direction/directions, the transmission security would be a problem, as their received modulation patterns are similar to the given one. To solve the problem, a two-ray model transmission has been analysed where signals via LOS and reflected paths are combined at receiver side. With positional modulation technique, signals with a given modulation pattern can only be received on desired locations, but scrambled for positions around them. A closed-form solution for weight coefficients to positional modulation design for a given array geometry is given, along with sparse array designs where reweighted l_1 norm minimisation method and group

sparsity are both introduced for finding a common set of antenna locations for all constellation points. In design examples, the beam pattern, phase pattern and BERs are provided to verify the effectiveness of the proposed designs.

7.2 Future Work

DM has been applied to multi-carrier structure for wider frequency spectrum and exploited polarisation information on crossed-dipole array for a higher channel capacity in the case of a single carrier frequency separately. In future work, these two techniques would be combined for both benefits, and the conventional OFDM structure designed for complex values would be changed to a quaternion OFDM structure [90] for quaternion values as a set of quaternion-valued weight coefficients are used for signal polarisation. Moreover, this design can be applied to sparse arrays, where the cost function can be either smaller or with a similar level of cost function minimisation result, the number of antennas is reduced.

DM applied to planar arrays and volume arrays would also be a good supplement to the design on linear arrays, where the main beam may be narrower and sidelobe level may be lower than the counterparts on linear arrays, and their corresponding CS-based sparse array design including l_1 norm minimisation and reweighted l_1 norm minimisation may be the subsequent research subjects. The problem is that the antenna location optimisation would be considered for all symbols for two or three dimensions array, not like the current work for one dimension array (linear array).

Bibliography

[1] Y. S. Shiu, S. Y. Chang, H. C. Wu, S. C. H. Huang, and H. H. Chen, "Physical layer security in wireless networks: a tutorial," *IEEE Wireless Communications*, vol. 18, no. 2, pp. 66–74, April 2011.

[2] A. Babakhani, D. B. Rutledge, and A. Hajimiri, "Transmitter architectures based on near-field direct antenna modulation," *IEEE Journal of Solid-State Circuits*, vol. 43, no. 12, pp. 2674–2692, December 2008.

[3] ——, "Near-field direct antenna modulation," *IEEE Microwave Magazine*, vol. 10, no. 1, pp. 36–46, February 2009.

[4] A. H. Chang, A. Babakhani, and A. Hajimiri, "Near-field direct antenna modulation (nfdam) transmitter at 2.4GHz," in *Proc IEEE Antennas and Propagation Society International Symposium*, June 2009, pp. 1–4.

[5] A. Moffet, "Minimum-redundancy linear arrays," *IEEE Transactions on Antennas and Propagation*, vol. 16, no. 2, pp. 172–175, March 1968.

[6] H. L. Van Trees, *Optimum Array Processing, Part IV of Detection, Estimation, and Modulation Theory.* New York: Wiley, 2002.

[7] R. L. Haupt, "Thinned arrays using genetic algorithms," *IEEE Transactions on Antennas and Propagation*, vol. 42, no. 7, pp. 993–999, July 1994.

[8] K. K. Yan and Y. l. Lu, "Sidelobe reduction in array-pattern synthesis using genetic algorithm," *IEEE Transactions on Antennas and Propagation*, vol. 45, no. 7, pp. 1117–1122, July 1997.

[9] K. Chen, Z. He, and C. Han, "Design of 2-dimensional sparse arrays using an improved genetic algorithm," in *Proc. IEEE Workshop on Sensor Array and Multichannel Signal Processing*, Waltham, Massachusetts, USA, July 2006, pp. 209–213.

[10] L. Cen, Z. L. Yu, W. Ser, and W. Cen, "Linear aperiodic array synthesis using an improved genetic algorithm," *IEEE Transactions on Antennas and Propagation*, vol. 60, no. 2, pp. 895–902, February 2012.

[11] M. B. Hawes and W. Liu, "Location optimisation of robust sparse antenna arrays with physical size constraint," *IEEE Antennas and Wireless Propagation Letters*, vol. 11, pp. 1303–1306, November 2012.

[12] A. Trucco and V. Murino, "Stochastic optimization of linear sparse arrays," *IEEE Journal of Oceanic Engineering*, vol. 24, no. 3, pp. 291–299, July 1999.

[13] G. Prisco and M. D'Urso, "Exploiting compressive sensing theory in the design of sparse arrays," in *Proc. IEEE Radar Conference*, Kansas City, MO, USA, May 2011, pp. 865–867.

[14] L. Carin, "On the relationship between compressive sensing and random sensor arrays," *IEEE Antennas and Propagation Magazine*, vol. 51, no. 5, pp. 72–81, October 2009.

[15] L. Cen, W. Ser, W. Cen, and Z. L. Yu, "Linear sparse array synthesis via convex optimization," in *Proc. IEEE International Symposium on Circuits and Systems*, Paris, France, May 2010, pp. 4233–4236.

[16] G. Oliveri and A. Massa, "Bayesian compressive sampling for pattern synthesis with maximally sparse non-uniform linear arrays," *IEEE Transactions on Antennas and Propagation*, vol. 59, no. 2, pp. 467–481, February 2011.

[17] G. Oliveri, M. Carlin, and A. Massa, "Complex-weight sparse linear array synthesis by bayesian compressive sampling," *IEEE Transactions on Antennas and Propagation*, vol. 60, no. 5, pp. 2309–2326, May 2012.

[18] M. B. Hawes and W. Liu, "Compressive sensing based approach to the design of linear robust sparse antenna arrays with physical size constraint," *IET Microwaves, Antennas & Propagation*, vol. 8, no. 10, pp. 736–746, July 2014.

[19] M. P. Daly and J. T. Bernhard, "Beamsteering in pattern reconfigurable arrays using directional modulation," *IEEE Transactions on Antennas and Propagation*, vol. 58, no. 7, pp. 2259–2265, March 2010.

[20] T. Hong, M. Z. Song, and Y. Liu, "Dual-beam directional modulation technique for physical-layer secure communication," *IEEE Antennas and Wireless Propagation Letters*, vol. 10, pp. 1417–1420, December 2011.

[21] M. P. Daly and J. T. Bernhard, "Directional modulation technique for phased arrays," *IEEE Transactions on Antennas and Propagation*, vol. 57, no. 9, pp. 2633–2640, September 2009.

[22] M. P. Daly, E. L. Daly, and J. T. Bernhard, "Demonstration of directional modulation using a phased array," *IEEE Transactions on Antennas and Propagation*, vol. 58, no. 5, pp. 1545–1550, May 2010.

[23] H. Z. Shi and A. Tennant, "Direction dependent antenna modulation using a two element array," in *Proc. European Conference on Antennas and Propagation (EUCAP)*, Rome, Italy, April 2011, pp. 812–815.

[24] ——, "Characteristics of a two element direction dependent antenna array," in *Proc. Loughborough Antennas & Propagation Conference*, Loughborough, UK, November 2011, pp. 1–4.

[25] ——, "An experimental two element array configured for directional antenna modulation," in *Proc. European Conference on Antennas and Propagation (EUCAP)*, Prague, Czech Republic, March 2012, pp. 1624–1626.

[26] ——, "Enhancing the security of communication via directly modulated antenna arrays," *IET Microwaves, Antennas & Propagation*, vol. 7, no. 8, pp. 606–611, June 2013.

[27] B. Zhang, W. Liu, and X. Gou, "Sparse antenna array design for directional modulation," in *Proc. Sensor Array and Multichannel Signal Processing Workshop (SAM)*, Rio de Janerio, Brazil, July 2016, pp. 1–5.

[28] ——, "Compressive sensing based sparse antenna array design for directional modulation," *IET Microwaves, Antennas & Propagation*, vol. 11, no. 5, pp. 634–641, November 2017.

[29] B. Zhang, W. Liu, and X. Lan, "Directional modulation design based on crossed-dipole arrays for two signals with orthogonal polarisations," in *Proc. European Conference on Antennas and Propagation (EuCAP)*, London, UK, April 2018.

[30] B. Zhang and W. Liu, "Multi-carrier based phased antenna array design for directional modulation," *IET Microwaves, Antennas & Propagation*, vol. 12, no. 5, pp. 765–772(7), April 2018.

[31] Y. Ding and V. Fusco, "Directional modulation transmitter synthesis using particle swarm optimization," in *Proc. Loughborough Antennas and Propagation Conference*, Loughborough, UK, November 2013, pp. 500–503.

[32] ——, "Directional modulation far-field pattern separation synthesis approach," *IET Microwaves, Antennas & Propagation*, vol. 9, no. 1, pp. 41–48, December 2015.

[33] T. S. Ng, "Generalised array pattern synthesis using the projection matrix," *IEE Proceedings H - Microwaves, Antennas and Propagation*, vol. 132, no. 1, pp. 44–46, February 1985.

[34] Y. Ding and V. Fusco, "Experiment of digital directional modulation transmitters," in *Forum for Electromagnetic Research Methods and Application Technologies (FERMAT)*, 2015.

[35] ——, "Directional modulation transmitter radiation pattern considerations," *IET Microwaves, Antennas & Propagation*, vol. 7, no. 15, pp. 1201–1206, December 2013.

[36] ——, "Constraining directional modulation transmitter radiation patterns," *IET Microwaves, Antennas & Propagation*, vol. 8, no. 15, pp. 1408–1415, September 2014.

[37] Q. J. Zhu, S. W. Yang, R. l. Yao, and Z. P. Nie, "A directional modulation technique for secure communication based on 4d antenna arrays," in *Proc. European Conference on Antennas and Propagation (EuCAP)*, Gothenburg, Sweden, April 2013, pp. 125–127.

[38] Q. J. Zhu, S. W. Yang, R. L. Yao, and Z. P. Nie, "Directional modulation based on 4-D antenna arrays," *IEEE Transactions on Antennas and Propagation*, vol. 62, no. 2, pp. 621–628, February 2014.

[39] W. Liu and S. Weiss, *Wideband Beamforming: Concepts and Techniques.* Chichester, UK: John Wiley & Sons, 2010.

[40] M. B. Hawes and W. Liu, "Sparse array design for wideband beamforming with reduced complexity in tapped delay-lines," *IEEE/ACM Transactions on Audio, Speech, and Language Processing*, vol. 22, no. 8, pp. 1236–1247, August 2014.

[41] S. A. Vorobyov, A. B. Gershman, and Z. Q. Luo, "Robust adaptive beamforming using worst-case performance optimization: A solution to the signal mismatch problem," *IEEE Transactions on Signal Processing*, vol. 51, no. 2, pp. 313–324, February 2003.

[42] J. Li, P. Stoica, and Z. Wang, "On robust capon beamforming and diagonal loading," *IEEE Transactions on Signal Processing*, vol. 51, no. 7, pp. 1702–1715, July 2003.

[43] L. Lei, J. P. Lie, A. B. Gershman, and C. M. S. See, "Robust adaptive beamforming in partly calibrated sparse sensor arrays," *IEEE Transactions on Signal Processing*, vol. 58, no. 3, pp. 1661–1667, March 2010.

[44] L. Yu, W. Liu, and R. J. Langley, "Novel robust beamformers for coherent interference suppression with DOA estimation errors," *IET Microwaves, Antennas & Propagation*, vol. 4, no. 9, pp. 1310–1319, September 2010.

[45] C. C. Chen, B. A. Kramer, and J. L. Volakis, "Considerations on size reduction of UWB antennas," in *Proc. IEEE International Symposium on Antennas and Propagation*, Honolulu, HI, USA, June 2007, pp. 6011 –6014.

[46] C. Research, "CVX: Matlab software for disciplined convex programming, version 2.0 beta," http://cvxr.com/cvx, September 2012.

[47] M. Grant and S. Boyd, "Graph implementations for nonsmooth convex programs," in *Recent Advances in Learning and Control*, ser. Lecture Notes in Control and Information Sciences. Springer-Verlag Limited, 2008, pp. 95–110, http://stanford.edu/~boyd/graph$_$dcp.html.

[48] E. J. Candès, M. B. Wakin, and S. P. Boyd, "Enhancing sparsity by reweighted l_1 minimization," *Journal of Fourier Analysis and Applications*, vol. 14, no. 5, pp. 877–905, December 2008.

[49] G. Prisco and M. D'Urso, "Maximally sparse arrays via sequential convex optimizations," *IEEE Antennas and Wireless Propagation Letters*, vol. 11, pp. 192–195, February 2012.

[50] B. Fuchs, "Synthesis of sparse arrays with focused or shaped beampattern via sequential convex optimizations," *IEEE Transactions on Antennas and Propagation*, vol. 60, no. 7, pp. 3499–3503, May 2012.

[51] L. Litwin and M. Pugel, "The principles of OFDM," *RF signal processing*, vol. 2, pp. 30–48, January 2001.

[52] V. Chakravarthy, A. S. Nunez, J. P. Stephens, A. K. Shaw, and M. A. Temple, "TDCS, OFDM, and MC-CDMA: a brief tutorial," *IEEE Communications Magazine*, vol. 43, no. 9, pp. S11–S16, September 2005.

[53] Y. S. Cho, J. Kim, W. Y. Yang, and C. G. Kang, *Introduction to OFDM*. John Wiley & Sons, Ltd, August 2010, pp. 111–151. [Online]. Available: http://dx.doi.org/10.1002/9780470825631.ch4

[54] L. Hanzo, Y. J. Akhtman, L. Wang, and M. Jiang, *Introduction to OFDM and MIMO-OFDM*. Wiley-IEEE Press, 2011, pp. 1–36. [Online]. Available: http://ieeexplore.ieee.org/xpl/articleDetails.jsp?arnumber=5713400

[55] ——, *Introduction to OFDM and MIMO-OFDM.* Wiley-IEEE Press, 2011, pp. 1–36. [Online]. Available: http://ieeexplore.ieee.org/xpl/articleDetails.jsp?arnumber=5713400

[56] A. Gangwar and M. Bhardwaj, "An overview: Peak to average power ratio in OFDM system & its effect," *International Journal of Communication and Computer Technologies*, vol. 1, no. 2, pp. 22–25, September 2012.

[57] S. Sharma and P. K. Gaur, "Survey on PAPR reduction techniques in OFDM system," *International Journal of Advanced Research in Computer and Communication Engineering*, vol. 4, no. 6, pp. 271–274, June 2015.

[58] M. Bala, M. Kumar, and K. Rohilla, "PAPR reduction in OFDM signal using signal scrambling techniques," vol. 3, no. 11, pp. 140–143, May 2014.

[59] X. D. Li and L. J. Cimini, "Effects of clipping and filtering on the performance of OFDM," *IEEE Communications Letters*, vol. 2, no. 5, pp. 131–133, May 1998.

[60] X. Zhu, W. Pan, H. Li, and Y. Tang, "Simplified approach to optimized iterative clipping and filtering for papr reduction of OFDM signals," *IEEE Transactions on Communications*, vol. 61, no. 5, pp. 1891–1901, May 2013.

[61] R. W. Bauml, R. F. H. Fischer, and J. B. Huber, "Reducing the peak-to-average power ratio of multicarrier modulation by selected mapping," *Electronics Letters*, vol. 32, no. 22, pp. 2056–2057, October 1996.

[62] W. X. Lin, J. C. Lin, and Y. T. Sun, "Modified selective mapping technique for PAPR reduction in OFDM systems," in *Proc. International Conference on ITS Telecommunications*, Taipei, China, November 2012, pp. 764–768.

[63] S. H. Muller and J. B. Huber, "OFDM with reduced peak-to-average power ratio by optimum combination of partial transmit sequences," *Electronics Letters*, vol. 33, no. 5, pp. 368–369, February 1997.

[64] J. C. Chen, "Partial transmit sequences for PAPR reduction of OFDM signals with stochastic optimization techniques," *IEEE Transactions on Consumer Electronics*, vol. 56, no. 3, pp. 1229–1234, August 2010.

[65] S. Hu, G. Wu, Q. Wen, Y. Xiao, and S. Li, "Nonlinearity reduction by tone reservation with null subcarriers for WiMAX system," *Wireless Personal Communications*, vol. 54, no. 2, pp. 289–305, July 2010.

[66] H. He, P. Stoica, and J. Li, "Wideband MIMO systems: Signal design for transmit beampattern synthesis," *IEEE Transactions on Signal Processing*, vol. 59, no. 2, pp. 618–628, February 2011.

[67] Q. Shen, W. Liu, W. Cui, S. L. Wu, Y. D. Zhang, and M. Amin, "Low-complexity direction-of-arrival estimation based on wideband co-prime arrays," *IEEE/ACM Transactions on Audio, Speech, and Language Processing*, vol. 23, no. 9, pp. 1445–1456, September 2015.

[68] Y. Kou, W. S. Lu, and A. Antoniou, "New peak-to-average power-ratio reduction algorithms for multicarrier communications," *IEEE Transactions on Circuits and Systems I: Regular Papers*, vol. 51, no. 9, pp. 1790–1800, September 2004.

[69] M. Mohamad, R. Nilsson, and J. van de Beek, "A novel transmitter architecture for spectrally-precoded OFDM," *IEEE Transactions on Circuits and Systems I: Regular Papers*, pp. 1–14, February 2018.

[70] H. He, P. Stoica, and J. Li, "On aperiodic-correlation bounds," *IEEE Signal Processing Letters*, vol. 17, no. 3, pp. 253–256, March 2010.

[71] J. A. Tropp, I. S. Dhillon, R. W. Heath, and T. Strohmer, "Designing structured tight frames via an alternating projection method," *IEEE Transactions on Information Theory*, vol. 51, no. 1, pp. 188–209, January 2005.

[72] W. Liu, "Channel equalization and beamforming for quaternion-valued wireless communication systems," *Journal of the Franklin Institute*, vol. 354, no. 18, pp. 8721 – 8733, December 2017.

[73] O. M. Isaeva and V. A. Sarytchev, "Quaternion presentations polarization state," in *Proc. IEEE Topical Symposium of Combined Optical-Microwave Earth and Atmosphere Sensing*, Atlanta, US, April 1995, pp. 195–196.

[74] L. H. Zetterberg and H. Brandstrom, "Codes for combined phase and amplitude modulated signals in a four-dimensional space," *IEEE Transactions on Communications*, vol. 25, no. 29, pp. 943–950, September 1977.

[75] R. T. Compton, "On the performance of a polarization sensitive adaptive array," *IEEE Transactions on Antennas and Propagation*, vol. 29, no. 5, pp. 718–725, September 1981.

[76] ——, "The tripole antenna: An adaptive array with full polarization flexibility," *IEEE Transactions on Antennas and Propagation*, vol. 29, no. 6, pp. 944–952, November 1981.

[77] A. Nehorai and E. Paldi, *Digital Signal Processing Handbook*. CRC Press, 1998, ch. Electromagnetic vector-sensor array processing, pp. 65.1–65.26.

[78] S. Miron, N. Le Bihan, and J. I. Mars, "Quaternion-MUSIC for vector-sensor array processing," *IEEE Transactions on Signal Processing*, vol. 54, no. 4, pp. 1218–1229, April 2006.

[79] X. M. Gou, Y. G. Xu, Z. W. Liu, and X. F. Gong, "Quaternion-Capon beamformer using crossed-dipole arrays," in *Proc. IEEE International Symposium on Microwave, Antenna, Propagation, and EMC Technologies for Wireless Communications (MAPE)*, November 2011, pp. 34–37.

[80] M. B. Hawes and W. Liu, "Design of fixed beamformers based on vector-sensor arrays," *International Journal of Antennas and Propagation*, vol. 2015, March 2015.

[81] J. J. Xiao and A. Nehorai, "Optimal polarized beampattern synthesis using a vector antenna array," *IEEE Transactions on Signal Processing*, vol. 57, no. 2, pp. 576–587, February 2009.

[82] X. Lan and W. Liu, "Fully quaternion-valued adaptive beamforming based on crossed-dipole arrays," *Electronics*, vol. 6, no. 2, p. 34, April 2017.

[83] G. A. Deschamps, "Techniques for handling elliptically polarized waves with special reference to antennas: Part II - geometrical representation of the polarization of a plane electromagnetic wave," *Proceedings of the IRE*, vol. 39, no. 5, pp. 540–544, May 1951.

[84] X. R. Zhang, W. Liu, Y. G. Xu, and Z. W. Liu, "Quaternion-valued robust adaptive beamformer for electromagnetic vector-sensor arrays with worst-case constraint," *Signal Processing*, vol. 104, pp. 274–283, April 2014.

[85] M. B. Hawes, W. Liu, and L. Mihaylova, "Compressive sensing based design of sparse tripole arrays," *Sensors*, vol. 15, no. 12, pp. 31 056–31 068, December 2015.

[86] H. Shi and A. Tennant, "Secure communications based on directly modulated antenna arrays combined with multi-path," in *Proc. Loughborough Antennas & Propagation Conference (LAPC)*, Loughborough, UK, November 2013, pp. 582–586.

[87] Y. Ding and V. Fusco, "MIMO-inspired synthesis of directional modulation systems," *IEEE Antennas and Wireless Propagation Letters*, vol. 15, pp. 580–584, July 2016.

[88] A. Kalantari, M. Soltanalian, S. Maleki, S. Chatzinotas, and B. Ottersten, "Directional modulation via symbol-level precoding: A way to enhance security," *IEEE Journal of Selected Topics in Signal Processing*, vol. 10, no. 8, pp. 1478–1493, December 2016.

[89] Y. Ding and V. Fusco, "A synthesis-free directional modulation transmitter using retrodirective array," *IEEE Journal of Selected Topics in Signal Processing*, vol. 11, no. 2, pp. 428–441, March 2017.

[90] L. G. P. Meloni, "Hypercomplex OFDM schemes for cross-polarized antennas," in *Proc. International Symposium on Communications and Information Technologies (ISCIT)*, Gold Coast, QLD, Australia, October 2012, pp. 502–507.